Institute of Physical Chemistry of the Polish Academy of Sciences

ul. Kasprzaka 44/52, 01-224 Warsaw, Poland

Spectroscopy of porphycene and its derivatives in supersonic-jet conditions by conventional heating and/or laser desorption techniques

Doctoral Thesis

Ephriem Tadesse Mengesha

Supervisor: Prof. dr hab. Jerzy Sepioł

This PhD dissertation was prepared with in the International Doctoral Studies at the Institute of Physical Chemistry of the Polish Academy of Sciences in Warsaw, Poland

Project operated within the Foundation for Polish Science International PhD Projects Program co-financed by the European Regional Development Fund, Operational Program Innovative Economy 2007-2013

INNOVATIVE ECONOMY
NATIONAL COHESION STRATEGY

FNP
Foundation for Polish Science

EUROPEAN UNION
EUROPEAN REGIONAL DEVELOPMENT FUND

September 2014, Warsaw

Spectroscopy of porphycene and its derivatives in supersonic-jet conditions by conventional heating and/or laser desorption techniques

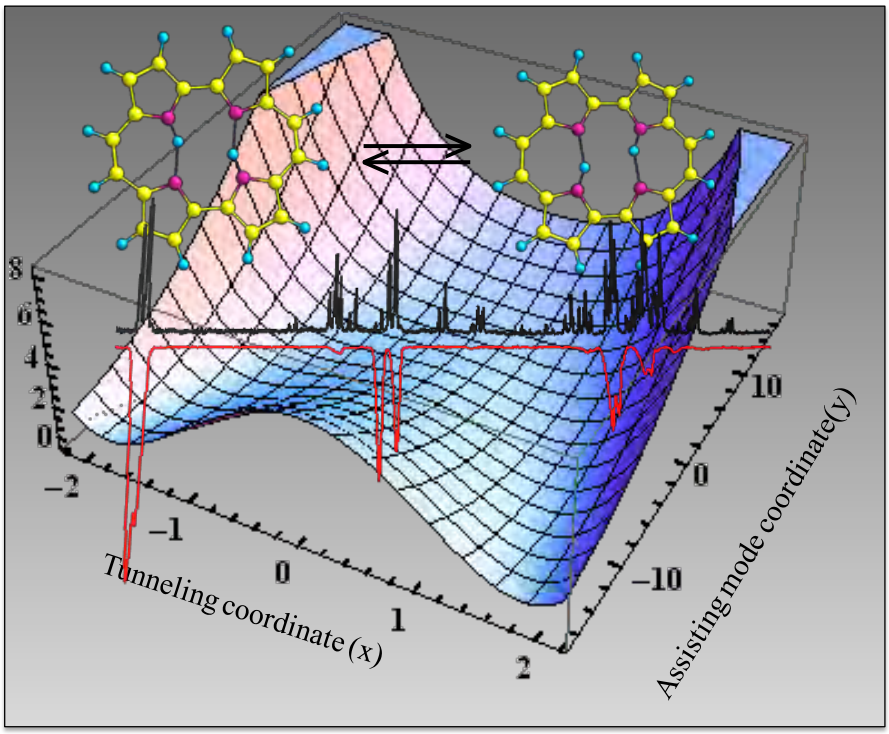

Doctoral Thesis

Ephriem Tadesse Mengesha

Supervisor: Prof. dr hab. Jerzy Sepioł

Department of Photochemistry and Spectroscopy, Institute of Physical Chemistry of the Polish Academy of Sciences, Warsaw, Poland

September 2014, Warsaw

Acknowledgments

I felt so blessed that I have a lot of wonderful people in my life to be thankful for!

First of all, I would like to express my deepest appreciation to my supervisor prof. dr hab. Jerzy Sepioł , not only for his consistent guidance, inspiration, encouragement and invaluable advices ever since I started the study, but also for trusting me in the judgments and decisions I made during the study, dziękuję bardzo! I would also like to thank Dr. Paweł Borowicz for his help and constructive ideas during the laboratory work. My sincere thanks goes to prof. dr. hab Jacek Waluk for his fruitful discussions, ideas, comments and encouragment througout my study. I would also like to thank Dr. Sylwester Gawinkowski, who I always run to whenever I needed porphycene samples, thank you!

My special thanks goes to my mentor and advisor in France, prof. Anne Zehnacker-Rentien for her generous support, valuable discussions and unlimited time she spend in the laboratory with me. Anne, I am grateful for everything you have done for me, merci beaucoup! I will also take this oportunity to thank all collegues in Institut des Sciences Moléculaires d'Orsay (ISMO) for all your help and the lunch and coffee times together. I thank specially prof. Claudine Crepin-Gilbert for the fruitful discussions on porhyrin staff. I was so moved by the excellent working environment during my stay in France, God bless you all!

I would also like to thank Dr. Tomasz Roliński for performing the theoretical modeling in this thesis and Michał Kijak for the Gaussian calculations and his valuable suggestions. I am grateful for all the helps and ideas I got from collegues in the department IX, IChF. I would also like to acknowledge Dr. Michał Gil, Urszula Szczepaniak (MSc) and Dr.Sebastian Peukert not only for the fruitful discussions but also for your good friendship.

I sincerely thank prof. Anna Grabowska for her valuable comments , suggestions and time to read my thesis. I am also grateful for the time I had with prof. Zbigniew R. Grabowski, it was an absolute privilege to meet him in person.

My sincere thanks also goes to prof. Alina Ciach, Dr. Monika Kuczyńska and all administration staffs of IChF for helping me during all the official procedures.

I cordially acknowledge the Foundation for Polish Science for providing the financial support and the Institute of Physical Chemistry (IChF) and Institut des Sciences Moléculaires d'Orsay (ISMO) for all the facilities I received during my study. I acknowledge the use of the computing facility cluster GMPCS of the LUMAT federation (FR LUMAT 2764). Because of these opportunities, I had the chance to see a different world and life experiences that helped me grow up in life!

I will not miss this opportunity to thank my friends Dr. Taye B. Demissie, Dr. Meressa Abrha and Birhanu Desalegn. Thank you for all the discussions and memories we had together during our time in Warsaw. My special thanks goes to all my Ethiopian friends in Warsaw, especially to Birtukan Negash, Yared Shegumo, Issayas Techane, Tobia Tadele, Lemlem, Senait and Aster Brzozowska. I have never missed home during holidays because of you, እግዚአብሄር ይስጥልኝ!

Finally I would like to thank my parents, families and friends for the unconditional love. Mom, I am grateful that I have you in my life, you always see the best in me. My deepest appreciations goes to my brothers Dr. Abi T. Mengesha and my sister-in-law Rahel Abebe, for always being there for me. Thank you both for being friends and families at the same time. My sincere thanks to my best friend Dawit Befekadu for his best friendship I could ever imagine. I am also indebted to my brother Belew T. Mengesha who opened my eyes to appreciate science since childhood, thank you bro!

ስለ ሁሉም ነገር እግዚአብሔር ይመስገን!!

Abstract

Supersonic jet-isolated porphycene (Pc) and its isotopomers have been studied using the techniques of laser induced fluorescence (LIF) excitation, single vibronic level fluorescence (SVLF) and hole burning spectroscopy, combined with quantum mechanical calculation of geometry and vibrational structures of the ground (S_0) and lowest electronically excited (S_1) states. Porphycene is a model for coherent double hydrogen tunneling in a symmetrical double well potential, as evidenced by tunneling splitting observed in electronic absorption and emission. The results led to reliable assignment of low frequency modes in the S_0 and S_1 electronic states. The values of tunneling splitting were determined for ground state vibrational levels. In the case of tautomerization promoting $2A_g$ mode, values of tunneling splitting were found to increase with vibrational quantum number in the ground state of Pc. Replacement of one or two hydrogens in the NH cavity by deuterons lead to drastic decrease of tunneling splitting. Different values of tunneling splitting were observed for co-excitation of two or more vibrations.

The effect of weak perturbations brought about by hydrogen/deuterium substitution on the outer rim of porphycene has been studied in detail and reported for jet-cooled heterogenous, perdeuterated Pc samples (Pc-d_{mix}) with the prevailing contribution of rim deuterated Pc-d_{12} isotopologue. In this case, laser desorption method was successfully applied to introduce the samples in the jet. The samples introduced into the gas phase were then studied by means of LIF excitation and SVLF measurements, in combination with quantum chemical calculations. The influence of molecular symmetry is studied by comparing Pc, Pc-d_{12} and Pc-d_{11}. The 0-0 transition in the LIF spectrum of Pc-d_{12} shows a blue–shift of about 32 cm^{-1} relative to that of the parent undeuterated Pc, although similar spectral patterns were observed in the two isotopologues. Comparable tunneling splitting was observed in the two isotopomers, both for the 0-0 transition and the most efficient promoting $2A_g$ mode. In contrast, an unexpected isotopic effect is observed for the totally symmetric $4A_g$ mode. While this vibration behaves as a neutral mode in Pc, neither enhancing nor decreasing the tunneling efficiency, it strongly promotes hydrogen transfer in Pc-d_{12}. This observation is explained in terms of modification of the displacement vectors of the $4A_g$ mode upon deuteration.

Symmetric mode coupling (SMC) model was applied to map effect of mode coupling in two dimensional potential surfaces (one along the tunneling coordinate and the other along the coordinate of the promoting $2A_g$ mode) of porphycene. The experimental values of tunneling splitting were well reproduced using this model.

More stringent electronic and structural perturbation on proton tunneling is reported for jet cooled 2,7,12,17-tetra-tert-butylporphycene (TTPc). LIF and SVLF measurements by conventional heating method, in combination with quantum chemical calculations show the presence of two Trans- (one C_{2h} and the other C_s symmetries) and one Cis- (C_{2v}) isomers of

TTPc in the supersonic jet. The trans-C_{2h} TTPc was found to be the most stable in the gas phase. A tunneling splitting of about 10 cm^{-1} is found for the Cis-form while no tunneling splitting is found for either of the trans isomers. This observation is in accordance with the shortest NH….N distance calculated for the Cis isomer. Interestingly, the presence of only the Cis-form of TTPc was manifested in the LIF spectrum measured in supersonic jet using laser desorption method.

Abstrakt

Porficen (Pc) i jego izotopomery badano w naddźwiękowej wiązce molekularnej stosując laserowe wzbudzanie fluorescencji (LIF), pomiary fluorescencji dyspersyjnej wzbudzanej selektywnie do pojedynczych stanów wibronowych (SVLF) i dwukolorową spektroskopię „wypalania-dziur" , włączając w to również obliczenia kwantowo-mechaniczne geometrii i struktury wibronowej stanu podstawowego (S_0) i najniższego electronowo wzbudzonego stanu (S_1). Porficen jest modelem dla koherentnego dwuprotonowego tunelowania w symetrycznej studni potencjału, o czym świadczy rozszczepienie tunelowe obserwowane w elektronowej absorpcji i emisji. Wyniki prowadzą do wiarygodnego oznaczenia modów niskoczęstościowych w stanach elektronowych S_0 and S_1. Wartości rozczepień tunelowych zostały określone dla stanów wibronowych stanu podstawowego. W przypadku modu A_{2g} wspomagającego tautomeryzację, wartości rozszczepienia tunelowego rosną wraz z wibracyjną liczbą kwantową. Zastąpienie jednego lub dwóch wodorów we wnęce z grupami NH przez deuterony prowadzi do drastycznego zmniejszenia rozszczepienia tunelowego. Różne wartości rozszczepienia tunelowego były obserwowane dla współwzbudzonych dwóch lub więcej wibracji.

Efekt słabego zaburzenia powodowany zastąpieniem protonów na obwodzie szkieletu porficyny poprzez deutery był szczegółowo badany i został opisany dla próbki heterogenicznej (Pc-d_{mix}) o różnym stopniu zdeuterowania ale z dominującym udziałem obwodowo deuterowanego izotopologu Pc-d_{12}. W tym przypadku, zastosowano z sukcesem metodę desorpcji laserowej w celu badania próbki w wiązce naddźwiękowej. Badano fluorescencję Pc-d_{mix} (LIF i SVLF) jak również przeprowadzono odpowiednie obliczenia. Wpływ symetrii molekularnej był analizowany porównując spektroskopie Pc, Pc-d_{12} i Pc-d_{11}. Przesunięte w kierunku niebieskim (c.a. 32 cm^{-1}) widma Pc-d_{12} pokazują podobne rozszczepienia tunelowe zarówno dla przejścia elektronowego 0-0 jak też aktywnego modu $2A_g$. Jednakże nieoczekiwany efekt zaobserwowano dla całkowicie symetrycznego modu $4A_g$. Jest on neutralny w Pc podczas gdy w Pc-d_{12} zwiększa rozszczepienie. Ten efekt można wyjaśnić analizując wektory przesunięcia atomów w modzie $4A_g$ po deuteracji.

Model symetrycznego sprzężenia modu (SMC) został zastosowany do śledzenia efektu sprzężenia modu na dwuwymiarowej powierzchni potencjału (jeden wymiar wzdłuż współrzędnej tunelowania i drugi wzdłuż współrzędnej modu wspomagającego $2A_g$) porficenu. Wyniki doświadczalne rozszczepienia tunelowego zostały dobrze odtworzone przez powyższy model.

Mocniejsze perturbacje zaobserwowano w zjawisku tunelowania protonów dla 2,7,12,17-cztero-tert-butylo-porficenu (TTPc) w naddźwiękowej wiązce molekularnej. Wyniki pomiarów widm LIF i SVLF dla TTPc wprowadzanego do wiązki molekularnej poprzez konwencjonalne grzanie piecyka a także obliczenia chemii kwantowej wskazują na obecność w fazie gazowej

trzech izomerów: dwóch *trans* (jeden o symetrii C_{2h} i drugi o symetrii C_s) i trzeciego *cis* (o symetrii C_{2v}) . Rozszczepienie tunelowe około 10 cm^{-1} zaobserwowano dla struktury *cis* podczas gdy nie zaobserwowano rozszczepienia dla obu form *trans*. Jest to w zgodzie z obliczoną najkrótszą długością wiązania NH...N formy *cis*. Interesującym jest, że widmo LIF mierzone z zastosowaniem desorpcji laserowej wskazuje na obecność w wiązce naddźwiękowej tylko izomeru *cis*.

List of Publications

Related to the PhD Dissertation:

1. ***Mengesha, Ephriem****; Zehnacker-Rentien, Anne; Sepiol, Jerzy; Kijak, Michał; Waluk, Jacek*, "Spectroscopic Study of Jet-Cooled Deuterated Porphycenes: Unusual Isotopic Effects on Proton Tunneling", **J. Phys. Chem. B, DOI: 10.1021/jp505553z (2014)**

2. ***E.T. Mengesha****, J. Sepiol, P. Borowicz and J. Waluk* , Vibrations of porphycene in the S_0 and S_1 electronic states: Single vibronic level dispersed fluorescence study in supersonic jet, **J. Chem. Phys. 138,174201 (2013)**.

3. *E.T. Mengesha, J. Sepiol, P. Borowicz, T. Roliński, M. Gil and J. Waluk* : Low frequency assisted proton tunneling in porphycene: Theory and Experiment (manuscript in preparation)

Others:

1. *J. Sepiol, A. Grabowska, M.Kijak, P. Borowicz,* ***E. Mengesha*** *and J. Nowacki* 'Partial deuterium substitution as a tool for identification of the most stable conformer of a polyatomic molecule. A case of the 2,5-bis(2-benzoxazolyl)-1,4-dimethoxy benzene in supersonic jet ' **Chem. Phys. Lett. , 554 (2012) 43-46**.

2. *Michał Kijak, Ephriem Mengesha, Anna Grabowska, Jerzy Sepioł*, Michał Gil*,* 'Supersonic jet spectroscopy of 1,4-diazatriphenylene and its complexes. Structural distortion and state inversion effects.' (manuscript in preparation).

3. *E.T. Mengesha, T. B. Demissie, Mesfin Redi-Abshiro and Ahmed M. Mohammed,* "Excitation Wavelength and Solvent Polarity Dependence of the Dual Fluorescence of (E)-N-4-(dimethylamino)benzylidene-2H-1,2,4-triazol-3-amine" (Manuscript in preparation).

Poster and Oral Presentations

Poster presentations:

1. *E.T. Mengesha , J. Sepioł , P. Borowicz, T. Roliński , M. Gil and J. Waluk* "Phenomena of atom gihsting: : Low frequency vibration assisted double proton tunneling in porphycene; theory and experiment " Microsymposium, IChF PAS, 7-9 January, **2014**, Warsaw.

2. *M. Gil, M. Kijak, E. Mengesha, P. Borowicz , J. Sepioł and A. Grabowska,* "Supersonic jet spectroscopu of 1,4-diazatriphenylene. Easily detectable signature with water and othe proton donors" Microsymposium, IChF PAS ,8-10 January **2013,** Warsaw.

3. *E.Mengesha, P. Borowicz, J. Sepiol and J. Waluk, "*New spectroscopic results of porphycene in supersonic-jet*",* Polish Photoscience Seminar , **2011** , Krutyn, Poland

Oral presentations:

1. *E.T. Mengesha , J. Sepioł , P. Borowicz, T. Roliński , and J. Waluk* "Quantum weirdness in action" Annual PhD days, May **2013**, ISMO, Orsay, France.

2. *Mengesha, Ephriem; Zehnacker-Rentien, Anne; Sepiol, Jerzy; Kijak, Michał; Waluk, Jacek*, "Laser-desorption supersonic-jet spectroscopy of porphycene isotopologues", Seminaire ISMO, October 15, **2013**, France.

List of Acronyms

CW- Continuous Wave

DF- Dispersed Fluorescence

DFT- Density Functional Theory

DNA- Deoxyribonucleic acid

fs- femtosecond

HOMO- Highest Occupied Molecular Orbital

IR- Infra Red

IVR- Intramolecular Vibrational energy Redistribution

LIF- Laser Induced Fluorescence

LUMO- Lowest Unoccupied Molecular Orbital

NMR- Nuclear Magnetic Resonance

OPA- Optical Parametric Amplifier

OPO- Optical Parametric Oscillator

Pc- Porphycene

Pc-d_1- Porphycene isotopologue where one of the internal NH hydrogen is substituted by deuterium

Pc-d_2- Porphycene isotopologue where both of the internal NH hydroges are substituted by deuteriums.

Pc-d_{11}- Porphycene isotopologue where eleven of the external CH hydrogens are substituted by deuteriums.

Pc-d_{11+1} - Porphycene isotopologue where eleven of the external CH hydrogens and one of the internal NH hydrogen are substituted by deuteriums.

Pc-d_{12}- Porphycene isotopologue where all of the external CH hydrogens are substituted by deuteriums.

Pc-d_{12+1}- Porphycene isotopologue where all of the external CH hydrogens and one of the internal NH hydrogen are substituted by deuteriums.

Pc-d_8- Porphycene isotopologue where all except the meso- positions of the porphycene ring are substituted by deuteriums.

Pc-d_{mix} – mixtures of perdeuterated porphycene isotopologues.

PES – Potential Energy Surface

S_0- Ground electronic state

S_1 – First excited electronic state

SMC- Symmetric Mode Coupling

STM- Scanning Tunneling Microscopy

SVL- Single Vibronic Level

SVLF- Single Vibronic Level Fluorescence

TD-DFT- Time Dependent Density Functional Theory

TPP0- 22,7,12,17-tetraphenylporphycene

TTPc- 2,7,12,17-tetra-tert-butylporphycene

Table of Contents

Chapter One

Introduction

1.1 Porphyrins: "pigments of life"

Porphyrins are a class of naturally occurring macrocycles containing four pyrrole rings linked via methine bridge of which free base porphyrin being the simplest member . The word porphyrin is derived from the Greek word "*porphura*" meaning purple. They are in fact a large class of deeply colored pigments, of natural or synthetic origin, having in common a substituted aromatic macrocycle ring and consist of four pyrrole rings linked by four methine bridges. Their numerous analogues and derivatives are materials of tremendous importance in chemistry, materials science, physics, biology and medicine [1,2]. They are the red color in blood (heme) and the green in leaves (chlorophyll). The essential role of porphyrins in these vital processes of life ranging from electron transfer, oxygen transport and storage and photosynthesis [3,4] made them labeled as "*pigments of life*". Figure1.1 presents a few examples of essential porphyrin derivatives in life and medical application.

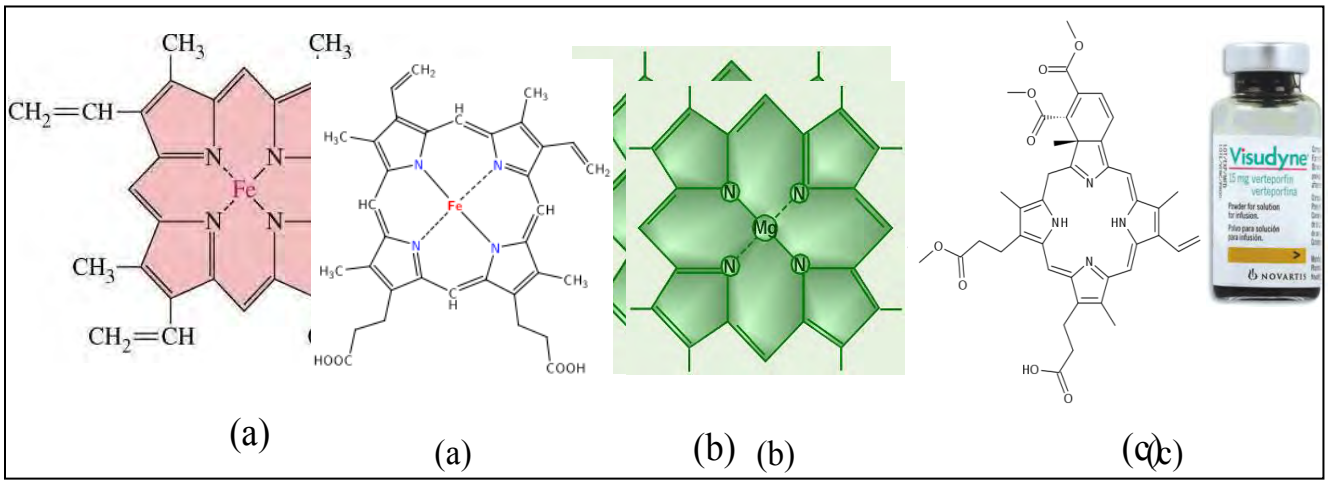

Figure 1.1 Derivatives of porphyrin which appear in essential processes of life. (a) The heme group of hemoglobin (b) part of chlorophyll a and (c) Vertporphin , a photosensitizer for photodynamic therapy sold under the trade name Visudyne [5].

The importance of porphyrins in essential life processes could be further shown by the effects they reveal in the body during abnormal conditions in metabolism of theses pigments. In this

respect, porphyrins are associated with *porphyria*, a rare inherited or acquired disorder of certain enzymes that normally participate in the production of porphyrin and heme. They manifest with either neurological complications or skin problems or occasionally both [6,7]. Figure 1.2 shows the first cases of porphyria, the Miranda family, in Brazil.

Figure 1.2 Boys of the Miranda family of Brazil, with congenital erythropoietic porphyria. Left to right, Pedro, two years old, Manoel, four, and Gesner, six. The photograph was taken in August, 1957, prior to splenectomy, later performed on the two older boys. The mutilations- a consequence of photosensitivity- are evident in the amputations required in Gesner's right hand and left ear. The distended bellies are not owing to the ascites of Schistosomiasis or of protein malnutrition, seen frequently in Northern Brazil, but to splenomegaly, a characteristic concomitant of congenital porphyria [6].

I found it more expressive to use the words of David L. Drabkin from his article about porphyria directly about the contribution of the Brazilian family in understanding the disease:

" *I wish to enter here a tribute to the subjects with debilitating disease, who look to us for aid but who faithfully serve us, frequently at the expense of their personal comfort and with only a vague hope that eventually we may be guided to understand their needs*." The photograph shows one of the saddest moments where we have to learn science the hard way!

Another interesting history associated with light sensitivity of porphyrins was recorded (in 1913) when a German physician, Frederich Meyer-Betz, injected himself with 200 mg of hematoporphyrin (Figure 1.3a) and registered no ill effect until he exposed himself to sunlight whereupon he suffered extreme swelling (Figure 1.3 b). This photosensitivity remained for several months [7].

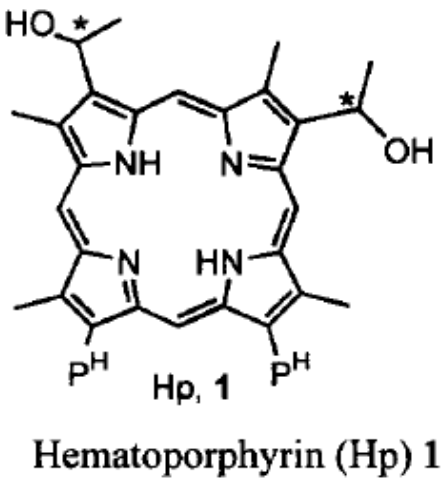

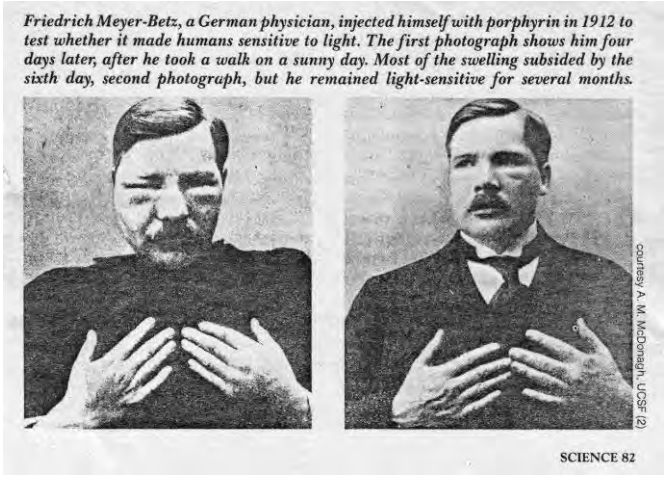

Figure 1.3 (a) the structural formula of hematoporphyrin Meyer-Betz injected himself [8] and (b, left) Mayer-Betz four days later, after he took a walk on a sunny day and (b, right) Mayer –Betz by the sixth day after injection. [photo taken from wikipedia][9]

From the perspective of coordination chemistry, porphyrins are excellent ligands that can coordinate with almost every metal in the periodic table. Grounded in natural systems, they are incredibly versatile and can be modified in many ways; each new modification yields derivatives, demonstrating new chemistry, physics and biology, with a vast array of medicinal [7] and technical applications [10,11,12]. Because porphyrins possess extended π-electron systems and exhibit large stability, they are finding applications, to an increasing extent, in advanced materials as components in organic metals, molecular wires, and other devices [3]. In medicine, porphyrins are experiencing a renaissance due to the advent of photodynamic therapy of great promise in the treatment of cancer and dermatological diseases [4].The interdisciplinary interest porphyrins thus generate has provided the impetus to develop porphyrin-like molecules anticipated to exhibit special properties, by structural variation of the tetrapyrrolic macrocycle

while maintaining a (4n+2) π main conjugation pathway. The pursuit of this concept has proven to be highly successful as evidenced by the synthesis of expanded [13,14], reshuffled [15], inverted [16], contracted [17], and otherwise modified porphyrins [18].

1.2 Porphyrin Isomers

As stated above, one method of modification is simple reshuffling of the macrocyclic ring of parent porphyrin which results in the formation of constitutional isomers presented in Figure1.4.

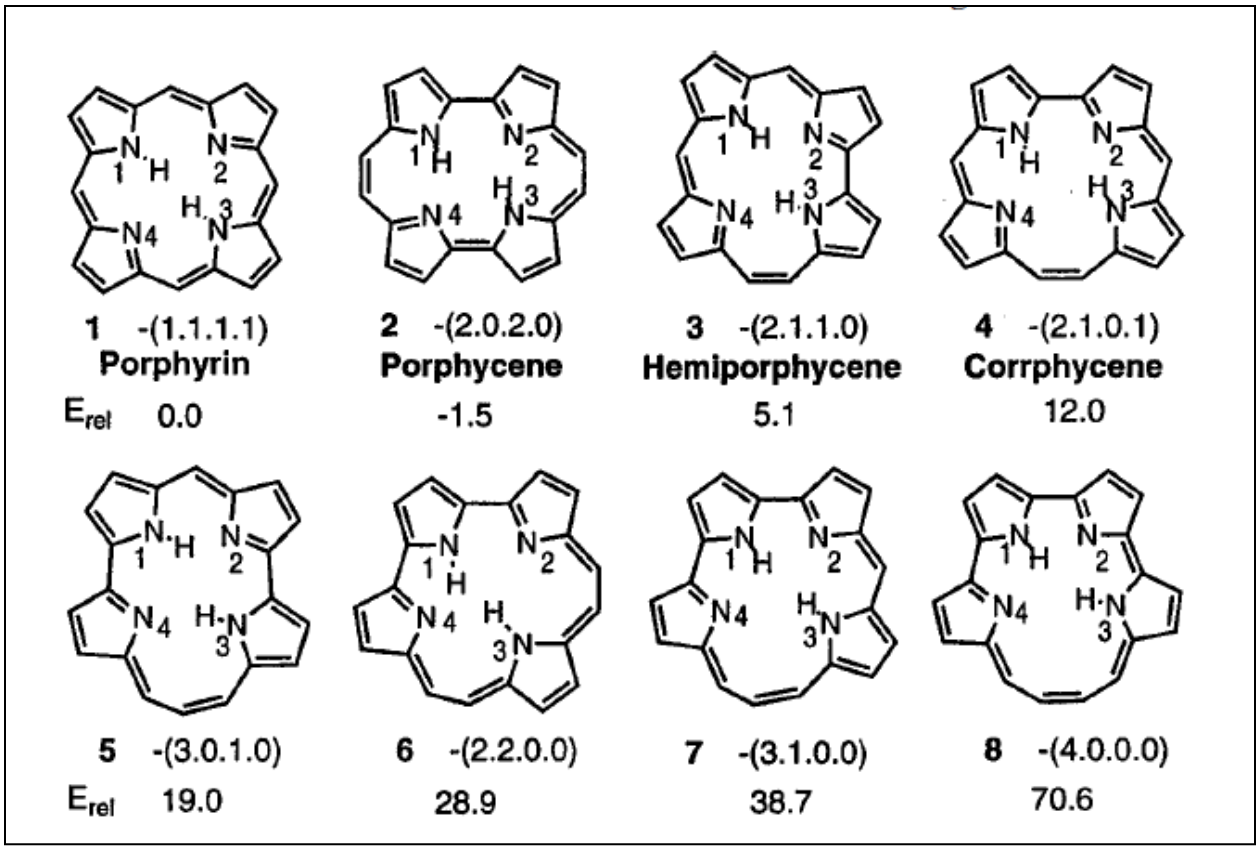

*Figure 1.4 Porphyrin and its seven (Z)-configured constitutional isomers with an N_4-core metal coordination centre. The calculated relative energies (Kcal/mol) by BLYP/6-31G**// BLYP/3-21G are also shown (the formulae represent the most stable NH tautomer in each case)* [19].

They differ formally by the arrangement of the four methine units linking the pyrroles. The numbers in the parenthesis denotes the number of carbon atoms between adjacent pyrrole units. The X-ray crystal structures and NMR spectra indicate that compounds **2-4** are all planar and aromatic, just like porphyrin. They all possess the ability to bind metal ions, and their redox

properties are similar to that of porphyrin [20,21]. Structures **5-8** are much higher in energy than porphyrin and porphycene due to sever angle strains in their geometries; whether the synthesis of these compounds can be achieved, largely depends on their stability. Table 1.1 shows the results of calculations by Wu et.al [19] on the relative stability of the constitutional isomers.

Table **1.1** Calculated relative stabilities (Kcal/mol) of compounds **1-8** [19]

isomer	PM3	BLYP/ 3-21G	BLYP/ 6-31G**//3-21G	BLYP/ 6-31G**
1	0.0	0.0	0.0	0.0
2	1.7	−6.2	−1.5	−2.0
3	8.6[a]	2.5	5.1	4.5
(*E*)-**3**		42.9	39.2	
4	20.9	12.0	12.0	11.8
(*E*)-**4**	30.1	28.1	28.7	
5	23.6	17.7	19.0	
(*E*)-**5**	24.9	28.3	26.2	
6	37.6	31.8	28.9	
7	39.7	42.7	38.7	
(*E*)-**7**	29.8	31.6	29.5	
8	53.9	78.6	70.6	
(*E*)-**8**	34.8	43.1	38.4	

From all the structural isomers, porphycene (**2**) was found to be the most stable, even more stable than parent porphyrin (**1**). This was attributed to the presence of stronger hydrogen bond in the former. Porphycene was first synthesized by E. Vogel et. al in 1986 [22]; and in their report they said " to our great surprise, there was no evidence in the literature for porphycene or derivative of porphycene even though the synthesis of structural variants of porphyrin has long been pursued intensively in porphyrin research"[23] . It will be discussed latter that, of course the synthesis of this constitutional isomer initiated plenty of researches both in fundamental and application regimes. Successful exploitation of these "pigments of life" can be achieved; however, via understanding of their fundamental chemical and photophysical properties.

One of the most fundamental chemical processes occurring in free base porphyrin is the exchange of two inner hydrogens between two inner nitrogens in the so called tautomerization reactions. Strong interest in tautomerization reaction in porphyrins has many causes. On one hand, such studies probe basic chemical notions, such as coupling between vibrations of the

protons and heavy atoms, role of tunneling, and cooperativity. On the other hand, tautomerization, especially when induced by light can be exploited for practical purposes, e.g. in optical read and write systems. Porphyrins constitute important models for theoretical treatment of intramolecular tautomerization, because the process occurs in a reaction center of well-defined geometry, located inside a molecule and isolated from the environment [24].

1.3. Proton transfer reactions and the role of quantum tunneling

Proton transfer reactions are known to play crucial roles in various physical , chemical and biological processes [25-30]. Exploitation of these reactions in synthetic and biological chemistry had been reported [31,32]. Proton transfer reactions also play roles in enzymatic reactions [33], cellular respirations [34,35], photosynthesis [36], DNA damage and repair [37] etc. From technological perspective, proton tautomerization reactions have been proposed for application in laser dyes and molecular memory devices [32].

Proton transfer reactions are common in molecules having inter or intra-molecular hydrogen bonds where the proton moves back and forth between two electronegative atoms (F, O or N) along the proton transfer coordinate. An impressive characteristics of this reaction is the non-zero probability of the reaction to take place even in the presence of potential barrier via "proton tunneling". This could be understood by treating the proton as a quantum "wave packet" as it has considerable de Broglie wavelength in cases of small transfer distances and hence the wave nature of the particle becomes significant [38]. Löwdin [39] had discussed the implication of proton tunneling in DNA which could alter the genetic code and give rise to mutations (Figure 1.5). These mutations whether they are reversible or not, could be the cause of several medical conditions that come about as a result of degraded or corrupted genetic material such as aging or cancer [40].

Since hydrogen transfer reactions represent a range of processes, from a simple acid base reaction to complex biochemical reactions, it has been difficult to achieve the level of understanding to gain real control over the reaction [41]. Therefore, the primary goal should be characterization of the reaction potential energy surfaces. In this perspective, the first step is to select a simple model system where accurate experimental measurement and quantitative theoretical analysis of the potential energy surface could be made. One simple case is tautomerization reaction in "*narcissistic*" systems where the reactant and product are chemically identical. The potential energy surface of such systems could be represented by symmetrical double minimum potential.

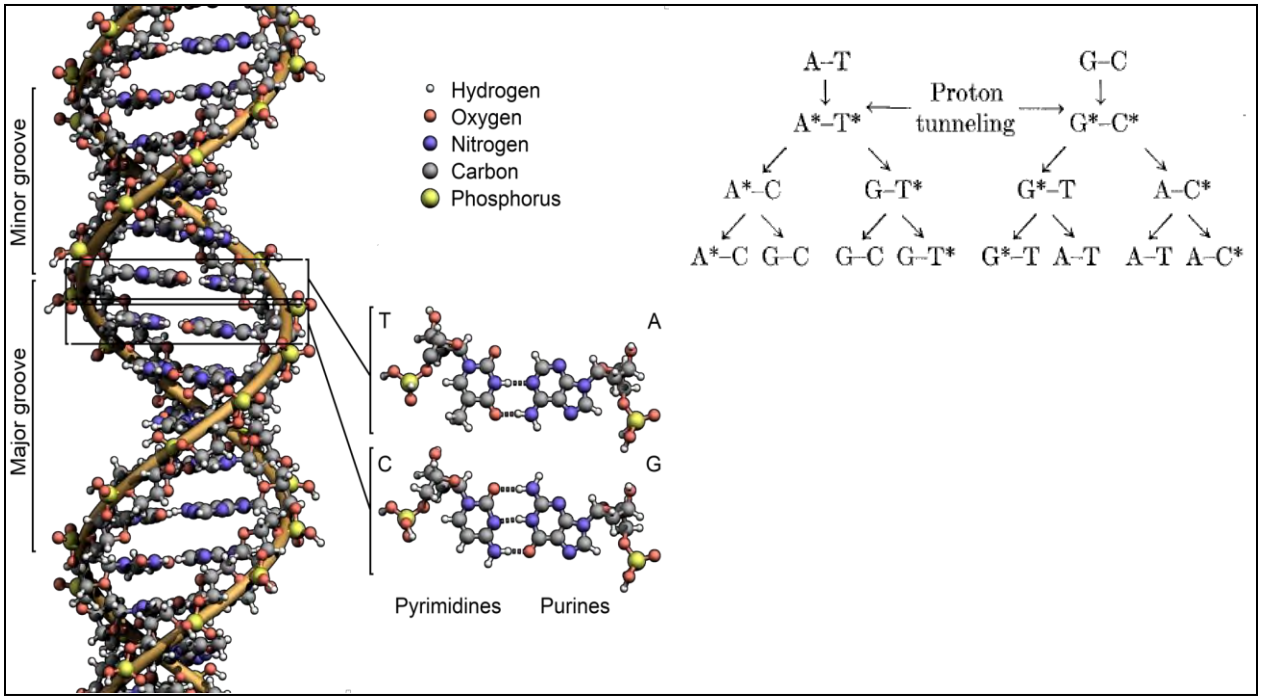

Figure 1.5 Hydrogen bonding in DNA base pairs. The inset shows the effect of proton tunneling in the hydrogen bonded base pairs responsible for mutation. [httpa://oscarbonilla.com/2011/04/radiation/].

1.3.1 Proton transfer in "narcissistic" systems

Molecules which are characterized by symmetric double minimum potential energy surfaces are interesting to study spectroscopically because of splitting of Eigen states of the molecule and parity selection rules result in tunneling splitting which are readily observable in spectra [38,41]. The tunneling splitting can lead to doublet transitions in the absorption or fluorescence excitation spectra as was observed in the case of malonaldehyde [42,43], tropolone [44a], 9-hydroxyphenalenone and derivatives [44], porphycene [45] and benzoic acid dimer [46]. For a symmetric double minimum potential well, the parity-allowed electronic transitions are + ↔ + and - ↔ - as shown in figure 1.5. The transition originating from 0 - level can be treated as a "hot" band.

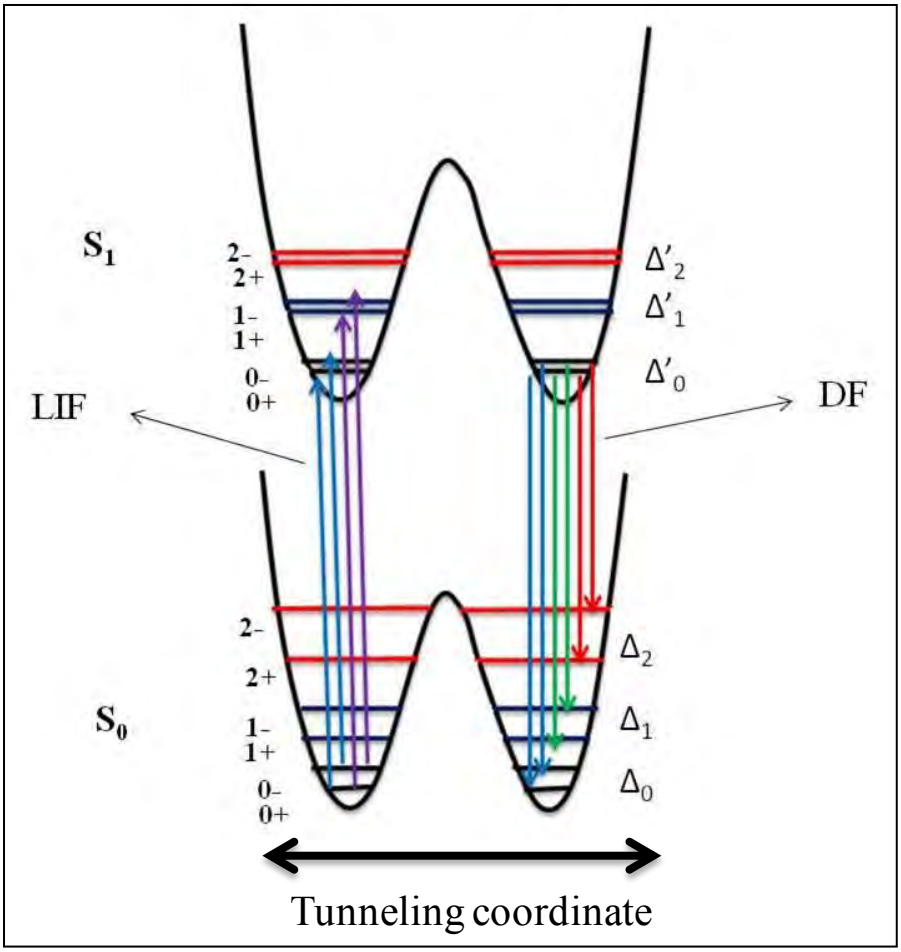

Figure 1.5 Schematic diagrams of symmetric double minimum potential energy curves in the S_0 and S_1 state along the proton transfer coordinate.

The problem of tunneling in symmetric double minimum potential was first considered by Dennison and Uhlenbeck [47] in connection with the doubling of lines in the vibrational spectrum of ammonia, and most of its subsequent applications have been to spectroscopy. The quantitative treatment of the problem of quantum tunneling in a symmetric double minimum potential is reviewed in ref [38].

If one considers the potential wells in isolation, there will be a series of non degenerate energy levels in each well as shown in figure 1.6 (Eigen states ψ_1 and $\psi_{2)}$. As the barrier height is lowered however, the wave functions which penetrate the barrier walls, will interact both constructively and destructively to produce two new wave functions which can be described mathematically by the linear combination, $\psi_1 \pm \psi_2$.

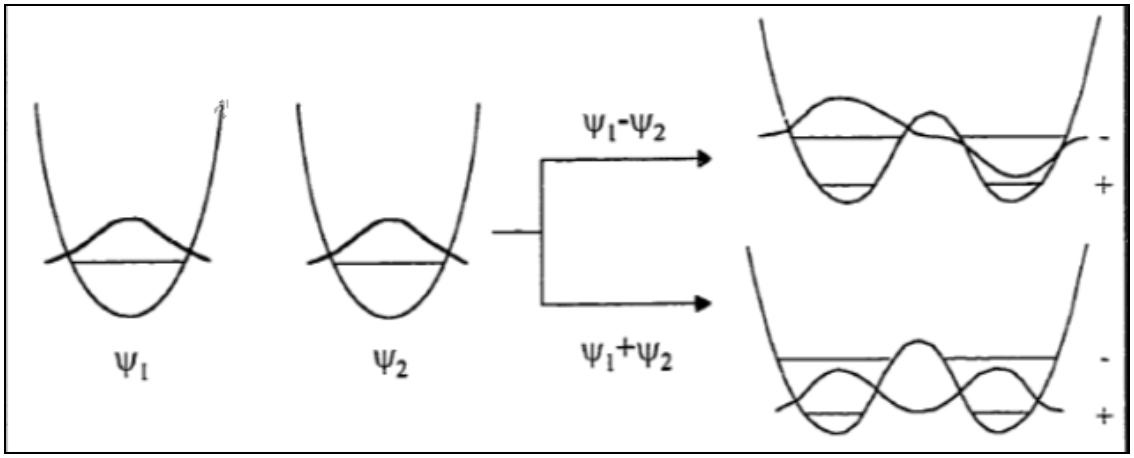

Figure 1.6 Schematic diagram showing the origin of removal of +, - parity degeneracy of the wavefunctions in a symmetric double minimum potential well [41].

To a first approximation, the two new wave functions could be written as ψ_+ and ψ_- where:

$\psi_+ = 2^{-1/2}[\psi_1 + \psi_2]$..... (1)

$\psi_- = 2^{-1/2}[\psi_1 - \psi_2]$..... (2)

Appropriate one dimensional quantum mechanical treatment with the help of Wentzel Krammer and Brillouins' (WKB) approximation [48-52] show that the tunneling splitting ($\Delta E = E_- - E_+$) is given by:

$$\Delta E = 2\hbar\nu exp^{[\frac{-\sqrt{2m}}{\hbar}\int_{-x_1}^{x_1}(V(x)-E_0)^{1/2}dx]} \quad \ldots\ldots\ldots (3)$$

and the tunneling frequency ν_t is given by:

$$\nu_t = \frac{2\Delta E}{h} = \frac{2\nu}{h} exp^{[\frac{-\sqrt{2m}}{\hbar}\int_{-x_1}^{x_1}(V(x)-E_0)^{1/2}dx]} \quad \ldots\ldots (4)$$

where h, ν, m, and E_0, represent the Planck's constant, vibrational frequency, tunneling mass and energy of vibration, respectively.

For a double-minimum potential, slight departure from symmetry produces a large decrease in tunneling frequency, and at the same time renders the problem much more difficult to treat theoretically. Crudely speaking, the decrease in tunneling frequency may be attributed to the fact that the introduction of asymmetry destroys the exact state of the resonance between the two wells. The stationary state wave functions can no longer be classified as symmetric or antisymmetric, as in the case of symmetrical case, and they no longer predict equal probabilities of finding the particle in the two wells. For example, if the right-hand well is slightly lower than the left-hand one, the lowest stationary state ψ_0 corresponds to a particle which is largely localized in the former, while for the next lowest state ψ_1 this localization is transferred to the left well. The non-stationary state in which the particle is definitely known to be in the left-hand well will be approximately represented by:

$$\psi_1 + c\psi_0$$

where $c^2 \ll 1$, and the average time which elapses before the particle appears in the right-hand well will be greater than that in the symmetrical case by a factor of the order of $1/c^2$. A similar difference arises if the shapes of the two wells are slightly different, even if their minima have exactly the same energies.

A number of authors have treated in detail the problem of tunneling between asymmetric double minima [53-57]. The problem is , however, a complex one and only some general conclusions have been drawn. Harmony [58] has given the approximate expression, valid when both the asymmetry and the tunneling probability are small.

If ν_t^0 and ν_t refer, respectively, to tunneling frequencies of the symmetrical and unsymmetrical systems and ΔV is the energy difference between the two minima in the latter (Figure 1.7), then

$$\frac{\nu_t}{\nu_t^0} = \frac{2h\nu_t^0}{[(2h\nu_t^0)^2 + 16(\Delta V)^2]^{1/2}} \text{.....} (5)$$

It can be easily observed from the equations above that the tunneling splitting is highly sensitive to the mass of the tunneling particle suggesting that the study of isotopic effects could be employed to confirm phenomena of tunneling. It is also highly dependent on the form of the potential and theinter minimal distance of the double minimum positions. Equation (4) shows the value of tunneling frequency can be obtained from measurement of the tunneling splitting . Another important factor is the symmetry of the double minimum potential. Equation (5) shows that the tunneling splitting is reduced by introduction of asymmetry between the two minima.

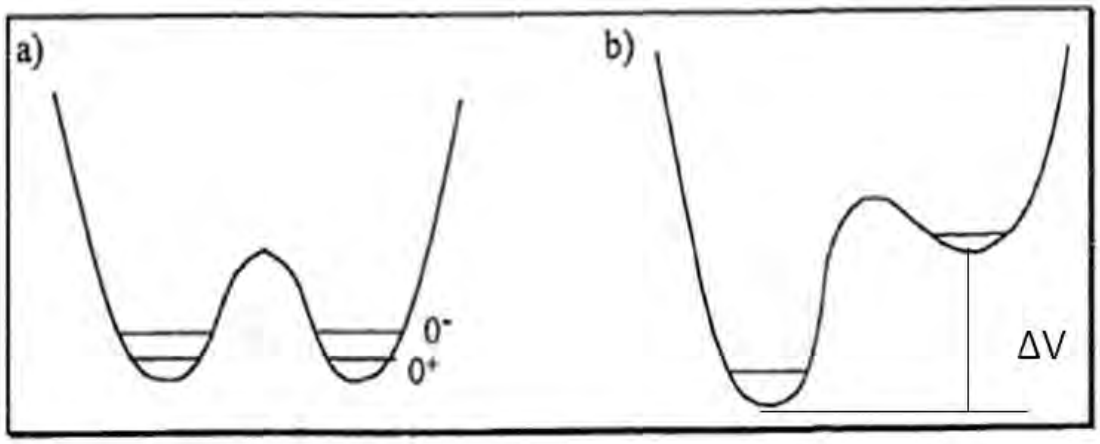

Figure 1.7 Schematic diagrams of (a) symmetric and (b) asymmetric potential energy curves for intramolecular proton transfer reactions [41].

1.3.2 Porphycene: a model system for double proton transfer reaction

Porphycene is a blue pigment with strongly reddish fluorescence. Ever since its synthesis [22] as the first known constitutional isomer of porphyrin, it continues to be a fascinating molecule for scientists both in fundamental and applied researches [59, 60]. Scheme 1 shows comparison of the structural formulae of porphycene and porphyrin.

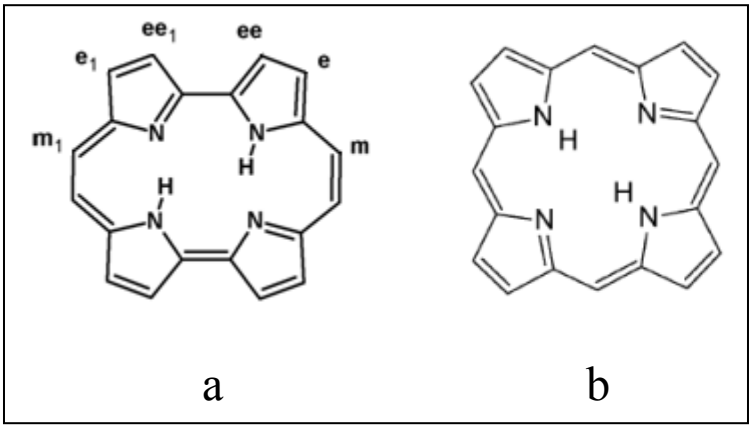

Scheme 1. Porphycene (a) and porphyrin (b). For porphycene, non-equivalent positions of hydrogens are marked.

Even though porphycene retains the central feature of porphyrin, it differs in the cavity shape, NH···N distance, and overall symmetry. The structural modification results in the change of symmetry, from D_{2h} in porphyrin to C_{2h} in porphycene. Consequently the strength of the hydrogen bond is larger in porphycene than in porphyrin which makes the former more stable! This, in turn, leads to a change in the intensity pattern of the electronic transitions and overall photophysical properties. For example, porphycene shows much stronger absorption coefficient in a physiologically relevant region (600-650 nm), which makes it a much better agent for photodynamic therapy than porphyrin as light of longer wavelength penetrate deeper in tissues (see Scheme II) [61-67]. This behavior is due to a larger |ΔHOMO-ΔLUMO| difference in porphycene than in porphyrin, where ΔHOMO and ΔLUMO stand for the energy splitting between the HOMO and HOMO-1, and LUMO and LUMO+1, respectively[68].

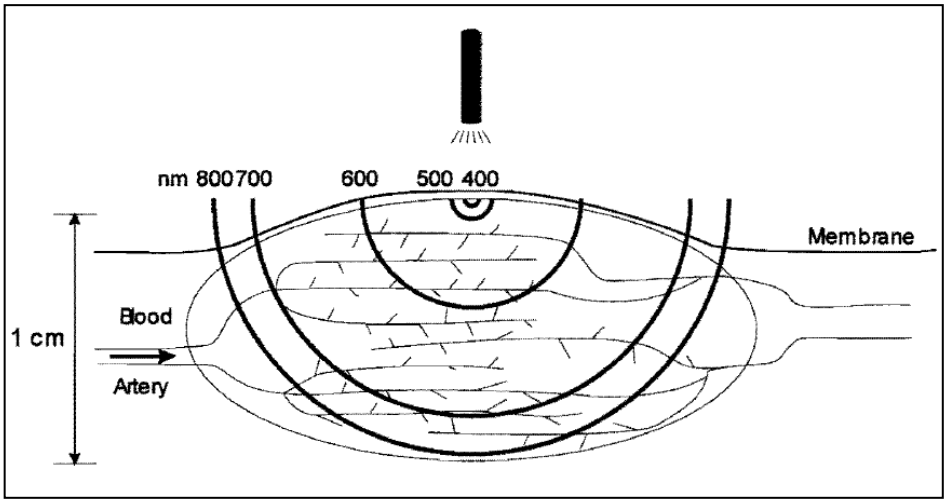

Scheme II . Wavelength dependence of the depth of penetration of light into a tumor [8].

Three tautomeric forms can be envisaged for porphycene, a trans species with protons on the opposite nitrogen atoms and two cis structures with protons localized on the adjacent nitrogens (Scheme III). Each of these tautomers has a chemically identical counterpart and can be represented by a symmetric double minimum potential. Theoretical calculations of relative energies for porphycene isomers in the gas phase predict the trans tautomer to be the most stable while cis-2 structure is found to be the least stable [69, 70]. (Table 1.2). Similar conclusions have been reached by Yoshikawa et.al [71].

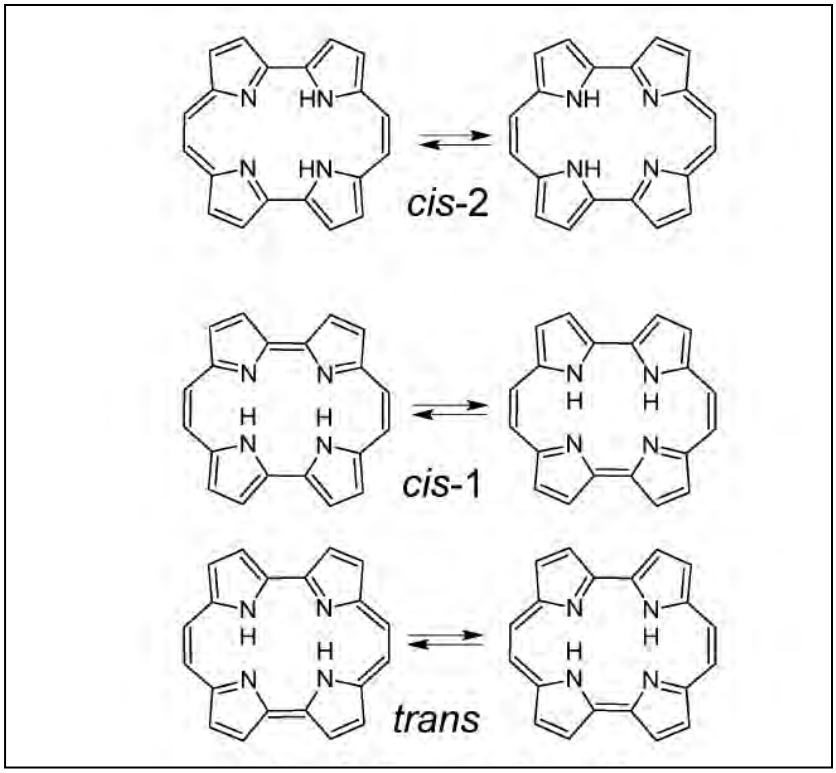

Scheme III. Tautomeric forms of porphycene

Table 1.2 Calculated relative energy for porphycene at stationary points in Kcal/mol *. [69]

Structure	SCC-DFTB	B3LYP
trans	0.0	0.0
Cis-1	3.7	2.2
Cis-2	16.2	30.2

*The 6-31G(d,p) basis set was used for B3LYP calculations

From experimental point of view, no evidence was found for the presence of cis-forms of porphycene in the gas phase; although both the trans and cis-1 forms of isolated 9,10,19,20-tetraalkyl porphycene derivatives have been observed in supersonic-jet [72]. In contrast, recent STM study of porphycene deposited on Cu (110) surface at 5K confirmed that the cis-1 structure is the most stable one [73].

In the most stable form of porphycene or porphyrin in the gas phase, the inner hydrogen atoms are in the *trans* position, corresponding to the inner hydrogens located at the opposite nitrogen atoms, as shown in Scheme I. Due to the symmetry of the system, these hydrogen atoms can migrate from one *trans* configuration to the equivalent one. Tautomerism in porphyrin and porphycene has been widely studied; both molecules act as model systems for the double hydrogen transfer reaction [24, 60, 70, 73, 74-99] . They strongly differ, however, in the rate and mechanism of tautomerization. The interconversion between the *trans* tautomers of porphyrin is strongly temperature-dependent and has been shown to proceed via a two-step mechanism, involving the *cis* form with the hydrogen atoms located at the neighboring nitrogen atoms as an intermediate. [74-76]

In contrast, NMR studies of crystalline porphycene (Figure 1.8) have shown that the interconversion between the two *trans* forms is still very fast on the NMR timescale even at 107 K. [77] This observation suggests the tunneling nature of the hydrogen exchange mechanism.

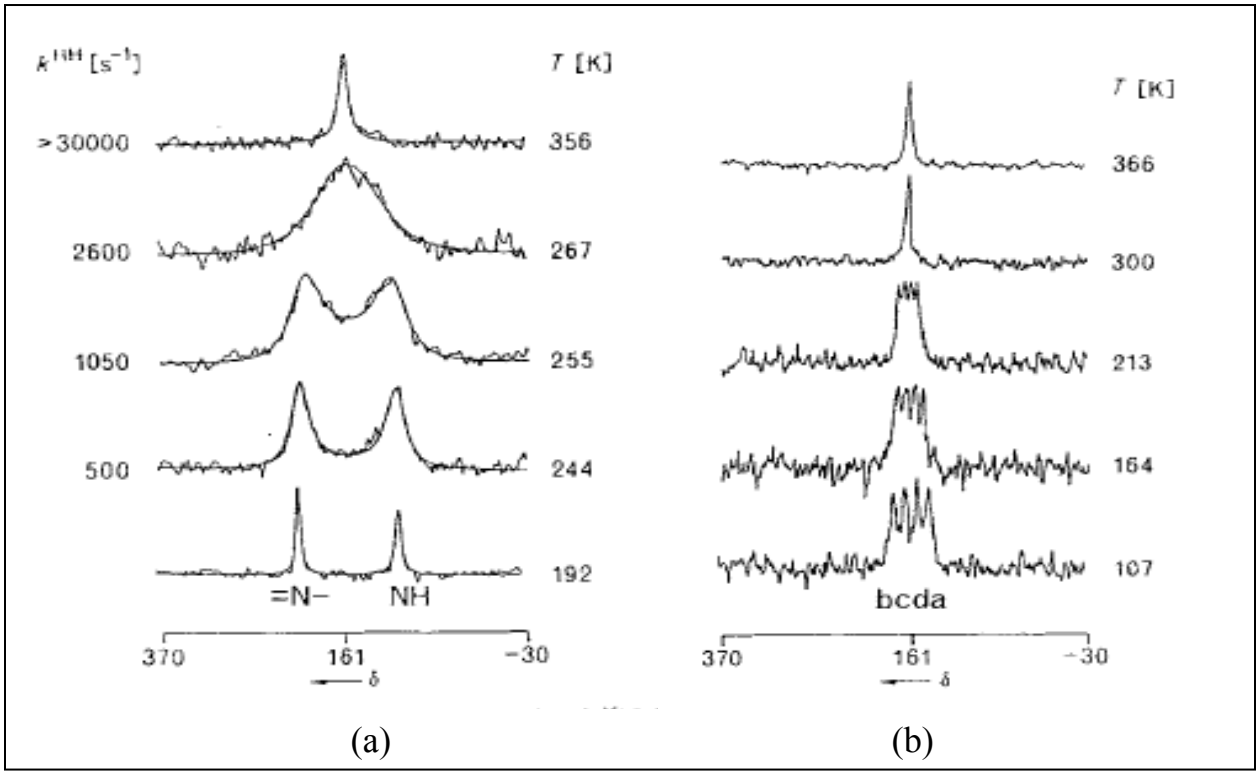

Figure 1.8 ^{15}N-CPMAS-NMR spectra of 95% ^{15}N-enriched Porphyrin (a) and Porphycene (b) at 9.12 MHz as a function of temperature. [77].

Low temperature experiments, performed in supersonic jet [45,72, 100] or helium nanodroplets [101] are especially informative in this respect. Sepioł *et. al*. [45] carried out the first supersonic jet study of porphycene which demonstrated that the 0-0 and all the vibronic bands observed in the laser-induced fluorescence (LIF) excitation spectrum were split into doublets (Figure 1.9). The doublets disappear upon exchange of one or both inner protons by deuterons. This observation, as well as the disappearance of splitting upon complexation with water or alcohol, was interpreted as evidence of coherent double hydrogen tunneling in a symmetric double minimum potential. Based on temperature dependent LIF excitation apectra of porphycene, the authors have also shown (Figure 1.9 c) that the "hot" 0‾ transition is red-shifted indicating greater tunneling splitting in the ground state than in the S_1 state.

High resolution optical spectroscopic study (LIF spectra) of porphycene doped in superfluid helium nanodroplets [101] showed tunneling splittings of 4.4 and 0.58 cm^{-1} for porphycene and monodeuterated porphycene (Pc-d_1), respectively, from LIF excitation spectral measurement. Dispersed fluorescence spectral measurement via excitation of the origin band revealed doublets for various vibrational modes, differing in the magnitude of the splitting and intensity distribution. The observed differences reflect different tunneling probabilities for the respective vibrational modes in the S_0 state. This picture was confirmed by theoretical studies based on Car- Parinello molecular dynamics simulations. [70] Notice that the hydrogen/deuterium exchange was done in the cavity NH hydrogens. The fact that the values of the ground-state splitting are much larger than those in the S_1 excited state indicates a higher energy barrier and/or a larger barrier width in the excited state than in the ground electronic state (Figure 1), a situation contrasting with most of the cases observed so far, whether intramolecular, like tropolone, or intermolecular, as in benzoic acid dimers. [44, 46] This hypothesis was confirmed by polarization spectroscopy measurements in condensed phases, carried out both in emission and transient absorption, which enabled determining the tautomerization rates in S_0 and S_1 for porphycene and several derivatives [88, 95, 102, 103]. The reaction rates in S_1 are several times lower than in S_0. Moreover, the values of the rates vary by four orders of magnitude (10^9-10^{13} s^{-1}) for differently substituted porphycenes. The isotope effects, measured at 293 K, are also substantial [94, 95]. These findings indicate the importance of tunneling, even at room temperature, and that of the overall symmetry on the process. In particular, in *meso*-alkylated porphycenes, the alkyl substitution leads to a decrease of the NH···N distance in the cavity, one of the key parameters in proton transfer dynamics. It has also been shown that the torsional modes of the substituents are coupled to the motion of internal protons, implying the multidimensional nature of tunneling [72, 90, 92]. Dispersed fluorescence spectrum obtained by excitation into the electronic origin band of porphycene revealed doublets for various vibrational modes, differing in the magnitude of the splitting and intensity distribution. The observed differences reflect different tunneling probabilities for the respective vibrational modes in the S_0 state. This picture was confirmed by theoretical studies, based on Car-Parinello molecular dynamics simulations. [70]

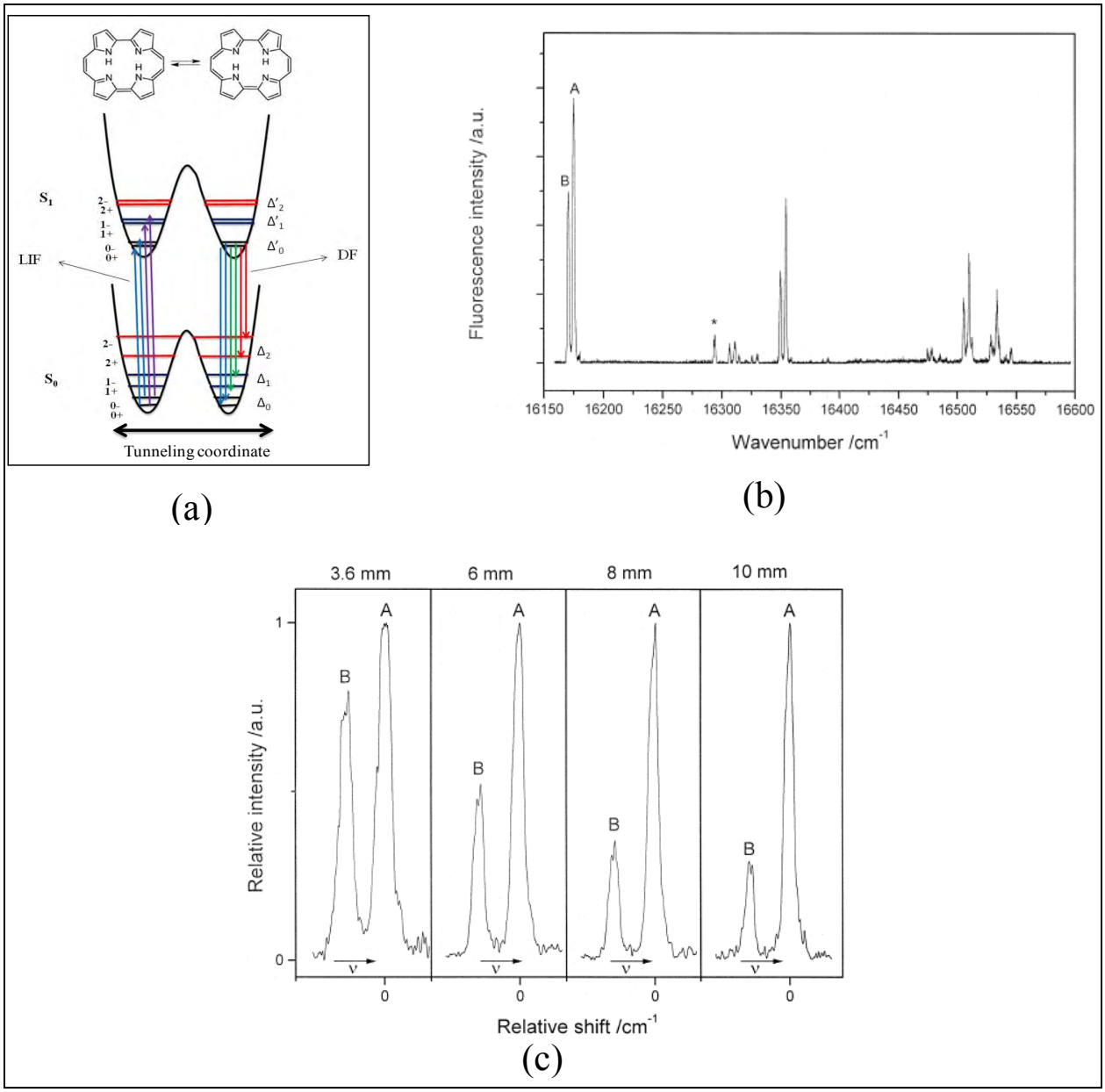

Figure 1.9 (a) Schematic cross section through the ground and excited state potential energy surfaces, (b) LIF excitation spectrum of porphycene in supersonic-jet and (c) laser-nozzle distance dependent LIF excitation spectrum of porphycene. The allowed transitions between tunneling levels are indicated by arrows. Throughout the text, we refer to the 0_-^- *transition as "hot band".*

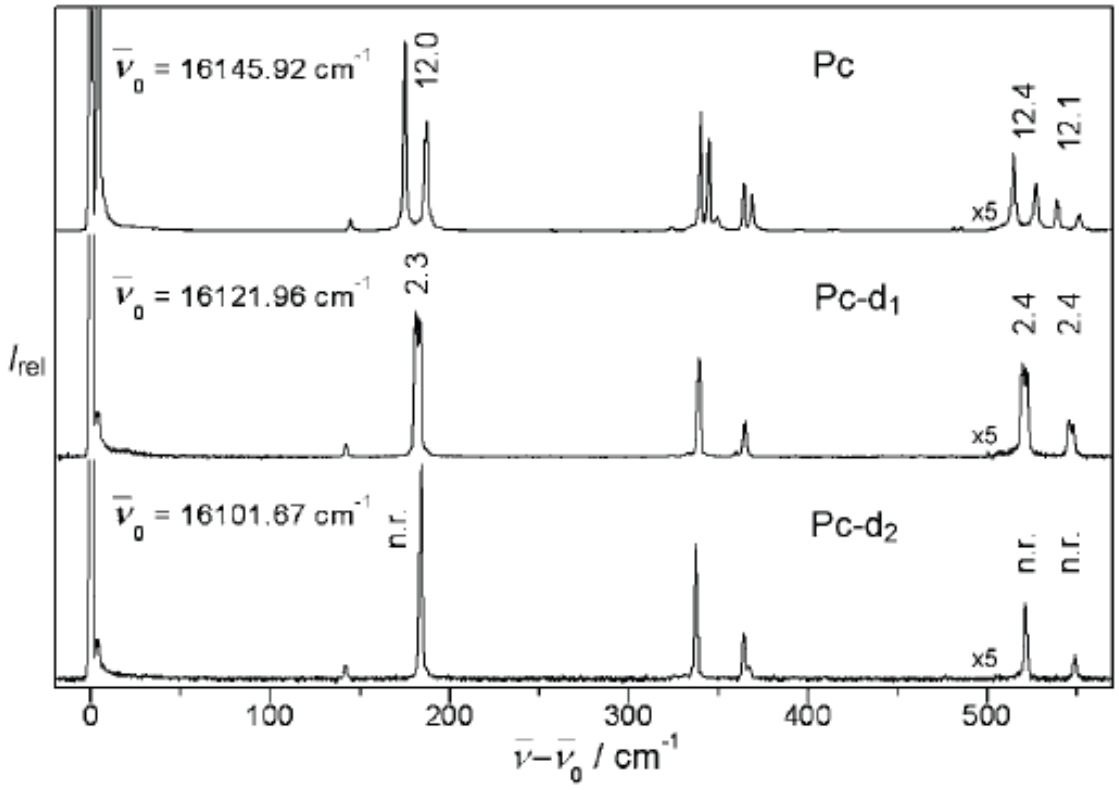

Figure 1.10 Emission spectra upon excitation at the respective electronic origin of Porphycene, singly deuterated porphycene (Pc-d_1) and doubly deuterated porphycene (Pc-d_2) in helium droplets (0.37K). The values of $\nu_0 = \nu_{exc}$ are given in each spectrum. The splitting values are indicated only for promoting modes and either given in units of cm^{-1} or assigned as not resolved (n.r).[101]

1.4 Objectives

The work presented in this thesis, along with previous studies, represents an effort towards a full and accurate characterization of the vibrational structure and proton tunneling dynamics of porphycene. The following objectives are intended to be addressed in this work.

1.4.1 Precise assignment of vibrations of porphycene both in the S_0 and S_1 states.

The first objective of the thesis is the precise assignment of vibrational modes both in S_0 and S_1 electronic states, since it helps to understand the pattern of mode coupling and hence dimensionality of hydrogen tunneling coordinate. This task is not trivial, not only due to the large number of fundamental vibrational mode in porphycene (108), but also because of the presence of tunneling splittings, different for various electronic and vibrational states. To overcome these difficulties, emphasis has been given to the analysis of LIF and single vibronic level dispersed fluorescence spectra of porphycene in supersonic jet. The fact that effective collisions, and hence random thermalizations, are highly prohibited in supersonic jet is exploited as an advantageto see fluorescence occurring from unrelaxed vibronic levels in the S_1 state, which can be used for precise assignments of vibrations, observation of mode-selective tunneling splittings, and the study of mode coupling.

1.4.2 Effect of selective excitation of low frequency modes on tunneling splitting

The second objective is to see the effect of vibrational excitation of low frequency modes on tunneling splitting. In this respect, I focused on the role of a low frequency mode of about 180 cm^{-1} both in the LIF and DF spectrum of porphycene in assisting proton tunneling. This mode was previously reported [101] to be the most promoting mode showing the largest tunneling splitting ($12cm^{-1}$) in the ground state of porphycene. However, its role could be explicitly assessed if one knows the value of tunneling splitting in higher quantum number of this mode. Fluorescence spectrum from a single vibronic level of a molecule is proved to be important in many cases in detecting the high vibrational levels of the ground state. I am intending to see the fluorescence spectrum via selective excitation of the fundamental and second harmonic of this mode. Of course, identification of the second harmonic of the mode is not trivial due to spectral congestion in that region. The same measurement will be undertaken for monodeuterated , Pc-d_1 (where one of the cavity NH hydrogen is substituted by deuterium) and doubly deuterated, Pc-d_2 (where both cavity NH hydrogens are substituted by deuterium) isotopologues of porphycene to see the isotopic effects. Following determination of the experimental values of tunneling splitting along the mode described above, I will model the process using two dimensional

potential energy surface, one along the tunneling coordinate and the other along the assisting coordinate. This will help me to predict the potential barrier and the extent to which the low frequency mode is facilitating the process. Further the value of the potential barrier will be compared with previous theoretical and experimental attempts.

1.4.3 Effect of weak structural perturbation: proton tunneling in per-deuterated porphycenes

Besides substitution of the inner hydrogen by deuteron (N-H/N-D), which has a dramatic effect on the tunneling efficiency as mentioned above, weaker perturbation can be brought about by hydrogen/deuterium substitution (C-H/ C-D) on the outer rim. The third objective will be therefore to study the effect of this weak structural perturbation on proton tunneling. Such a study will help us understand the importance of mode coupling between the motion of outer rim hydrogens with the tunneling coordinate, and effect of symmetry breaking (in the case of partially deuterated porphycenes) in influencing the proton tunneling path. In this case, laser desorption method combined with supersonic-jet were successfully applied.

1.4.4 Single vibronic level life time measurement in porphycene and Pc-d_{12}

Comparison of single vibronic level lifetime of porphycene and its deuterated isotopologue will reveal some dynamical information in the S_1 state. In this case, the dependence of the life times of each isotopomers on vibrational energy and symmetry of vibration will be explored.

1.4.5 Searching for N-H stretching band in Porphycene

Although harmonic calculations predict strong transition of the N-H stretching mode, experimental detection has been difficult in the past. In our case, two-color (IR/Visibe) experiments are applied to detect the N-H stretching vibration in porphycene.

1.4.6 LIF and DF spectra of selected porphycene derivatives

The last but not the least objective is the study of heavier derivatives of porphycene: 2,7,12,17-tetra-tert-butylporphycene (TTPC) and 2,7,12,17-tetraphenylporphycene (TPP0) in supersonic jet using laser desorption technique. In this case both the electronic structure and the potential energy surface will be strongly modified. And the consequence of these modifications on the tunneling path and mechanism will be explored.

Chapter Two

Experimental and Theoretical Methods

The experiments in this work include laser induced fluorescence (LIF) excitation, dispersed fluorescence (DF) and hole burning spectral measurements using one or two color excitation laser sources in a conventional heating or laser desorption based supersonic-jet setups. The measurements were carried out in two separate laboratories, one set of measurement in the Institute of Physical Chemistry Polish Academy of Sciences (**IChF PAN**), Warsaw and the other set in the Institut des Sciences Moléculaires d'Orssay (**ISMO**), France.

The size of Porphycene system precludes the use of correlated methods. Ground state geometry optimizations and frequency calculations were done within the frame of the density functional theory (DFT) at the B3LYP/6-31+ G(d,p) level. Time dependent DFT (TD-DFT) method was used for the excited state calculations with the same functional and basis set using the GAUSSIAN 09 program package. Indeed, this method has been shown to properly describe the $\pi\pi^*$ transition in related porphyrins.

2.1 Supersonic-jet Spectroscopy: Introduction

Spectroscopy allows study of the interaction of matter with electromagnetic radiation. It is arguably the most powerful experimental tool available for understanding molecular structure and dynamics.

Frequently the goal of spectroscopic study is the elucidation of intermolecular interactions that occur in solids, and of course in these cases the solid state is the sample of choice. In other cases, the goal of the experiment is to study those intramolecular properties that are only slightly affected by the solid matrix surrounding the molecule of interest. In these cases the solid sample , although not ideal, is still adequate. However, there are cases where the desire is the study of properties of the isolated molecule that are completely overwhelmed in the matrix by intermolecular interactions, and in these cases, the study must be carried out in the gas phase at lowest temperature consistent with adequate vapor pressure [104]. However, the low volatility of large molecules such as porphyrins requires high temperature in order to obtain sufficient vapour pressure [105,106]. This will result in a drastic thermal vibrational sequence congestion effects and inhomogeneous broadening where the typical line widths of electronic- vibrational transitions of large molecules are 100-1000 cm^{-1}. Therefore, the dual objectives of preparing an isolated gas

sample and of producing low internal temperature have been traditionally desired by spectroscopists.

The advent of supersonic-jet expansion comes to the rescue. The method allows the preparation of internally cold, isolated, gas phase molecules and thereby retains the advantage of solid state or matrix isolation spectroscopy without the disadvantage of overwhelming environmental interaction. One meaningful example is found from comparison of LIF spectra of porphycene in supersonic-jet [45] versus in argon matrix [107]. One could easily observe that the tunneling splitting in the 0-0 and 180 cm^{-1} ($2A_g$) mode of Pc observed in supersonic jet (see Figure 1.9 b) disappears in argon matrix (Figure 2.1) indicating interference of environmental effect with intramolecular processes.

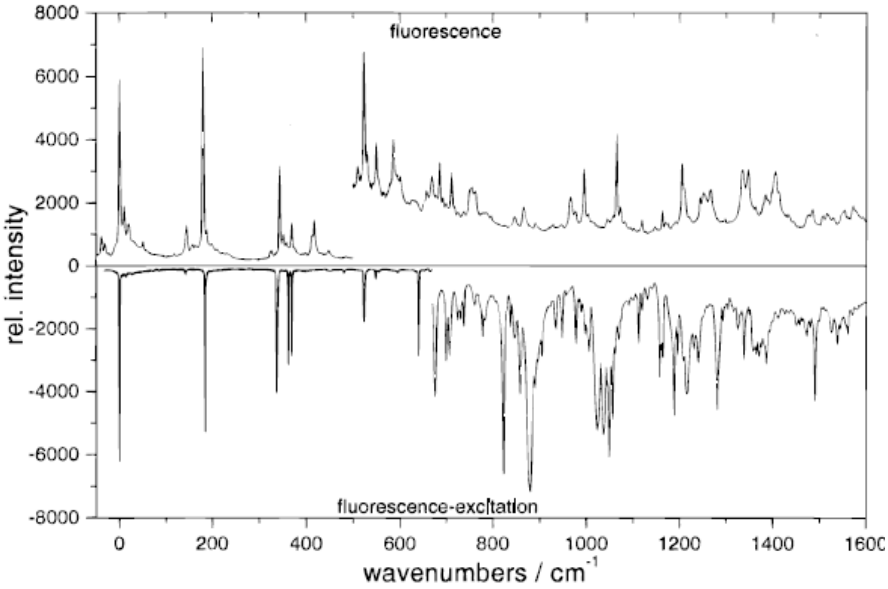

Figure 2.1 Site-selective fluorescence and fluorescence excitation spectrum of porphycene in argon matrix.

2.1.1 Principle of supersonic-jet expansion

In a supersonic free jet and molecular beams [104], molecules at moderately high pressures (usually in the range 0.7 to 100 atm) are expanded either neat or in a carrier gas through a small orifice (nozzle) or planar slit in to a region of relatively low pressure. The expansions cool the translational degrees of freedom of the gaseous mixture which creates a cold translational bath. This can significantly reduce the internal rotational and vibrational population distribution in

molecular species of interest. As the expansion progresses, the molecular concentration and thus collisional density decreases. Subsequently, the rotationally and vibrationally cooled molecules enter a collision free region where they can be spectroscopically probed with minimum of intermolecular interaction. The basic features of a free jet expansion are shown in Figure 2.2.

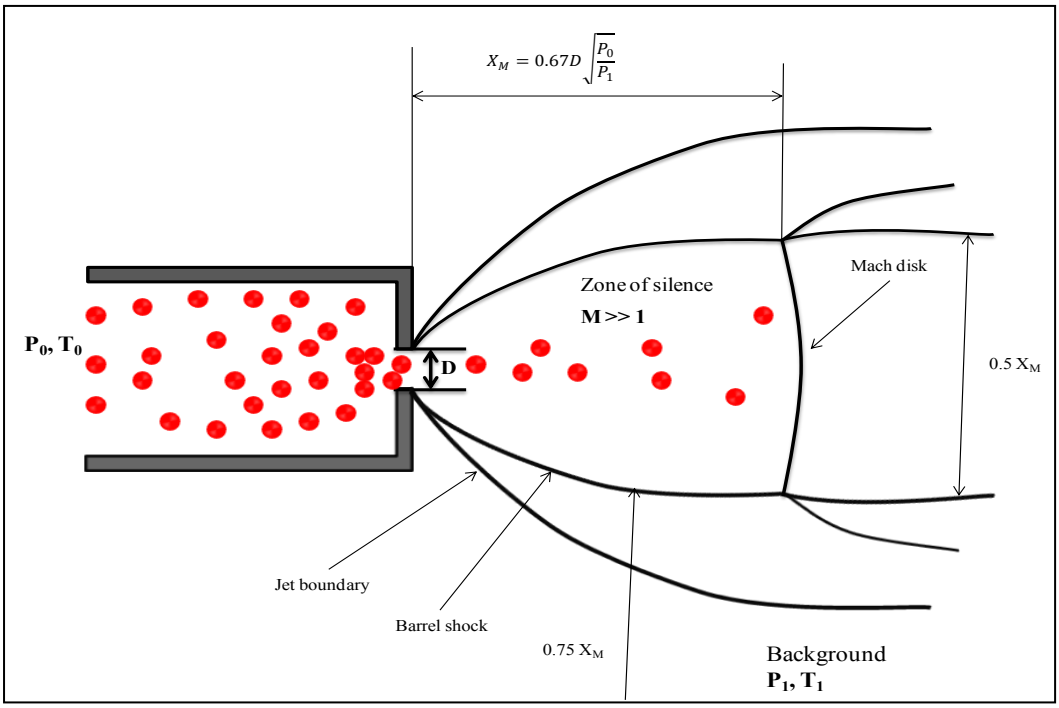

Figure 2.2 Schematic visualization of a continuous free jet expansion from a nozzle.

As the area of the nozzle decreases towards the exit, the pressure difference $(p_0 - p_1)$ will accelerate the carrier gas. If $\frac{p_0}{p_1}$ will be less than the critical value $G = \left(\frac{\gamma+1}{2}\right)^{\gamma/\gamma-1}$, where γ is the ratio of the heat capacities C_p/C_v, the flow will escape from the nozzle with a sonic speed (M= 1, Mach number (M) for the local speed of sound is given by v/a, v and a being the flow speed of the jet and sound velocity, respectively). On the other hand, if the ratio of pressures is less than the critical value (< 2.1 for all gases) a stream will exit from the nozzle with the speed lower than the speed of sound. In the last case, such an expansion to the low pressure region proceeds with relatively low number of collisions (mean free path, $\lambda_0 < D$, where D denotes the nozzle diameter) and not accompanied by the change in population distribution in the internal degree of freedom in the seeded molecules. Such an expansion with subsonic speed does not have the

previously described advantages of the supersonic expansion, which is very useful for spectroscopy [25,108].

A supersonic jet expansion is achieved if $\frac{p_0}{p_1} > G$ and $\lambda_0 << D$ and the pressure at the collision zone is independent of P_1 and is equal to $\frac{P_0}{G}$.

During the adiabatic expansion process, the molecules moving faster collide with the slower ones thereby decelerating the former and accelerating the latter. This results in a narrow velocity distribution. Such being the case, at low temperature the relative velocity between the molecules is low unless they collide with the wall of the vacuum chamber. However, there always exist a non-zero residual pressure in the vacuum chamber (P_1) due to some residual gases present inside the vacuum chamber and they are constantly shoved away by the expanding molecules. This results in the formation of a barrier of closely packed molecules, called the *Mach disk*. It is the edge of the cold zone, beyond which a large number of collisions occurs between atoms and molecules, thereby hindering the cooling process.

As shown in Figure 2.2 , the supersonic-jet is composed of various zones:

2.1.2 The collision zone

The collision zone is located at the exit of the nozzle (1-2 mm). The cooling of molecules and the formation of complexes occur in this zone. During a two-body collision, the carrier gas takes away the internal energy from the molecules of interest in the form of kinetic energy. As a result of undergoing collision, the molecules are said to be “cold”, with temperature in a range of a few Kelvins thereby indicating that only the lowest vibrational level (ν = 0) and a few rotational levels of the electronic ground state are populated [109]. In a similar three-body collision, the carrier gas makes the formation of a complex possible by carrying away the binding energy in the form of kinetic energy.

2.1.3 The silent zone

It is the isentropic region between the nozzle and the Mach disc, which cannot be penetrated by the residual gas atoms in the chamber. Here the isolated molecules move with the same velocity and in the same direction. It is in this zone where useful spectroscopic studies take place. It is also possible to skim the silent zone to take its most internal and hence coldest part.

2.1.4 The jet-boundary

It is the zone where the atoms of the carrier gas enter in to collisions with residual gas molecules or atoms present inside the vacuum. This boundary layer protects the zone of silence.

2.1.5 The Mach disk

It is the outer limit of the zone of silence located at a distance X_m from the nozzle. The distance from the nozzle to the Mach disk , X_M , is expressed by:

$$X_M = 0.67D\sqrt{\frac{P_0}{P_1}} \quad \text{..... (2.1)}$$

Where P_0 and P_1 are the pressures of the gas in the nozzle and in the vacuum chamber, respectively and D is the nozzle diameter.

The Mach disk and barrel shock diameters (see Figure 2.2) are approximately $0.5X_M \pm 25\%$ and $0.75X_M \pm 25\%$, respectively.

If one considers an ideal gas expansion, neglecting the effect of heat condution and viscosity, then the first law of thermodynamics can be used to estimate the changes in molecular denisty with distance, R from the nozzle. For Expansion with constant γ:

$$\rho = \rho_0 \left(1 + \frac{(\gamma-1)}{2} M^2(R)\right)^{-\frac{1}{\gamma-1}} \quad \text{..... (2.2)}$$

With such an approach molecular density, ρ depends only on initial density, ρ_0 and Mach number M(R), which itself depends on the distance from the nozzle. On sufficient distances (R/d>10) the jet can be approximated as a spherical expansion from a point source and the Mach number can be evaluated as:

$$M(R) = A\left(\frac{R}{D}\right)^{\gamma-1} - \frac{{}^{\gamma+1}/_{\gamma-1}}{2A({}^{R}/_{D})^{\gamma-1}} \approx A\left(\frac{R}{D}\right)^{\gamma-1} \quad \text{..... (2.3)}$$

Where for monoatomic gases γ=1.67 and A= 3.3

For closer distances (R/D<3), the approximation does not work and the following approximation should be applied:

$M(R) = 1 + A\left(\frac{R}{D}\right)^1 + B\left(\frac{R}{D}\right)^3$, where for ideal gases A remains the same as the previous equation and B = -1.541. [110]

2.1.6 *The valve*

The use of continuous supersonic molecular beams has been limited by the cost and complexity of the required vacuum systems. In addition, the maximum achievable density of a continuous molecular beam has been kept relatively low since it is limited by the pumping capability of vacuum systems. The use of a pulsed molecular beam source can overcome the above limitations to a large extent and the physical dimensions of the source of the molecular beam can be reduced. This reduction of system complexity makes the pulsed valve production quite attractive [111]. Pulsed nozzle supersonic jets have also been developed resulting in higher jet densities, better ro-vibrational cooling and less condensation relative to the corresponding continuous expansions. In addition, pulsed nozzle supersonic jets reduce stress on the pumping system required to sustain the supersonic expansion and are especially useful when corrosive gases are present in the expansion [25].

The disadvantage of such nozzles is that they have movable mechanical components which must be maintained and which place practical limitations on the valve pulsing frequency. Moreover, the need of synchronization of the valve with the light source gives additional complication.

The pulsed nozzles for supersonic expansions are now well established and various designs are also available to meet specific requirements. More elaborated discussions on the development and design of pulsed valves could be found in ref [25,111]. In the present work, the modified pulsed valve, General Valve Series 9, was used. The modification was done in our laboratory (IChF PAN). Figure 2.3 shows the schematic design of the pulsed valve used in our experiment. The valve is modified to heat samples to a temperature as high as 300^0C.

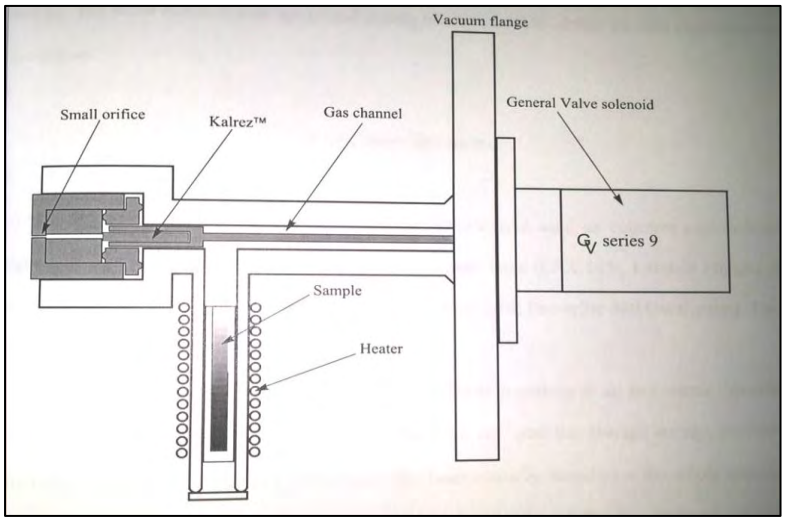

Figure 2.3 Schematic drawing of the modified "General Valve Series 9" pulsed valve.

Selenoid body was mounted on the massive metal flange to provide sufficient heat conductivity. Standard piston was replaced by the long metal needle. At the end of the needle a piece of high temperature resistant Kalrez ^{TM} was mounted which provided precise and seal closing of the orifice. The nozzle was operating with a repetition rate of 10 Hz with a pulse duration of 150-700 μs. The pulse duration was optimized during the measurement to obtain the best experimental conditions.

2.2 Optical detection

The optical system for signal detection in the supersonic-jet setup was constructed by dr. Jan Jasny. The schematic design is illustrated in Figure 2.4

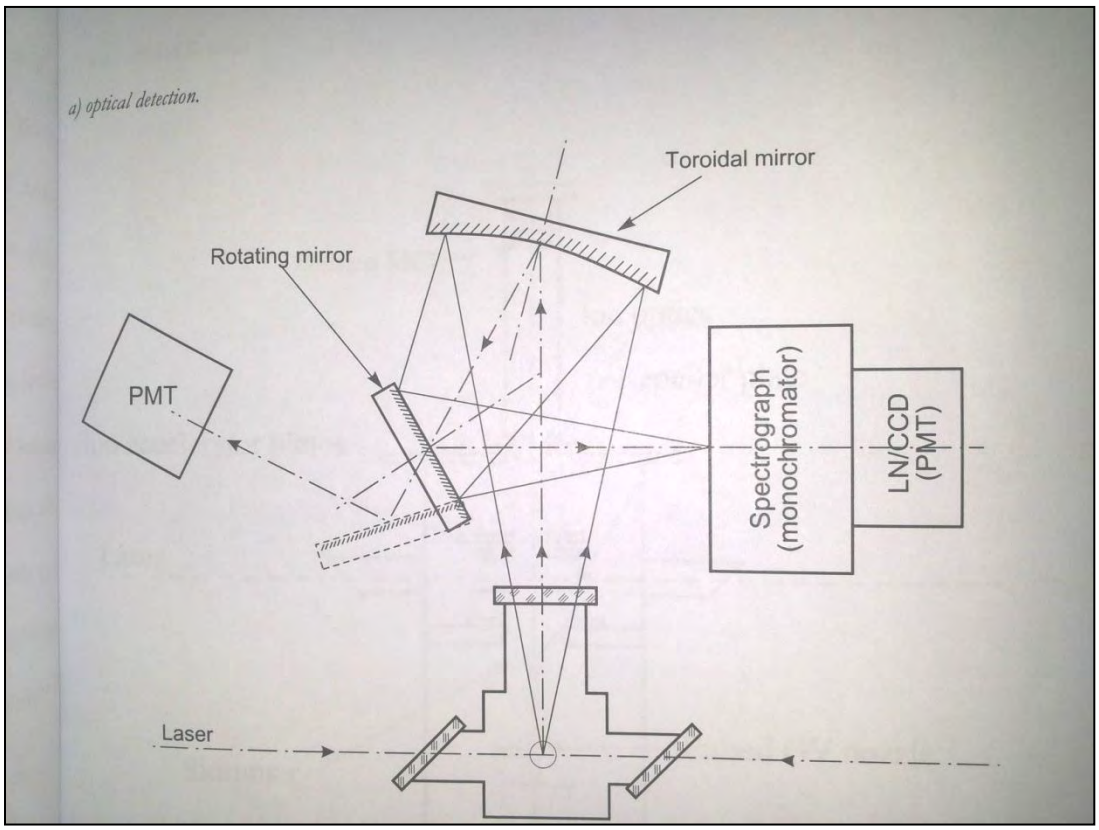

Figure 2.4 General scheme of the optical layout of the detection system. was constructed by dr. Jan Jasny of the Institute of Physical Chemistry, Polish Academy of Sciences (IChF PAN).

The detection system consists of a torroidal mirror, which serves as f/l optics and images the fluorescence on to the photomultiplier or monochromator slit. The rotating mirror allows a quick switching between the photomultiplier and the spectrograph/monochromator. The LIF excitation spectrum was detected by a Hamamatsu R2949 photomultiplier using a BG 645 cutoff filter to reduce scattered light signal. Dispersed fluorescence spectrum was measured using a 0.5 m monochromator (Sciencetech 9040), fitted with 1800 groove/ mm diffraction grating, attached to a CCD (Andor iDUS) camera. The system designed in this way allows to minimize the background signal from the scattered light and to improve the signal to noise ratio.

2.3 Conventional heating/Laser desorption based gas sample sources

In a conventional supersonic-jet spectroscopic set up, the molecules under study are often seeded in the carrier gas at a concentration of a few percent by evaporating the solid sample contained in an oven prior to the expansion. However, this technique is not always convenient when working with high molecular weight and/or fragile compounds. The reason for that might be two fold. On one hand, the sublimation point of these molecules may be very high and the valve will become unstable (limited to work up to 530 K in the case of General valve series 9) and hence proper production of the jet will be interrupted. On the other hand, the probability that the sample might be decomposed or modified due to side reactions increaseas, as it is exposed to high temperature in a furnace for long time. In such cases, the technique of choice will be laser desorption where a plume of ablated molecules are introduced directly in the collision zone by a “pick up” process.

2.3.1 Principle of laser ablation of molecules

The use of laser light allows to transfer fragile or high molecular weight (ranging from hundreds to hundreds of thousands atomic mass units) compounds from the condensed phase in to the gas phase with virtually no accompanying decomposition. The process is usually partitioned in to two, laser desorption molecules and laser ejection of molecules from a matrix. The division lies in the fact that laser desorption is rationalized using thermal models while laser ejection from a matrix is primarily a non thermal process. These two divisions are shown schematically in Figure 2.5 a and b.

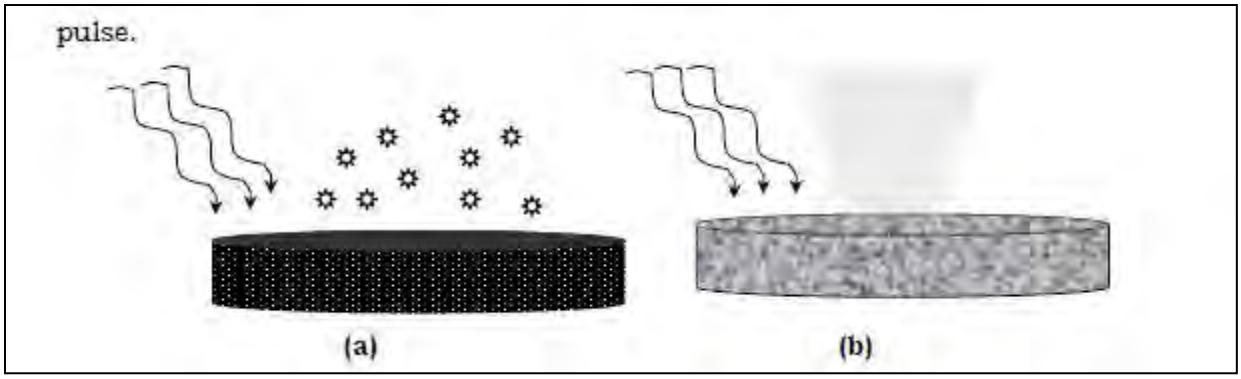

Figure 2.5 Schematic representation of (a) Thermal laser desorption of a substrate and (b) Non-thermal laser ablation of a homogeneous substrate adsorbate mixture. [110, 112]

Phenomenologically, laser-induced thermal desorption typically occurs from a neat film adsorbed on a light absorbing substrate, and monolayer or lower quantities are often desorbed by the heat generated at the surface. In laser ejection of molecules from a matrix, many monolayers are ejected per pulse, perhaps via an explosion like process.

The essence of laser methods to transfer molecules in to the gas phase relies on rapid energy deposition in to a condensed phase system [113]. The process of energy deposition is fast enough to assure that desorption or ejection occur before decomposition. The lasers used to deposit this energy vary widely in terms of pulse width (CW to fs), irradiance (50 kW to 100MW), and wavelength (151 nm to 10.6 μm). The molecular desorption process results from the extremely high heating rate present, $10^{10\pm2}\,K/s$. Such heating rates lead to a number of possible mechanisms for laser induced thermal desorptions that are described by kinetic, restricted energy transfer and collisional cooling models.

2.3.2 Mechanism of laser induced thermal desorption

Three mechanisms are primarily responsible for the ability to transfer a molecule from condensed phase into the gas phase using laser induced thermal desorption. The three mechanisms results from the high heating rates inherent in the laser desorption process. Typical heating rates range from 10^8 to $10^{13}\,Ks^{-1}$ and depend on laser pulse energy density and absorption cross-sections [114,123].

The first mechanism involves the kinetics of desorption and decomposition at extremely high heating rates [124-131]. In this model, the process with the highest pre-exponential factor becomes the major reaction channel at high enough heating rates to high enough temperatures regardless of the respective activation energies.

The second mechanism involves the efficiency of energy transfer during laser desorption [132-136]. A theoretical model based on vibrational energy transfer suggests that the efficiency of energy transfer is low during the desorption step for weakly coupled adsorbate surface systems.

The last mechanism, perhaps of less importance, is the effect of post-desorption collisions on the internal energy distributions of the desorbing species [137-143]. Both experimental and theoretical evidences suggest that post-desorption collisions serve to cool the internal energy and increase the translational energy distributions as well as sharpen the spatial distribution of the desorption products.

2.3.3 Kinetics of laser desorption

If the heating rate is high enough (10^8 to $10^{11}\ Ks^{-1}$) and the temperature excursion is large enough, molecular desorption can be obtained on a time scale that is short compared to many surface reactions [124]. Such heating rates allow energetically unfavorable reactions to be accessed by entropic means. Thus, even though the activation energy for desorption may be higher than that for decomposition, as long as the pre-exponential term in the rate expression is larger, the desorption reaction can be favored. A number of researchers have employed this model to rationalize molecular desorption of adsorbates which would otherwise decompose on the surface [127-130].

The physical principle behind the kinetic mechanism for molecular desorption in laser-induced thermal desorption can be understood using the Polanyi-Winger model [141] for the desorption rate. The rate expression for an adsorbate given a desorption and a reaction channel can be written as:

$$\frac{d[\theta]_{des}}{dt} = [\theta]^n_{ads} \,.\, \nu_{des}.\ exp\left[-\frac{E_{des}}{RT}\right] \text{..... (2.4)}$$

$$\frac{d[\theta]_{reac}}{dt} = [\theta]^n_{reac} \,.\, \nu_{reac}.\ exp\left[-\frac{E_{reac}}{RT}\right] \text{.....(2.5)}$$

Where equation 2.4 describes the rate for desorption given the energy barrier for desorption E_{des}, the frequency factor ν_{des} and the adsorbate coverage $[\theta]_{ads}$, the gas constant R and temperature T. Equation 2.5 describes the rate for the formation of surface reaction (decomposition) product in terms of the energy barrier for the reaction, E_{reac} , and the frequency factor, ν_{reac}.

For a given surface desorption process, the barrier for desorption can exceed the barrier for decomposition. However, the pre-exponential frequency factor for desorption often exceeds that

for decomposition because of steric and/ or entropic reasons. To determine the branching ratios and the total number of product channel molecules, the rate equation must be integrated as a function of the heating rate by using the appropriate kinetic parameters. Hall [124] gives the function necessary for this integration as:

$$N_{react} = \int_{t=0}^{\infty} \int_{r=0}^{\infty} [\boldsymbol{\Theta}(t)].\nu.exp\left[\frac{-E_a}{RT_{(r,\ t)}}\right].2\pi.dr.dt \quad \text{..... (2.6)}$$

Where t is the time after the laser fires and r is the radial distance from the centre of the laser spot.

From the integration which uses the kinetic constraints described previously, one observes that at sufficiently high heating rates, the desorption rate can exceed the decomposition rate by many orders of magnitude.

2.3.4 Energy transfer during laser-induced desorption process

As seen in the previous section, the temperature of the surface can approach thousands of degrees K, but fragile molecules can still be desorbed intact. Another model based on relatively long vibrational relaxation time has been put forth by several investigators to account for molecular desorption. In a simulation of laser desorption of isolated NO from LiF [125]. Lucchese and Tully [132] found that all degrees of freedom of the gas phase NO were considerably less populated than expected from the surface temperature. This non equilibrium distribution was attributed to the rapid, $10^{15}\ Ks^{-1}$, temperature jump to 2000 K. The results of this study suggested that the vibrational temperature was coolest (209 K), followed by the rotational temperature (302 K). The normal translational temperature was the warmest (638 K) but was still a factor of three from the mean surface temperature upon desorption (1900 K). Three models were proposed to account for the observed energy deficit: (i) energy was employed to surmount the attractive well of the NO bond to the surface, (ii) the molecules were desorbed before the maximum surface temperature was attained, and (iii) there is incomplete equilibration of the thermal energy due to differing relaxation times.

To illustrate mechanism (iii), the investigators point out that to transfer one quanta of vibrational energy at 1904 cm^{-1} to the highest energy phonon band of the substrate at 600 cm^{-1} would require 10 ns [133], while the transfer of one quantum of rotational energy would require < 1ns, and the transfer of translational energy should proceed at gas kinetic rates. Thus, because vibrational energy transfer requires the most time, it is the least populated in the pulsed laser desorption experiment. Further evidence for this model was obtained by varying the vibrational frequency of the NO in the simulation. Lowering the frequency from 1904 to 1000 cm^{-1} produced an increase in the vibrational temperature of the desorbed NO from 37 K to 209 K.

In an attempt to quantify this model, Zare and Levine [134] developed an expression based on the adiabaticity parameter ξ, commonly referred to as the bottle neck model. In essence, the critical parameter for energy transfer from one vibrational mode, such as the surface adsorbate bond having frequency ν, to another vibrational mode, such as an internal vibration in the adsorbate having frequency ν', is the mismatch of the vibrational frequencies and the time allowed for energy transfer, τ. The adiabaticity parameter is derived from gas-phase energy transfer concepts [135]. For the case of energy transfer through the surface adsorbate bond, the adiabaticity parameter is defined as:

$$\xi = 2\pi\left(\frac{\nu'}{\nu}\right) \quad \text{.....(2.7)}$$

To determine the amount of energy transferred through the surface adsorbate bond, a kinetic energy for energy transfer is written as

$$\frac{\partial E}{\partial t} = \frac{dE_0(t)}{dt} - kE(t), \quad \text{.....(2.8)}$$

Where $E_0(t)$ is the initial energy found in the surface adsorbate bond, $kE(t)$ is the quantity of energy flowing in to the adsorbate's internal vibrational mode and $\frac{dE}{dt}$ is the quantity of energy remaining in the surface adsorbate bond.

The rate constant for energy flow in to the adsorbate's vibrational mode is:

$$k = \nu \exp(-\xi) \quad \text{.....(2.9)}$$

When integrated, equation 2.8 provides the amount of energy lost at time τ:

$$E(\tau) = D_0(1 - k\tau) \quad \text{.....(2.10)}$$

Where the E_0 has been set to the bond dissociation energy, D_0.

If $k\tau$ is small ($k\tau < 1$), no energy transfer in to the internal mode of the adsorbate. Thus, one finds that the criteria for desorption of internally cold molecules is :

$$\nu\tau < \exp(\xi) \quad \text{.....} \quad (2.11)$$

The theory predicts that if the product of the surface adsorbate bond frequency and the interaction time is less than the quantity exp (ξ), then little energy will flow from the surface adsorbate bond in to the internal modes of the adsorbate. A key issue for this model is the residence time of an adsorbate on the surface during the laser induced thermal desorption experiment. If the measured residence time is less than the time scale for vibrational energy transfer, molecules can desorb intact after laser-induced thermal desorption [136].

2.4 The working laser desorption setup

In our experiment, the samples were introduced into the gas phase using a home-made desorption device. The sample was prepared by brushing a few mg of porphycene on a 4 cm long and 0.5mm wide carbon bar. With this technique, we were able to work with small sample quantities, about 0.25 mg/hr of desorbed matter. A frequency-doubled Nd:YAG laser (532 nm) (Continuum Minilite) was used as the desorption source. The beam was propagated by an optical fiber to the surface of the carbon bar with 1.5 to 2 mJ energy per pulse. The sample holder was fixed on a linear translation system, with a translation speed of 1 cm/hour, attached to a pulsed valve (General Valve- Parker) with a nozzle diameter of 300 µm.

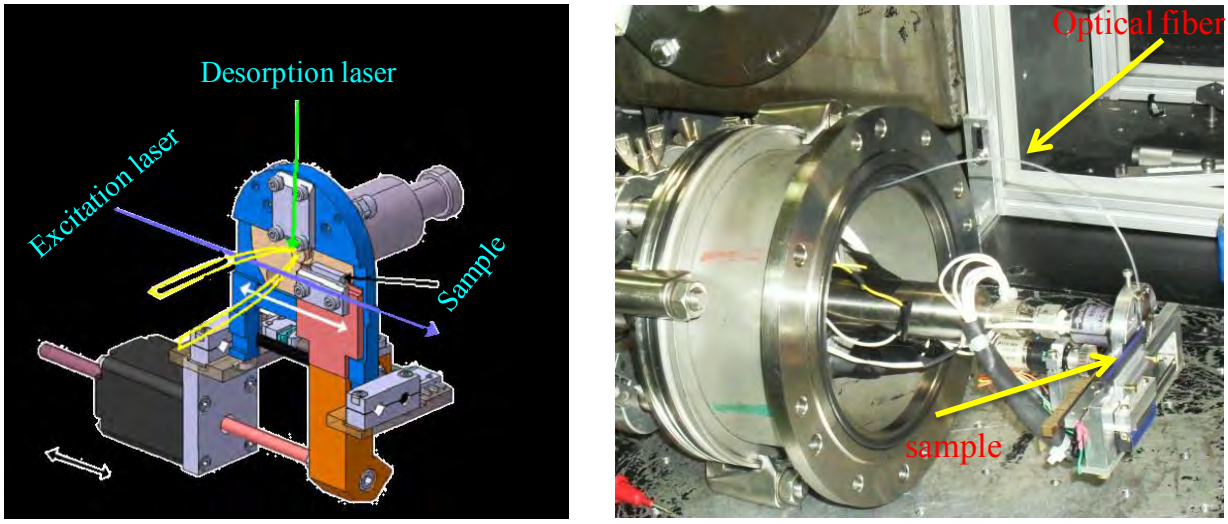

(a) (b)

Figure 2.6 (a) Schematic representation of the laser-desorption set up and (b) a digital phototgraph of the setup used in the experiment.

2.4.1 Optimization of the ablation system

The ablation system used before my arrival in Orsay laboratory was composed of a mount holding the sample at about 0.5 mm from the nozzle. A green light from Nd:YAG laser was captured by an optical microscope objective and focused to an optical fiber which was fixed at about 0.5 mm from the nozzle, opposite the sample. The optical fiber has four layers as shown in Figure 2.7. The glass core of about 10 cm was pealed and fixed above the nozzle. But it was

extremely difficult to stripe the inner thinnest membrane away and when it was possible the exposed glass fiber is so fragile (brittle) that it was not easy to put in and take out the flange in to the vacuum chamber. Thus instead we keep the thin layer and fix it to the nozzle (of course we exposed the glass core only at the tip where it faces the sample and this was quite easy). In doing so, we maintain the flexibility of the optical fiber..

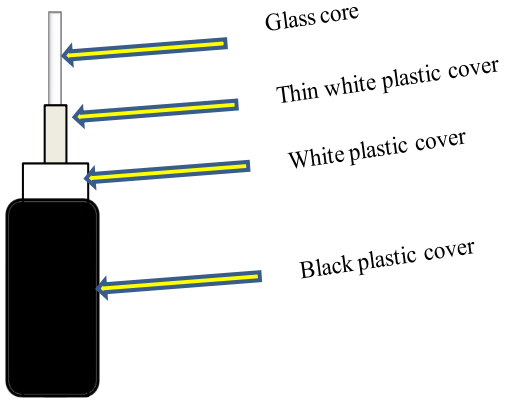

Figure 2.7 Scheme of the side view of the optical fiber.

Since the sample is exposed to strong laser pulse for a long period of time, a hole would be dug in to the pellet which might lead to inefficient gas sample production. This is why the mount was fixed on a motor allowing fast back and forth translation (speed of 1-3 cm/s). In the previously-used ablation system the sample was prepared as a pellet (30% sample and 70% carbon) pressed by a KBr pellet press at about 3 tons. This sample can be used for several weeks; it only requires to be flattened with sand paper every day to offer a fresh surface to the ablation laser. However, it takes plenty of samples to be made (about 400 mg) which is not convenient for our situation where we have < 10 mg of each porphycene derivatives.

The new ablation system uses remote controlled motor at much lower speed, of the order of 1cm/h, and a mount on which a rectangular rod of carbon is mounted (Figure 2.6). The sample is then introduced by forming a thin layer of the substance on the carbon rod. In this arrangement, one could easily control the extent to which a single spot on the pellet is exposed to the laser pulse by adjusting the speed of the motor. It was thus possible to avoid formation of deep hole on the carbon rod. Moreover, it was possible to expose fresh sample to be desorbed as the sample is constantly shifting perpendicular to a fixed desorption laser during the whole spectral measurement.

Because the ablation system was new, it was necessary to optimize the experimental conditions to get the best fluorescence emission signal. We have used naproxene [144a] and hydroquinine [144b] as test samples since their spectra in this supersonic jet setup is well characterized.

2.4.2 Sample preparation

The sample was first prepared by forming a thin layer on the carbon rod after wetting the top of the rod with ethanol. In such procedure (along with optimization of other parameters explained later) we had a reasonable signal, though its stability was not lasting long enough. This procedure might not be "so convenient" because if we are dealing with samples that could potentially form stable complexes with ethanol, we might misinterpret the signal from the complex to be that of a bare molecule [145]. After having the signal for naproxene (our favorite standard), the LIF spectrum of naproxene was measured in the 0-0 region as a function of speed of the motor. The results are presented in figure 2.8.

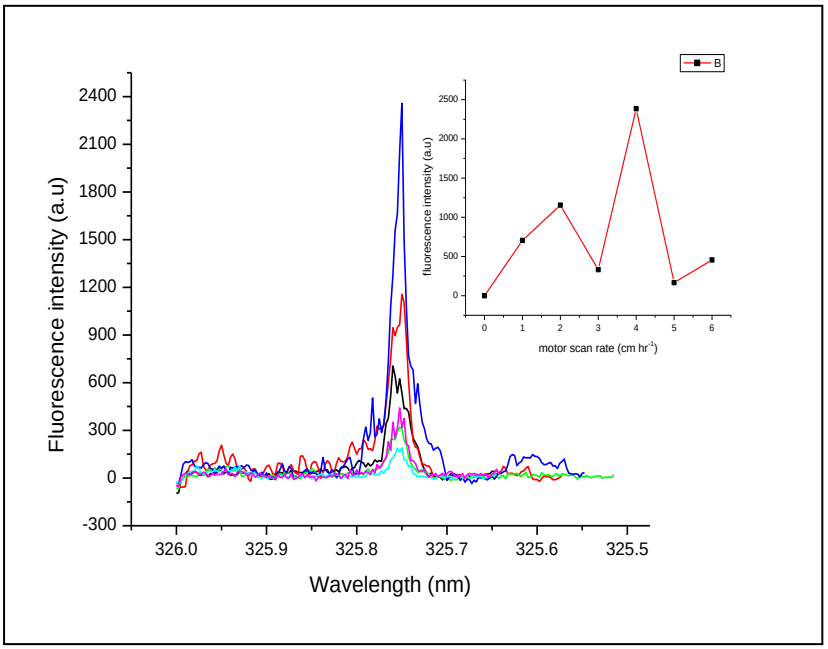

Figure 2.8 LIF spectrum of naproxene near 0-0 region as a function of the speed of ablation motor. Valve delay= 434 µs, minilite 824.39 µ sec, Sirah 844.67 µs. The inset shows the value of intensity maxima at different translational speeds of the pellet pasted with the test molecule.

As shown in the figure the best signal is obtained at 4 cm hr^{-1}. It is reasonable that higher motor speed the ablation laser encounters fresher sample (as long as the sample forms a uniform layer on the carbon rod). But high speed of the motor is also a disadvantage in that we cannot use the

sample for long time as the length of the rod is only about 4 cm. Therefore,a speed of 1cm/hr was preferentially used in the experiment.

We have also tried to prepare a layer of sample on the carbon rod without wetting the pellet. Instead we crushed the sample with a mortar to produce fine powder and the rod is gently brushed against the fine powder. This procedure produces a layer with much better uniformity and the fluorescence signal was much better both in terms of intensity and stability even at 1cm hr^{-1} speed of the motor. With this procedure the sample could last up to 5 hrs.

In all measurements we have used Ne as a carries gas (5atm stagnation pressure). The diameter of the nozzle was 300 μm and the valve opening time range from 260-280 μ sec.

2.5 Spectroscopic detection of samples

In our experiments, four different kinds of measurements, laser induced fluorescence excitation (LIF) spectrum, single vibronic level dispersed fluorescence (SVLF) spectrum, hole burning (active base line subtraction method), and single vibronic level life time measurements have been carried out. In this section I will explain the principles behind each measurement.

2.5.1. Laser Induced Fluorescence excitation (LIF) spectrum

LIF excitation spectrum is obtained by monitoring changes of total fluorescence intensity as a function of excitation wavelength. Therefore, it is basically the measurement of the electronic absorption spectrum of a molecule in the jet. But one should notice that the fluorescence excitation spectrum could not be identical with the absorption spectrum if the fluorescence quantum yields are not identical for different vibronic transitions. This measurement is important to probe the vibronic states of the molecule in the excited state. Figure 2.9a shows the schematic representation of the principle of LIF excitation spectrum.

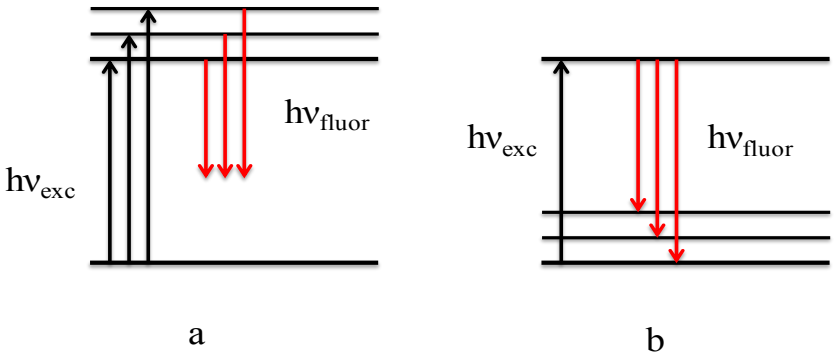

Figure 2.9 Schematic representations of (a) Fluorescence excitation spectroscopy and (b) dispersed fluorescence spectroscopy

2.5.2. Single Vibronic Level dispersed Fluorescence (SVLF) spectrum

In dispersed fluorescence, the fluorescence originating from a particular excited state of a molecule is dispersed by a monochromator and the distribution of energy as a function of wavelength (wavenumber) is detected by a CCD camera. As shown in fig 2.9b. a molecule excited in a specific vibronic level undergoes transition to different vibrational levels in the ground state. Hence this measurement provides information about the ground state vibrational structure of a molecule. Dispersed fluorescence spectrum from a single vibronic level also provides information complementary to the excitation spectrum. It maps the overlap of the nuclear wave functions of the excited and ground electronic states and hence such measurements are essential for precise assignment of vibrational levels both in the ground and excited states.

2.5.3. Spectral "hole burning" (active baseline subtraction)

Spectral "hole burning" (also called two color laser depletion) is a pump probe technique where a pump laser is fixed at a wavelength resonant with an electronic transition of a selected species while scanning with the probe laser. The measurement is done with the pump laser on and off using a shutter at each step of the scan, which results in two LIF excitation spectra (a so-called active baseline procedure). Because the fluorescence intensity is proportional to the number of ground state species, it decreases for the selected species after pumping. Since the time for total recovery of the initial ground state population is usually long (>1 μs), lowering of the intensity of vibronic bands belonging to the selected species is observed, while the intensity of the bands belonging to the other species are unaffected by the pumping process.

2.6 Coherent Light Sources

Optical parametric oscillator (OPO) and Tunable dye Lasers had been used as monochromatic excitation light sources during the experiments.

2.6.1 Optical Parametric Oscillator (OPO)

The operation principle of OPO is based on the parametric interaction of the strong pumping wave $\boldsymbol{\omega_p}$ with molecules in a media (crystal in this case), which has a large non-linear susceptibility. This phenomena can be illustrated as an inelastic scattering of the pump photon $\boldsymbol{\omega_p}$ by a molecule where pumping photon is absorbed and two new photons $\boldsymbol{\omega_s}$ (signal frequency) and $\boldsymbol{\omega_i}$ (idler frequency) are generated. Two main conditions have to be fulfilled to start parametric oscillation:

i) The phase matching condition $\boldsymbol{k_p = k_s + k_i}$, which may be regarded as the conservation of momentum for the three photons elaborated in the parametric process.

ii) Conservation of energy at all points of the active media $\boldsymbol{\omega_p = \omega_s + \omega_i}$

The phase matching condition selects infinite number of waves $\boldsymbol{\omega_s + \omega_i}$ and only single pair $\boldsymbol{\omega_s, k_s}$ and $\boldsymbol{\omega_i, k_i}$ is determined by the orientation of the non-linear crystal with respect to $\boldsymbol{k_p}$. If nonlinear crystal is placed inside an optical resonator, oscillations on signal and idler waves can start when the gain exceeds the total losses.

In this work, a narrow band (< 0.1 cm^{-1}) optical parametric oscillator (OPO, Sunlite Ex, Continuum) pumped by a seeded Nd:YAG laser (Powerlite 8000, repetition rate 10Hz) was used as an excitation source for LIF and DF spectral measurements. This set up covers a spectral range of 440-1800 nm.

An Optical parametric oscillator/ amplifier (OPO/OPA) (Laser Vision) has been used as a tunable IR source as a pump laser during IR/Vis double resonance experiment. This system, shown in Figure 2.10 , is an integrated, multistage nonlinear device designed to convert the fixed frequency output of an unseeded Nd:YAG laser in to tunable radiation in the mid infrared. The system produces an output that is tunable from 710 to 885nm and from 1.35 to 5 μm using a set of nonlinear crystals from the combination of a 532 nm pumped OPO and a 1064 nm pumped OPA.

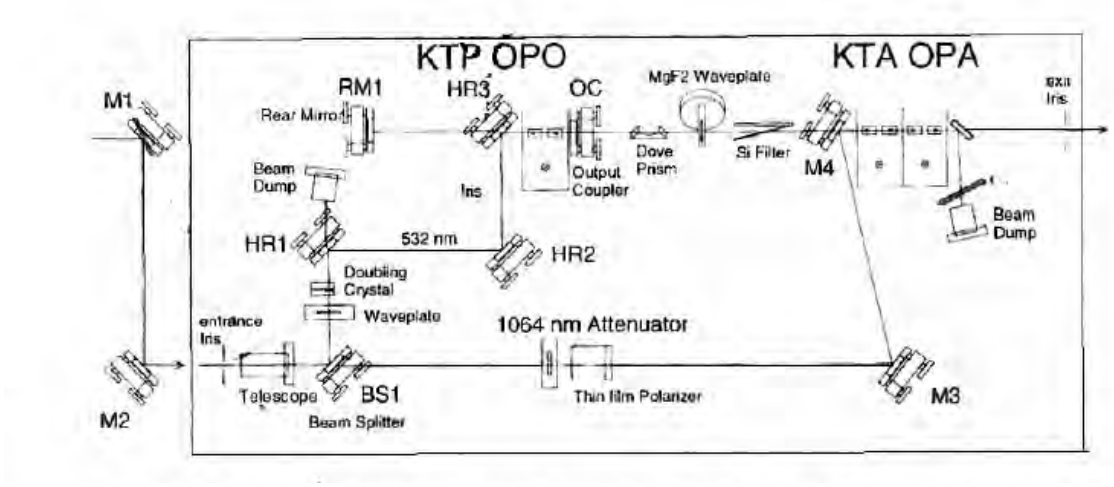

Figure 2.10 Layout of Laser vision Parametric Oscillator and Amplifier used in this work (taken from reference 110).

2.6.2 Tunable dye Laser

A tunable dye laser (Sirah equipped with Rh6G) pumped by the second harmonic of a Nd:YAG laser (Quanta Ray, Spectra Physics) was used as an excitation source for the experiments in Orsay. On the other hand, a homemade dye-laser (Rhodamine B in methanol) pumped by the second harmonic of a Nd:YAG laser (Surelite I-10, continuum) was used as a pumping source for two-color experiments in Warsaw . The typical resolution of both dye lasers was < 0.2 cm^{-1}.

2.7 Samples and reagents

The synthesis and purification of porphycene has been described in reference [22]. Pure sample of porphycene was kindly provided by Dr.Sylwester Gawinkowski (PhD).

For isotopic studies, the deuteration of the inner NH hydrogen atoms could be achieved during interaction of the Pc with heavy water (or MeOD) seeded in carrier gas (He or Ne).

Deuteration of rim hydrogen atoms: Perdeuteration of the outer rim hydrogen atoms was achieved by the procedure described in ref 99. Briefly, Pc was heated to 150^0C in 70% D_2SO_4 in D_2O for 24 hours and chloroform was added to the cold solution before being neutralized with diluted $NaOD/D_2O$. Finally, the organic layer was concentrated. The mass spectrum of the deuterated product proved that it contained 31% of Pc-d_{12}, 24% of Pc-d_{11}, 17% of Pc-d_{10}, and 11% of Pc-d_9, while the other isotopomers contributed in negligible amounts (Figure 2.11). The dominant contribution of Pc-d_{12} over other isotopomers was encouraging for us to study this heterogeneous sample, called hereafter Pc-$d_{mix.}$

Following the synthesis of Pc-d_{mix}, we measured LIF excitation spectra in a supersonic jet where the sample was heated in a furnace at about 230^0C to produce gas samples (Figure 2.12).

Successive LIF excitation spectra measured under the same experimental condition were found to be irreproducible. This problem was associated with the exposure of the sample to high temperature for a long period of time during which the deuterium atoms on the ring are back hydrogenated by traces of water impurities in the carrier gas. This back reaction results in the formation of several partially deuterated species at the expense of the fully deuterated sample with relatively close absorption lines. As a result, a systematic decrease of the narrow band at 617.4 nm assigned to Pc-d_{12} was observed. To avoid this effect, new measurements based on laser desorption technique have been undertaken, using a homemade desorption device in Orsay.

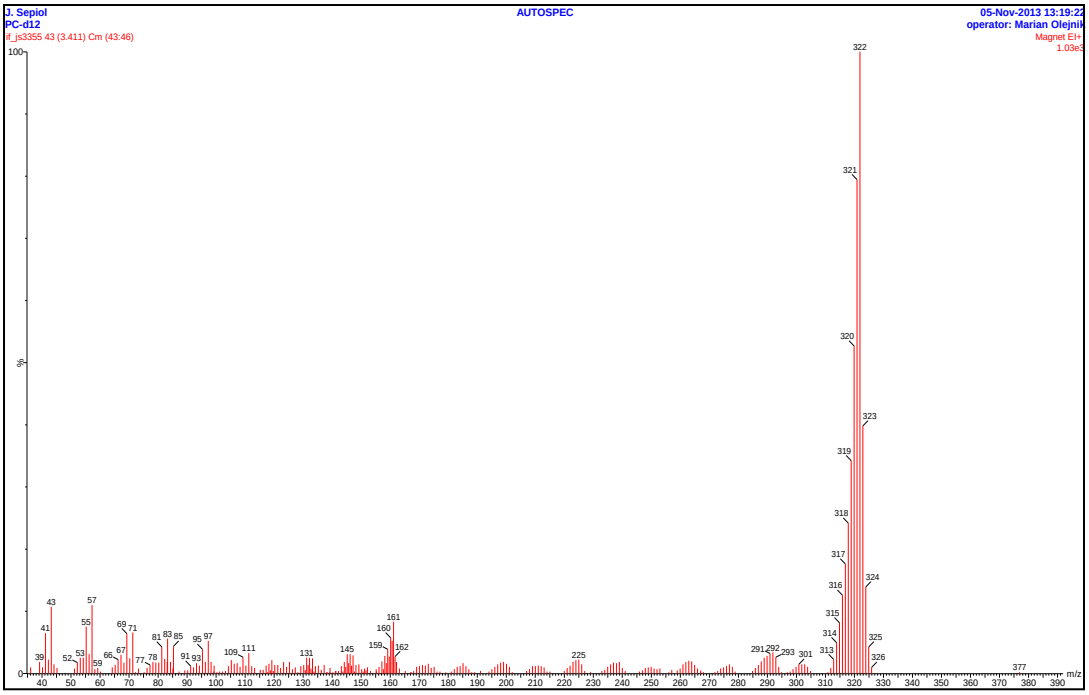

Figure 2.11 Mass spectrum of perdeuterated porphycene sample (Pc-d_{mix}).

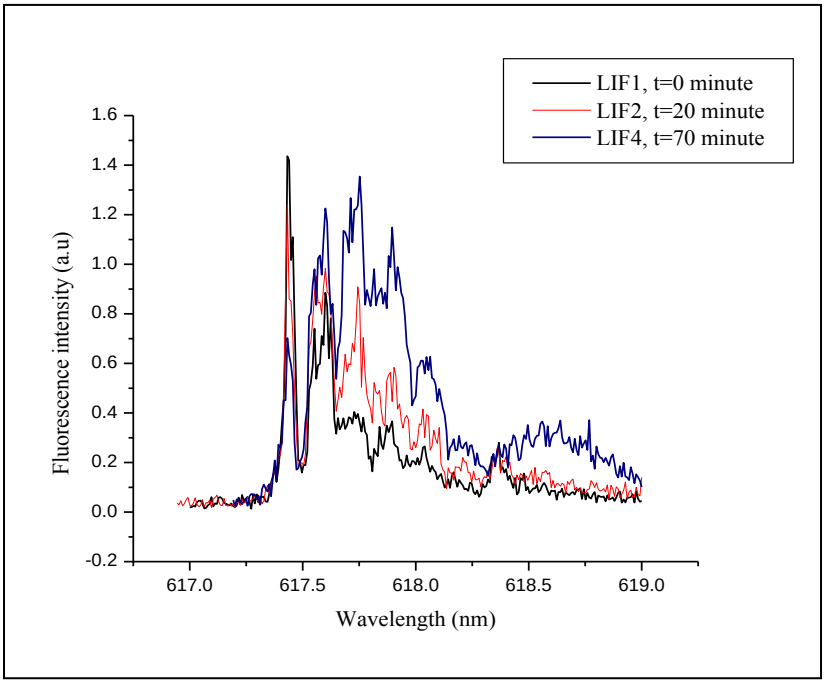

Figure 2.12 Successive LIF scans of Pc-d_{mix} in a supersonic-jet using conventional heating technique.

It has also been shown that at least partial deuteration of the cavity NH hydrogens could be achieved during interaction of the desorbed Pc with heavy water (or MeOD) seeded in carrier gas (Ne).

2.8 Vapor-phase absorption spectra

The vapor phase electronic absorption spectra of porphycene and derivatives were measured on Shimadzu UV 3100 spectrophotometer equipped with a variable temperature chamber (constructed by Mgr. Ing. A. Krupka), allowing temperature control starting from room temperature up to 400 ^{0}C.

An important experience that I have learned during the study is that the measurement of vapor-phase absorption spectra of molecules of interest could be taken as a prerequisite before directly going to measurement in the jet when working with conventional supersonic-jet set up where sublimation of solid samples is used to produce gas samples. This procedure is especially important when there is no previous data of the molecule of interest in the jet measurement. On one hand, the vapor phase spectrum helps to estimate the position of the 0-0 transition and hence guides us where to look for this signal in the jet. On the other hand, temperature dependent vapor-phase spectra gives insight of the optimal working temperature and the decomposition temperature of the molecule of interest. Figure 2.13 shows the temperature dependent vapor-phase spectra of porphycene.

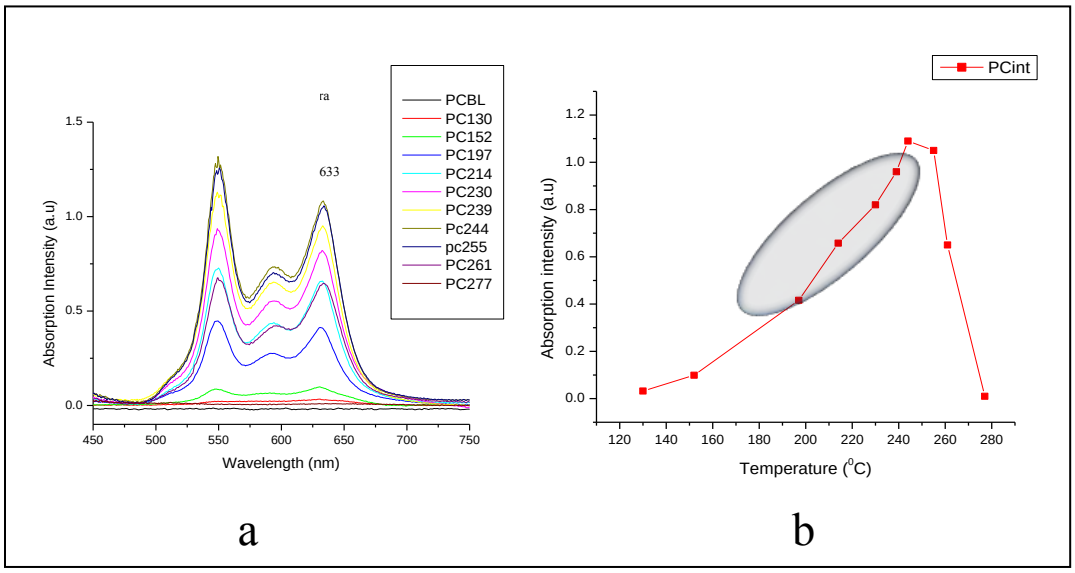

Figure 2.13 (a) Temperature dependent vapor-phase spectra of porphycene in the Q band region and (b) the plot of absorption maxima at 633 nm versus temperature.

It can be easily seen from the spectra that a reasonable vapor absorption is found starting from 200^0C while above 245^0C, there is a significant decomposition of the sample. The shaded region in Figure 2.13 b shows the most convenient range of temperatures for sublimation of porphycene in a conventional heating supersonic-jet set up.

Another important advantage of vapor-phase absorption measurement is presented in Figure 2.14

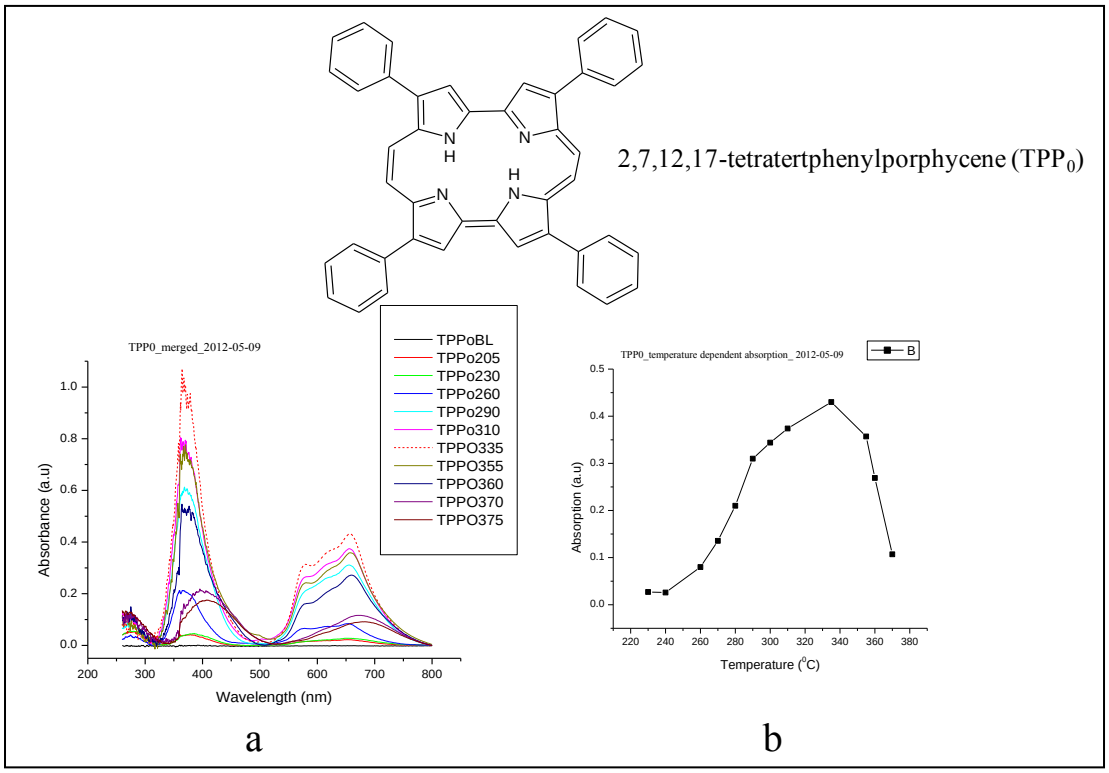

Figure 2.14 (a) Temperature dependent vapor-phase spectra of TTP0 and (b) the plot of absorption maxima at 654 nm versus temperature.

Based on the experience on porphycene, it could be seen that the molecule should be heated to a temperature of 300^0C to see a measurable signal in the jet. However, this temperature is almost the limiting temperature of the pulsed valve above which the proper production of supersonic-jet expansion will be compromised. Therefore, it is highly unlikely to get a signal from this compound in our conventional supersonic-jet setup. In this case, laser desorption technique will be the method of choice to produce gas samples in a supersonic jet.

The above measurements show that the classical vapor phase measurement is extremely important to decide on the mechanism of gas sample production and in terms of saving time, energy and resources especially when the samples are expensive.

2.9 Theoretical Methods

Geometry optimizations and frequency calculations were done at the density functional theory (DFT) level, using both double zeta (B3LYP/6-31G (d, p)) and triple zeta (B3LYP/6-311++G(d, p)) basis sets. Time-dependent DFT (TD-DFT) model was applied for the excited state calculations with the same functional and basis sets using Gaussian 09 program package [146]. The calculations have been done by Prof. Jacek Waluk and Michal Kijak (MSc).

Two dimensional symmetric mode coupling (SMC) model [147] has been applied by Dr. Tomasz Roliński to calculate the potential barrier for double proton tunneling in porphycene.

Hamiltonian for symmetric mode coupling (SMC) model:

$$\tilde{H} = -\frac{\hbar^2}{2m_x}\frac{\partial^2}{\partial\tilde{x}^2} - \frac{\hbar^2}{2m_y}\frac{\partial^2}{\partial\tilde{y}^2} + \frac{m_x\tilde{\omega}_x^2}{8\tilde{x}_0^2}(\tilde{x}-\tilde{x}_0)^2(\tilde{x}+\tilde{x}_0)^2 + \frac{1}{2}m_y\tilde{\omega}_y^2\,(\tilde{\alpha}(\tilde{x}^2-\tilde{x}_0{}^2)+\tilde{y}))^2$$

Where m_x, m_y , $\tilde{\omega}_x$, $\tilde{\omega}_y$, $2\tilde{x}_0$, and $\tilde{\alpha}$ are mass in the x direction, mass in y direction,

frequencies in x and y directions, distance between minima and coupling strength, respectively.

The following formulae:

$$x = \frac{\tilde{x}}{\tilde{x}_0}\ ;\ y = \frac{\tilde{y}}{\tilde{y}_0}\sqrt{\frac{m_y}{m_x}}\ ;\ \omega = \frac{\tilde{\omega}_y}{\tilde{\omega}_x}\ ;\ g = \frac{\hbar}{m_x\,\tilde{\omega}_x\tilde{x}_0{}^2}\ ;\ \alpha = \tilde{\alpha}\tilde{x}_0\sqrt{\frac{m_y}{m_x}}\ ;\ E(and\ H) = \frac{\tilde{E}(and\ \tilde{H})}{m_x\tilde{\omega}_x^2\tilde{x}_0{}^2}$$

scale the above Hamiltonian to a dimensionless form:

$$H_{SMC} = T + V_{SCM} = -\frac{g^2}{2}\left(\frac{\partial^2}{\partial x^2}+\frac{\partial^2}{\partial y^2}\right) + \frac{1}{8}\,(x-1)^2(x+1)^2 + \frac{1}{2}\omega^2(\alpha(x^2-1)+y)^2$$

In the SMC method it is assumed that the approximate potential is quartic along the high frequency mode (tunneling coordinate) and quadratic along the low frequency mode. The dimensionless form of this potential has two independent parameters: ω and α, where ω can be related to the ratio of the frequencies and α – to the coupling strength between the modes. The third parameter, g, can be related to the average kinetic energy of the mode where it plays the

role of . This model has two minima at $(x, y) = (\pm 1, 0)$ and one saddle point at (0, α); the y coordinates of the two minima are the same and are shifted from the coordinate of the saddle point. The barrier height, i.e, the potential difference between the saddle point and potential minima, is normalized to be 1/8 = 0.125. The frequency in the y direction is always $(\frac{\partial^2 V_{SMC}}{\partial y^2})^{1/2} = \omega_y$, while that in the x direction at the minima is normalized to unity. The potential contour is depicted in Figure 2.15.

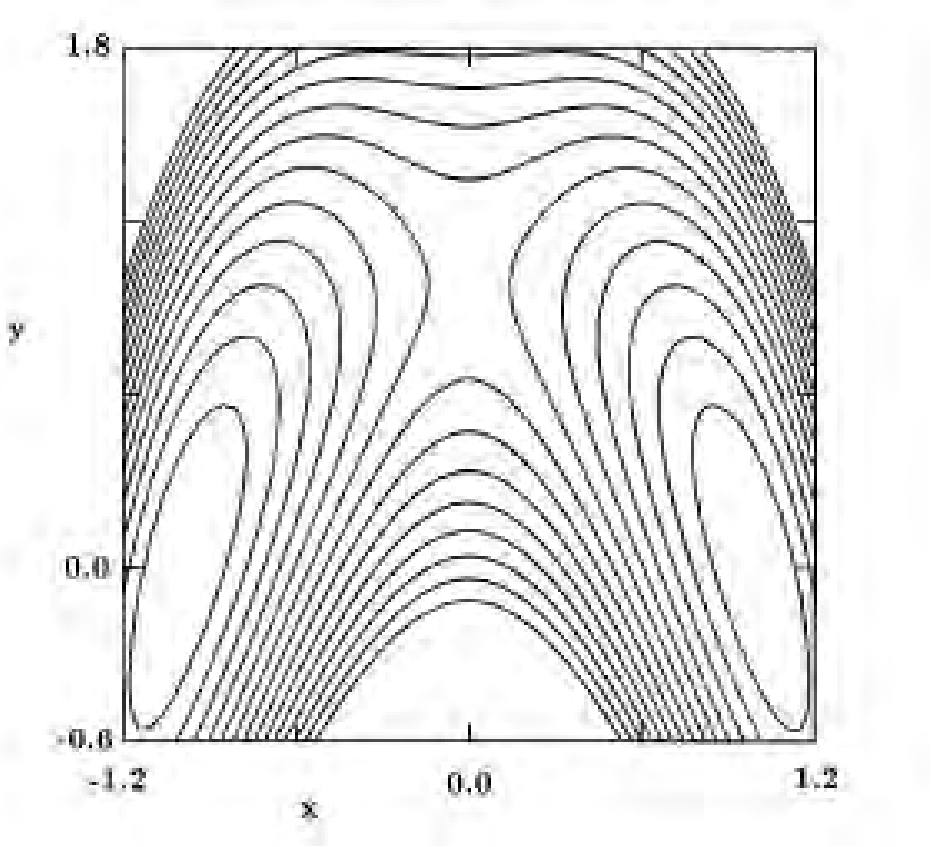

Figure 2.15 Contours of the symmetric mode coupling (SMC) potential for the parameters $(\omega_y, \alpha) = (0.5, 1)$. *The interval between the contours is 0.02 and the contours with the energy higher than 0.28 are omitted* [147].

This model has been used as a typical example of multidimentional tunneling in many fields [148,149], especially in the case of proton transfer in malonaldehydes [148] and tropolones [147,150].

Chapter Three

Vibrations of porphycene in the S_0 and S_1 electronic states: Single vibronic level dispersed fluorescence study

As stated in chapter one, porphycene provides a unique model system for studying multi-dimensional double proton tunneling in a symmetric double minimum potential. The multi-dimensional nature of the phenomena tells us that the tunneling coordinate is influenced by different vibrational modes in different ways. Therefore, proper understanding of the process should start with proper understanding of the nature of the vibrational levels of the molecule both in the ground and in the excited states.

The precise assignment of vibrations both in S_0 and S_1 electronic states should in turn help to understand the pattern of mode coupling (and hence dimensionality of proton tunneling coordinate). This task is not trivial, not only due to the large number of fundamental vibrations in porphycene (108), but also because of the presence of tunneling splittings, different for various vibrations and electronic states. To overcome these difficulties, emphasis was given on the analysis of LIF and single vibronic level dispersed fluorescence spectra of porphycene in supersonic jet. We exploit the fact that effective collisions, and hence random thermalizations, are highly prohibited in supersonic jet, and therefore the technique allows to see fluorescence occurring from unrelaxed vibronic levels in the S_1 state, which can be used for precise assignments of vibrations, observation of mode-selective tunneling splittings, and the study of mode coupling.

3.1 LIF excitation and "hole burning" spectra

Although the LIF excitation spectra of porphycene seeded in supersonic jet have already been reported, [45, 72, 101] our measurements were repeated in an extended range up to 1400 cm^{-1} above the 0-0 transition (Figure 3.1). To achieve higher sensitivity, the LIF spectra were obtained in the saturation regime. Instead of typical laser pulses of 10-100 μJ energy, pulses of ca. 1 mJ were applied. This enabled observation of many more transitions than detected before. For example, in addition to previously observed two transitions in the range below 200 cm^{-1} from the origin, four more transitions are identified, each composed of a doublet (Table 3.1).

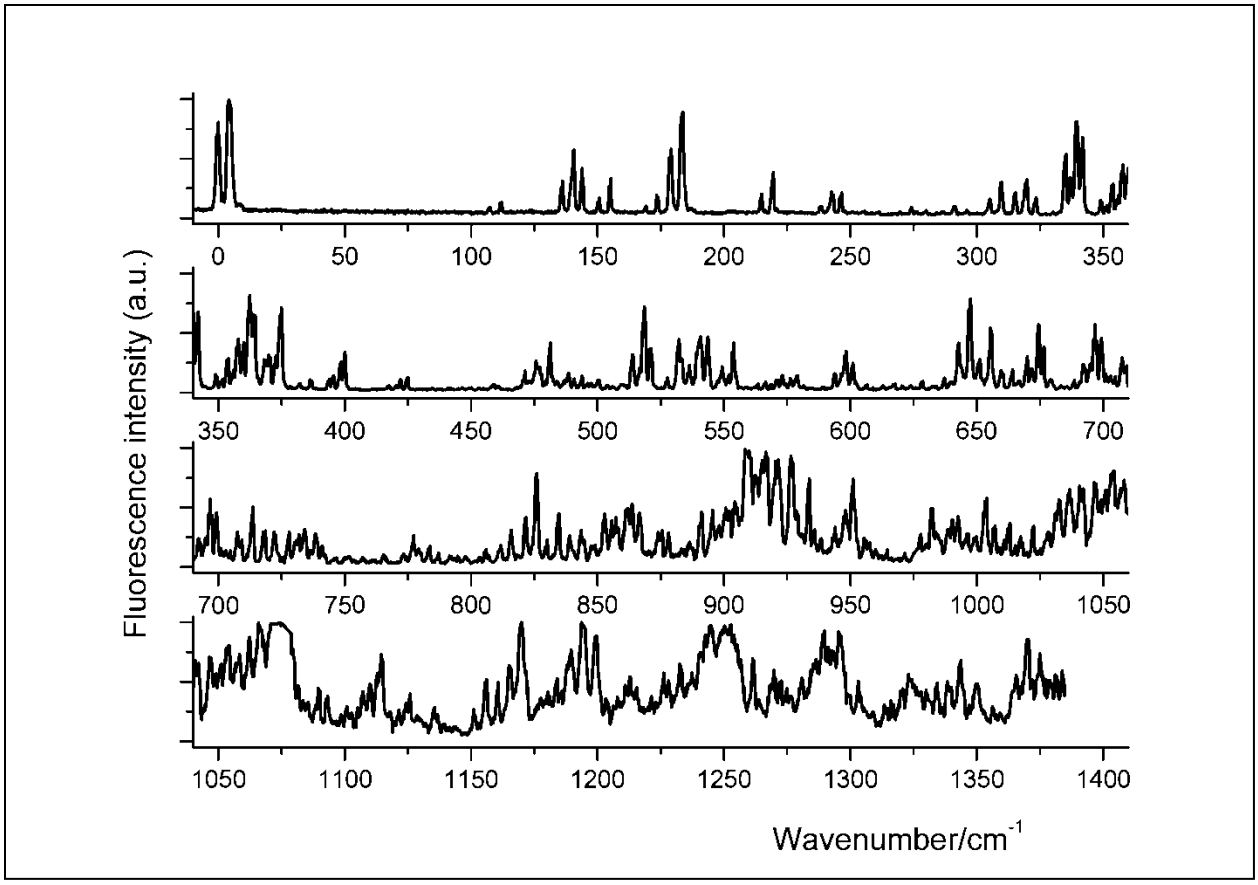

Figure 3.1. LIF excitation spectrum of porphycene in the range up to 1400 cm^{-1} excess energy above the origin of the S_0-S_1 electronic transitions.

The LIF excitation spectrum of porphycene shows well-resolved vibronic bands up to about 800 cm^{-1}. The spectrum becomes broader for excitation above 800 cm^{-1}, indicating an onset of fast excited state dynamics.

For the assignment of S_1 vibrations, it is helpful to note that the LIF spectrum consists of doublets, equally spaced for each vibrational mode by about 4.4 cm^{-1}. This behavior is a consequence of the fact that the tunneling splitting is practically negligible in S_1 (< 0.2 cm^{-1}). Therefore, the constant spacing between the components of each doublet reflects the value of the ground state splitting in the vibrationally unexcited level. Moreover, the selection rules dictate that only the transitions between the states of equal parity of nuclear functions are allowed. Since the "plus" combination of wave functions lies below the "minus" one, the 0^-_- electronic transition of "hot" nature is located ca. 4.4 cm^{-1} below 0^+_+.

Table 3.1. Ground (S_0) and excited state (S_1) vibrational frequencies of porphycene obtained form LIF and SVL fluorescence spectra.

$\tilde{\nu}$ (S_1) [a] exp	$\tilde{\nu}$ (S_1)[b] calc	$\tilde{\nu}$ (S_0)[c] exp	$\tilde{\nu}$ (S_0)[d] calc	$\Delta\tilde{\nu}$ (S_1-S_0) exp	$\Delta\tilde{\nu}$ (S_1-S_0) calc	Assignment
107, 112	107	112,116 117, 121	117	-10	-10	$1B_g$
136, 141	129	135,140 140, 145	130	-4	-1	$2B_g$
139sh,144	146	- 145	147	-4 [e]	-1	$1A_g$
150, 155	152	148, 152 152, 156	154	-2	-2	$2A_u$+$3A_u$
169, 174	174	162, 166 166, 170	168	3	6	$2x3A_u$
179, 184	179	169, 181 174, 186	185	1 [e]	-6	$2A_g$
215, 220	214	235 239	234	-20	-20	$2\times1B_g$
238, 242	237	260 -	260	-22	-23	$1B_g$+$2\times2A_u$
242, 246	236	260, 264 263	247	-22	-11	$1B_g$+$2B_g$
269, 274	258	-	260	-	-2	$2\times2\ B_g$

276, 280	275	-	277	-	-2	$1A_g+2B_g$
287, 291	286	-	302	-	-16	$2A_g+1B_g$
293, 297	298	-	301	-	-3	$1A_g+2A_u+3A_u$
305, 309	315	319 324	322	-14	-7	$2B_g+3B_g$
315, 320	308	310,319 310,318	315	6	-7	$2A_g+2B_g$
318, 323	325	- 324, 336	332	-12	-7	$1A_g+2A_g$
335, 339	340	335, 340 337, 341	342	-5	-2	$3A_g$
337, 342	344	- 361	369	-24	-25	$1A_u+5A_u$
349, 354	346	- 371	364	-23	-18	$2x1B_g+2B_g$
351, 356	360	-	381	-	-21	$1A_g+2x1B_g$
358, 362	358	358 345, 364	370	2 [e]	-12	$2x2A_g$
360, 364	367	357, 362 361,364	365	-2	2	$4A_g$
369, 373	365	-	377	-	-12	$1B_g+2\ x2B_g$
371, 375	366	- 392	387	-21	-21	$1Bg+2B_g+2x2A_u$
382, 387	382	-	394	-	-12	$1A_g+1B_g+2B_g$

	388	-	402	-	-14	$2x1B_g+2x3A_u$
394, 398	394	408,413 411,418	419	-19	-25	$2A_g+2x1B_g$
395, 400	355	399 398	390	-4	-35	$5B_g$
417, 422	416	-	442	-	-26	$2A_g+1B_g+2\times2A_u$
420, 425	415 410	- -	432 424	- -	-17 -4	$2A_g+1B_g+2B_g$ $2x2B_g+2A_u+3A_u$
471, 475	469	469, 474 -	472	-4	-3	$3A_g+2B_g$
476, 481	483	472,476 481	482	-5	1	$5A_g$
484, 489	472	-	494	-	-22	$2x(1B_g+2B_g)$
491, 494	489	-	511	-	-22	$1A_g+2x1B_g+2B_g$
496, 500	496	-	495	-	1	$4A_g+2B_g$
504, 509	494	-	507	-	-13	$1B_g+3\ x2B_g$
514, 518	519	509,522 514,526	527	-4 [e]	-8	$2A_g+3A_g$
516, 521	523	- 540,555	554	-30 [e]	-31	$2A_g+1A_u+5A_u$
528, 532	522	- 548, 563	549	-26 [e]	-27	$2A_g+2x1B_g+2B_g$
536, 541	537	- 542	555	-5	-18	$3x2A_g$

539sh, 544	546	- 536, 545	550	-7 [e]	-4	$2A_g+4A_g$
547, 552	544	-	562	-	-18	$2A_g+1B_g+2x2B_g$
549, 554	554	-	576	-	-22	$3A_g+2x1B_g$
594, 598	595	-	627	-	-32	$2x\ 2A_g+1B_g+2x2A_u$
596, 601	599	-	601	-	-2	$6A_g$
643, 647	650	- 661	664	-18	-14	$7A_g$
651, 656	650	-	664	-	-14	$2A_g+3A_g+2B_g$
660, 664	651	-	679	-	-28	$2A_g+2x(1B_g+2B_g)$
670, 674	668	-	696	-	-28	$1A_{g+}\ 2A_g+2x1B_g+2B_g$
672, 677	680	678 -	684	-6	-4	$2x3A_g$
692, 697	698	-	712	-	-14	$2x2A_g+3A_g$
695, 699	707	-	707	-	0	$3A_g+4A_g$
709, 714	701	-	734	-	-32	$2x2A_g+2x1B_g+2B_g$
812, 816	823	-	824	-	-1	$3A_g+5A_g$
822, 826	829	- 851	849	-29	-20	$2A_g+7A_g$
830, 835	836	-	837	-	-1	$3A_g+4A_g+2B_g$
839,844	830	-	864	-	-34	$2x\ (2A_g+1B_g+2B_g)$

[a] tunneling doublets observed in LIF, energy relative to the location of the 0_-^- transition; [b] B3LYP/6-31G++(d, p), scaling factor 0.9960; [c]observed shifts with respect to the excitation into the lower (first row) and higher energy (second row) doublet component; [d] B3LYP/6-31G++(d, p), scaling factor 0.9902; [e] S_0 frequency value approximated taking into account different tunneling splittings in the vibrationless and vibrationally excited levels.

This pattern is repeated for the observed vibronic transitions. A vibrational mode frequency in S_1 therefore corresponds to the difference between the value observed for the lower energy component of each doublet and the value of 0^-_- transition, the origin of the LIF spectrum.

The constant intensity pattern for the tunneling doublets is observed throughout the LIF spectra, the lower energy component always being weaker. Assuming the 4.4 cm^{-1} separation of the levels leads to an estimation of effective temperature of about 10 K.

Additional help in the vibrational assignments comes from hole-burning experiments, which allow differentiating between the transitions originating in the plus and minus ground state levels. An example is presented in Figure 3.2.

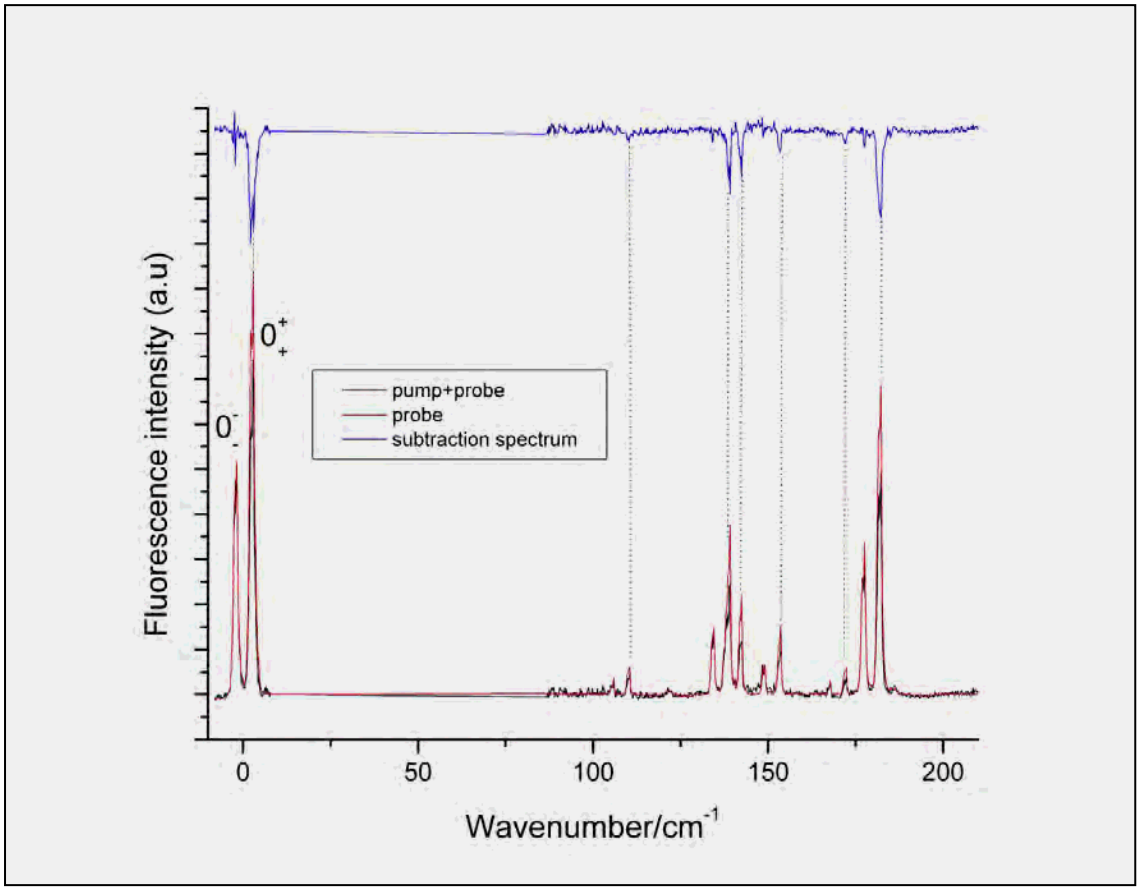

Figure 3.2 Active baseline subtraction spectrum (top, blue) of porphycene obtained while pumping the 0^+_+ band of the LIF excitation spectrum. The scanning probe laser was delayed by 200 ns with respect to the fixed pump laser. Bottom, the spectra obtained with and without pumping (black and red, respectively).

The bands which respond to hole burning while pumping at the O_+^+ band correspond to the transitions which originate from the "plus" level, the lowest energy level of S_0 whereas those which originate from the "minus" level, do not respond.

Hole burning spectroscopy has been also applied in order to detect the IR active asymmetric NH stretching frequency using IR/Vis pump/probe pulses in the laser desorption set-up. Proper alignment of the two lasers was checked using tetratertbutylporphycene (TTPC) as a standard. Figure 3.2 a show the results of hole burning spectra of TTPC in the CH stretching region. The conditions of the experiment are explained in the caption.

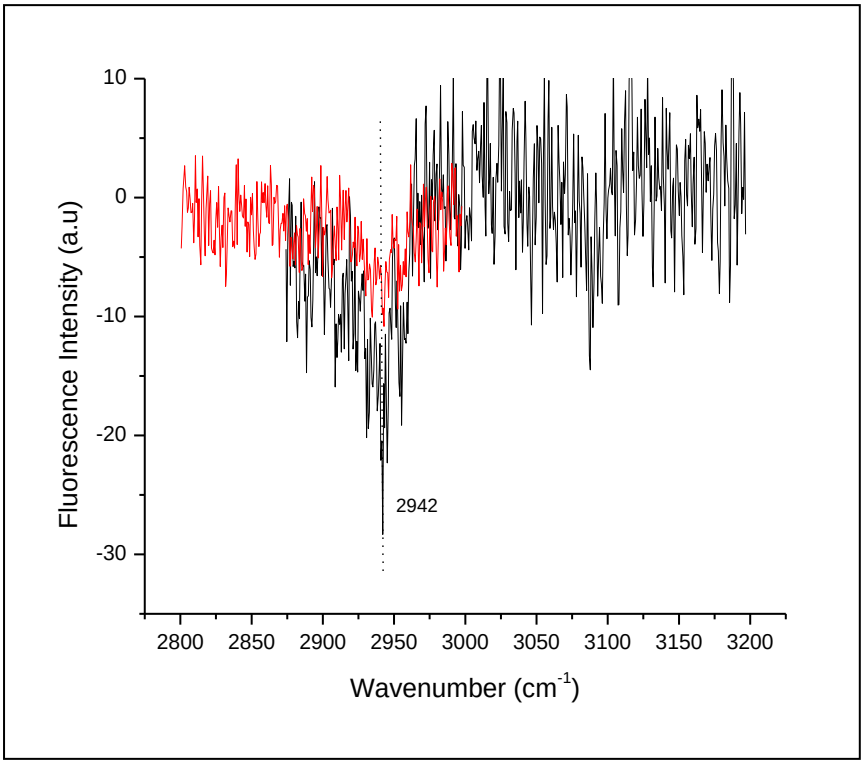

Figure 3.2a Two scans of hole burning spectrum (with active base line subtraction) were recorded in such a way that the visible laser (probe) is fixed at 0-0 position of TTPC while the IR (pump) is scanned. The time delay between the visible and IR lasers is about 100 ns.

As shown in the figure, a reproducible "hole" is observed at about 2940 cm^{-1} which certainly marked the position of IR band belonging to C-H stretch frequency of the tert-butyl substituents. The result proved the alignment of the pump and the probe laser was correct. Figure 3.2b shows the power output of the IR laser pulse in the scanning range.

Our first attempt to see the NH stretch (30 Bu mode) band of porphycene failed. This is not surprising since this mode was found to be extremely broad due to coupling with several other modes and hence its detection has been very difficult so far [97]. Unfortunately, further attempts were not possible by sudden defects of OPO IR-laser (Figure 3.2 b), and the attemps are proposed in the future.

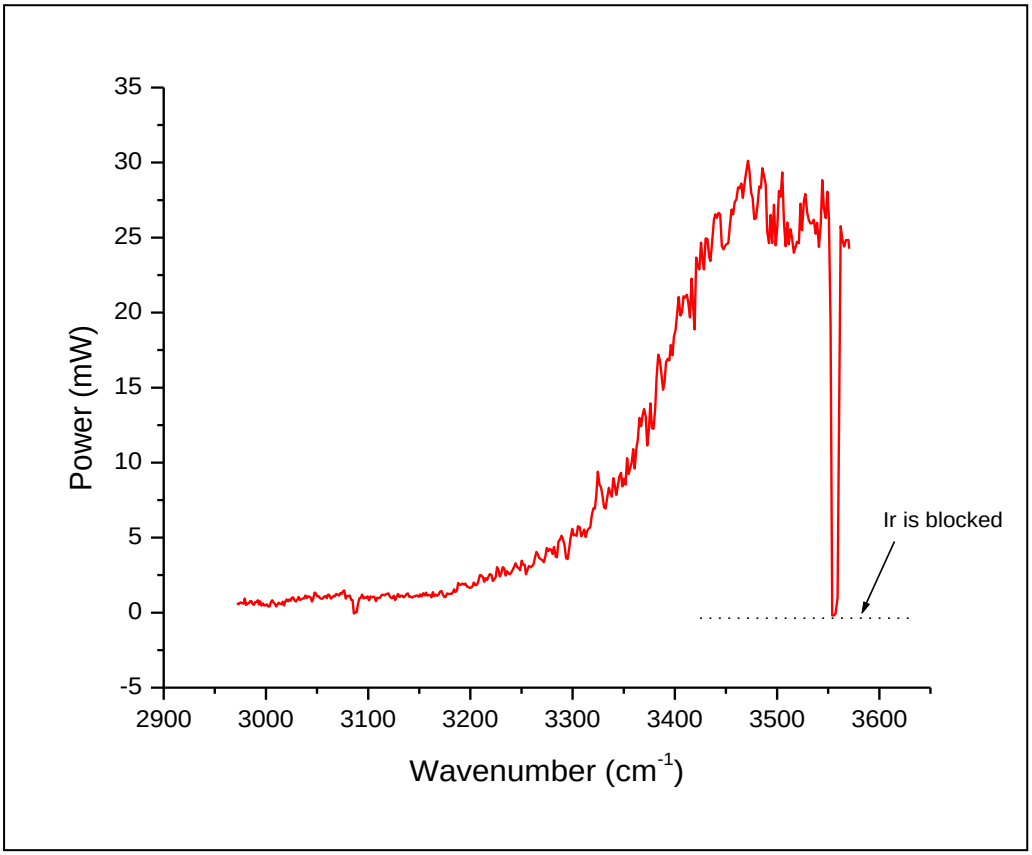

Figure 3.2b Energy profile of the IR laser pulse in the frequency range of interest, measured at the entrance of the experimental chamber.

Saturation conditions while recording the LIF spectra of porphycene resulted in the lack of simple one-to-one correspondence between the LIF excitation and origin-excited dispersed fluorescence spectra (Figure 3.3). The former reveal many more spectral features. For example, in the region below 180 cm^{-1}, only two bands appear in the dispersed fluorescence spectra at 152

and 145 cm^{-1}, whereas at least 5 bands are observed in the vicinity of 140 cm^{-1} in the LIF excitation spectrum. Even larger difference is observed in the range 200-300 cm^{-1}. Therefore, the assignment of corresponding vibrations in the S_0 and S_1 states is not straightforward. Unambiguous assignment of each vibronic state becomes possible after recording the dispersed fluorescence spectra following excitation into different vibronic bands.

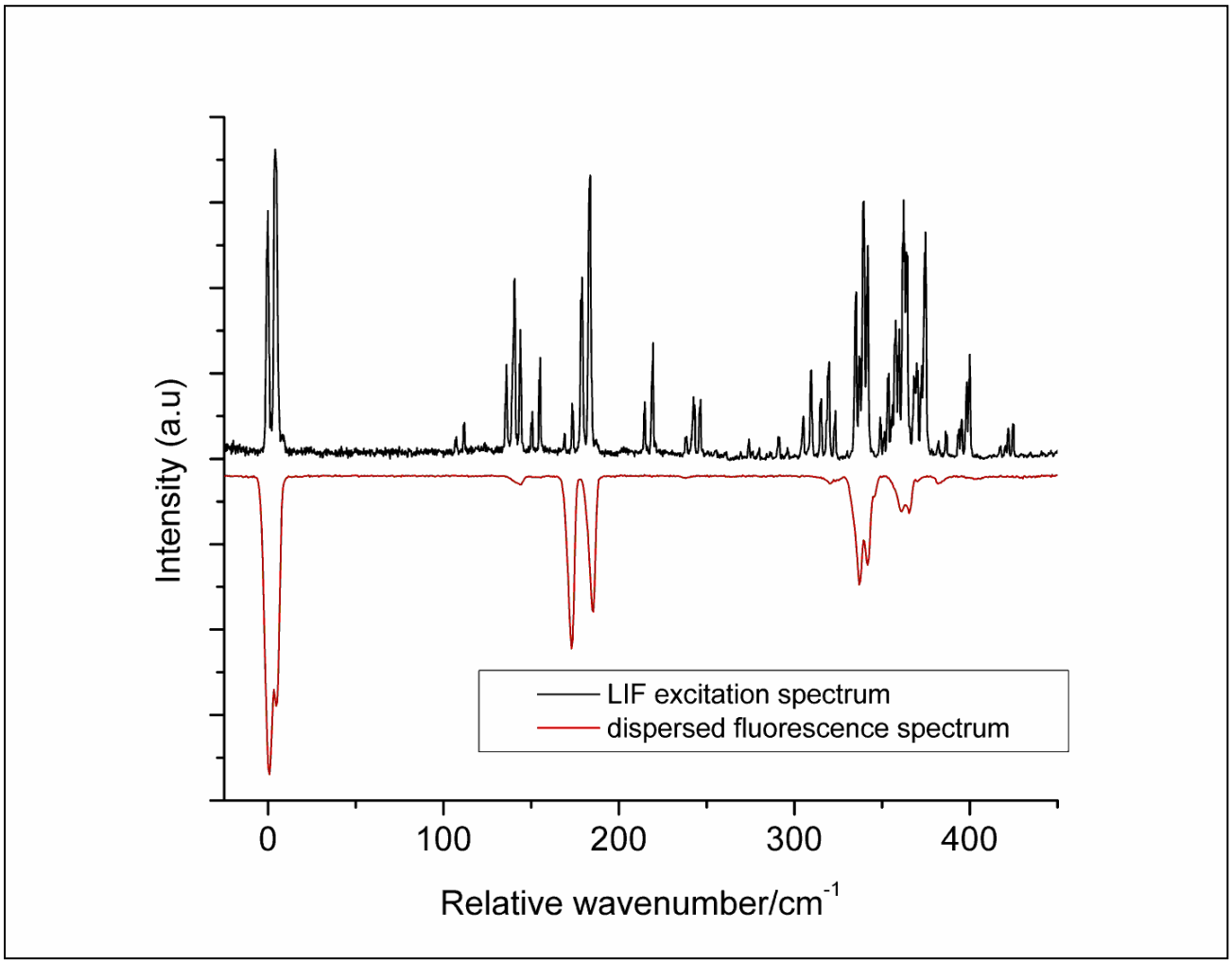

Figure 3.3 Comparison of LIF excitation (black, top) and dispersed fluorescence (red, bottom) spectra of porphycene in supersonic jet. Fluorescence intensity in the dispersed fluorescence spectrum is multiplied by -1 for easier comparison.

3.2 Single vibronic level dispersed fluorescence spectra

Dispersed fluorescence spectrum from a single vibronic level (SVL) provides information complementary to the excitation spectrum. It maps the overlap of the nuclear wavefunctions of the excited and ground electronic states and hence such measurements are essential for the precise assignment of vibrational levels both in the S_0 and S_1 states. [151-154] They also provide information about the extent of state mixing into the precursor of intramolecular vibrational energy redistribution (IVR). Single vibronic level fluorescence spectra originating from an excited vibrational level may provide detailed information on the ground state potential of analogous level. In this section, the dispersed fluorescence spectra of porphycene are presented and the bands are assigned with the aid of quantum chemical calculations.

3.2.A 0_0^0 *Excitation*

The dispersed fluorescence spectrum of porphycene obtained via excitation of the high-energy component of the origin doublet (16163 cm^{-1}) is presented in Figure 3.4. The spectrum exhibits features similar to those reported from earlier supersonic jet measurements, [72] but with better spectral resolution and sensitivity. Because of that, additional transitions could be detected.

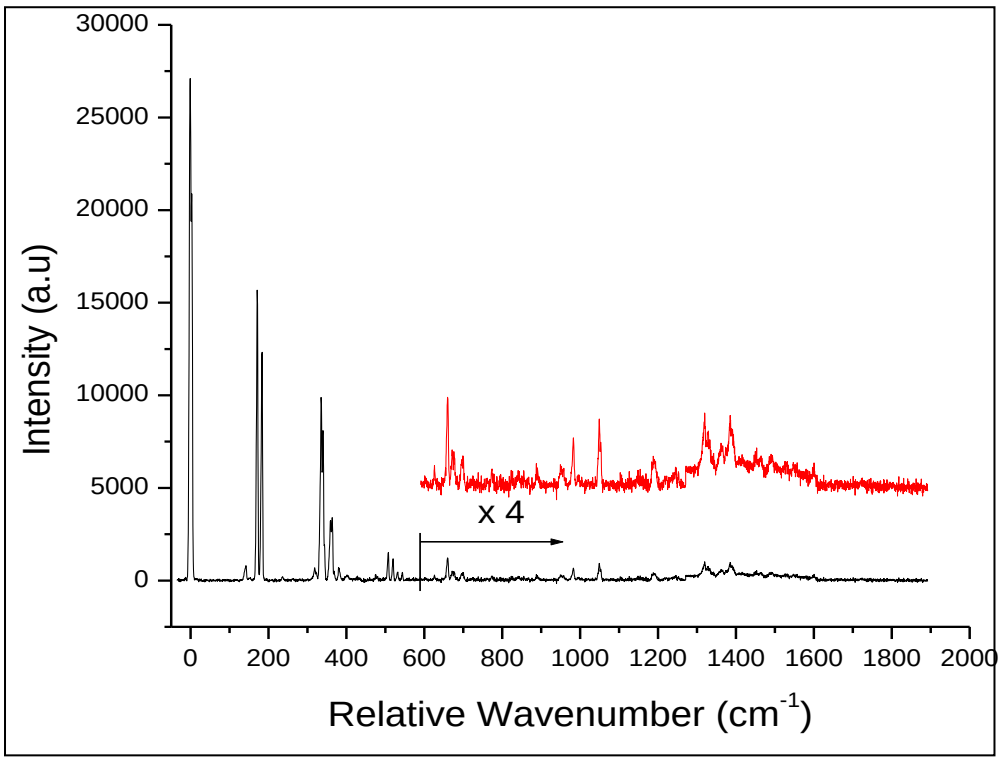

Figure 3.4. Dispersed fluorescence spectrum of porphycene recorded for excitation into the 0_+^+ *origin band (16163 cm-1). Frequencies are given in relative wavenumber from the excitation energy.*

In the region up to 800 cm^{-1}, several previously unobserved small intensity bands have been identified. The assignments of the vibrations are presented in Table 3.1.

3.2.B *Excitation into low-energy vibronic bands*

Figure 3.5 shows dispersed fluorescence spectra obtained for excitation into several representative tunneling doublets of porphycene. Similar spectroscopic features assigned to tunneling doublets have also been reported for malonaldehyde, [155-158] tropolone [159-172] and its derivatives, [173-177] 9-hydroxyphenalenones [178-184] and 6-hydroxybenzanthrone. [185]

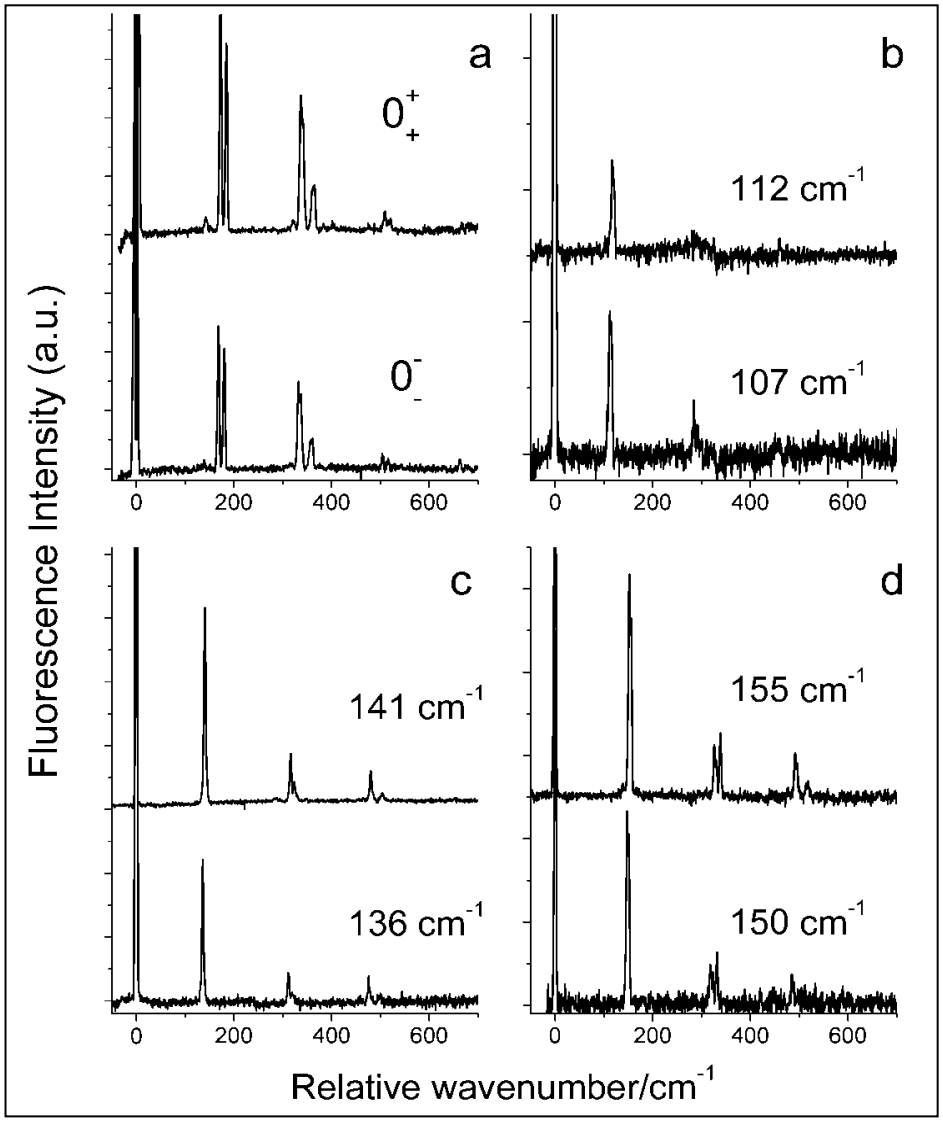

Figure 3.5 Comparison of dispersed fluorescence spectra obtained for selective excitation into both components of tunneling doublets: (a) 0^+_+ *and* 0^-_- *; (b) 107/112; (c) 136/141; (d) 150/155* cm^{-1}.

Figure 3.5a presents a comparison of disperse fluorescence spectra at 0_+^+ and 0_-^- excitations, respectively. The two spectra are very similar in the intensity distribution, as well as in the frequencies of the vibronic bands, except that, when plotted relative to the excitation energy, the vibronic pattern obtained for the 0_-^- excitation is shifted by 4-5 cm^{-1} towards lower values. This result is in line with the assignment of the bands at 16158 and 16163 cm^{-1} as the tunneling components of the zero-point-energy level. Guided by the 4.4 cm^{-1} characteristic splitting and similarity of the corresponding fluorescence emission spectra, we are able to identify numerous pairs of tunneling doublets in the LIF spectrum of porphycene (Table 3.1).

Analysis of the SVL fluorescence obtained after selective excitation of the low-energy transitions allowed detection and assignments of several vibrational levels which were not observed previously. Additional help in the assignment was provided by the doublet structure of the LIF spectra with constant spacing between the two components. The fluorescence spectra obtained for excitation into each of the two tunneling sublevels of the same vibrations are very similar, but they usually differ for excitation of different modes. This is crucial for reliable separation of nearby or even overlapping transitions. Some additional examples of SVL spectra obtained for excitation into different low-frequency vibronic bands are presented in Figure 3.6.

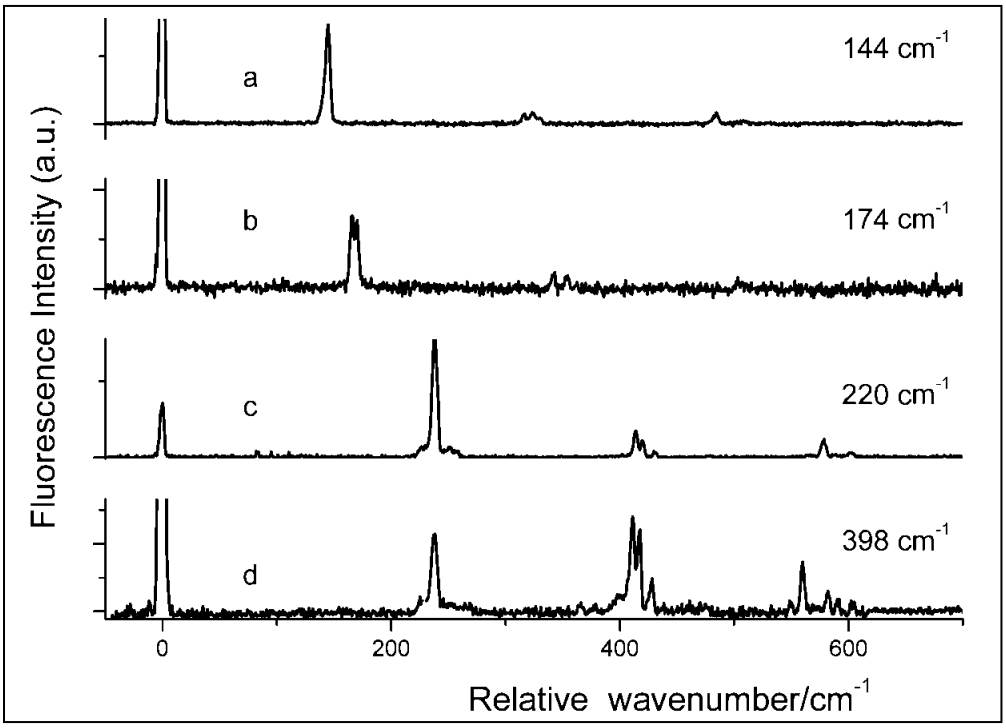

Figure 3.6. Dispersed fluorescence spectra obtained for excitation into low-frequency bands: (a) 144 cm^{-1}, (b) 174 cm^{-1}, (c) 220 cm^{-1}, (d) 398 cm^{-1}.

The spectra in Figures 3.5b-d and 3.6 are very simple and dominated in each case by one prominent band assigned as ν_1^1 band acting as an origin. The remaining bands are assigned to $\nu_1^1 x_1^0$ type cross-sequence transitions, where *v* and *x* correspond to two different modes. Only a few modes are active in the spectra built off ν_1^1 : they correspond to $2A_g$, $3A_g$, and $4A_g$ totally symmetric vibrations and their combinations; in some cases, weaker intensity transitions involving $1A_g$ mode are also observed. The same modes dominate the fluorescence recorded from the electronic origin. Also the relative intensities are quite similar. The assignment of vibrations based on 0-0 and single vibronic level emissions is presented in Table 3.1.

Nearly all bands observed in SVL spectra reveal doublet splittings similar to the values of 4.4 cm^{-1} observed in the LIF spectra. Since the spectral resolution of our setup is lower for the dispersed fluorescence than LIF, the doublets are not well resolved as in the LIF spectra, except for the $2A_g$ mode, its overtones and combinations, for which the splittings exceed 10 cm^{-1}. The observation of a constant spacing between the doublet components in the LIF spectrum allows us to assume a negligible tunneling splitting in S_1. We use the symbols Δ_0 and Δ_i to indicate the S_0 splitting for the vibrationless level and for the v=1 level of the *i*-th mode. Presenting the SVL fluorescence as a function of $\tilde{\nu}_{ex}$ - $\tilde{\nu}_{fl}$, where the former indicates the excitation energy and the latter, the recorded emission energy, one observes doublets separated by Δ_i. For the excitation from the lower (+) level, the two peaks are located at f +1/2(Δ_0 - Δ_i) and f +1/2(Δ_0 + Δ_i); for the excitation from the upper (-) level the corresponding locations are f -1/2(Δ_0 + Δ_i) and f +1/2(Δ_i – Δ_0). The centers of the doublets are located at f +Δ_0/2 and f + Δ_i/2 for excitation from (+) and (-), respectively. By f we denote the (v=0) → (v=1) transition energy that would have been observed had there been no splitting. This value should be compared with the calculated vibrational frequency. For a special case of $\Delta_0 = \Delta_i = \Delta$, the tunneling doublets observed in SVL are located at f and $f + \Delta$ for excitation from the (+) level, whereas for the excitation originating from (-) they are positioned at $f - \Delta$ and f. Given our accuracy of about 1 cm^{-1}, such situation is encountered most frequently. In Table 3.1 we present the frequency values obtained for excitation into both the (+) and (-) levels; the former are more reliable because of the greater population of the lower level, which results in higher emission intensity.

Excitation into the higher component of the 107/112 cm^{-1} doublet (Figure 3.5b) gives, in addition to the resonance fluorescence peak, a band peaking at 117 cm^{-1} with a shoulder at 121 cm^{-1}. The origin-excited dispersed fluorescence spectrum does not show any vibronic band at this frequency, but a peak was observed at 120 cm^{-1} in the inelastic neutron scattering (INS) spectrum. [97] The calculations for S_0/S_1 predict a vibration of B_g symmetry at 117/107 cm^{-1}. Therefore the 107 cm^{-1} band in the LIF spectrum and the 117 cm^{-1} transition in the emission are assigned to the $1B_g$ mode in the S_1 and S_0 states, respectively.

The fluorescence emission spectrum following the excitation of 136/141 cm^{-1} transition (Figure 5c) is also dominated by one prominent band at 140 cm^{-1} acting as an origin. This band is absent in the origin-excited dispersed fluorescence spectrum; a feature at 134 cm^{-1} has been observed by INS. [97] The calculations predict for S_1 a fundamental vibration of B_g symmetry at 129 cm^{-1}; the ground state frequency is calculated as 130 cm^{-1}. Therefore, the 136 cm^{-1} band in the LIF spectrum (a lower energy component of a doublet) and the 140 cm^{-1} transition in SVL fluorescence can be assigned to $2B_g$.

Figure 3.6a shows emission spectrum obtained via excitation of the 0+144 cm^{-1} band in the LIF excitation spectrum. The emission is dominated by one prominent band at 145 cm^{-1}. This feature is already observed in the origin-excited fluorescence emission spectrum and assigned as $1A_g$. Weak intensity bands are also observed at 316, 324, 330, 485, and 507 cm^{-1} from the excitation energy. Except for the 330 cm^{-1} feature (tentatively attributed to $2B_g+3B_g$), they can be assigned to the combination of $1A_g$ with $2A_g$, $3A_g$, and $4A_g$ modes. Because of large value of the tunneling splitting for $2A_g$, the two components are clearly resolved. This is not the case for $3A_g$, and $4A_g$, but the presence of doublets can be deduced from the larger widths of these peaks. On the other hand, the peak corresponding to the $1A_g$ mode is narrower. The origin of that may, in principle, be twofold: (i) small value of the tunneling splitting for this mode; (ii) lack of mechanism to populate both the "plus" and "minus" S_1 levels on the time scale of S_1 lifetime (ns). The latter is improbable, as we observe emission from both components for modes other than $1A_g$. For the particular case of the $1A_g$ vibration, it has been already demonstrated that it exhibits practically no tunneling splitting. [101] However, we will return to the general problem of equilibration of the two tunneling levels in a separate section.

Dispersed fluorescence emission spectrum following the 0+155 cm^{-1} band excitation is presented in Figure 3.5d. The spectrum is dominated by a prominent band at 152 cm^{-1}, exhibiting a doublet structure with a separation of 4 cm^{-1}. This band is not observed in the origin-excited dispersed fluorescence. Based on the results of calculations regarding both absolute frequencies, as well as the agreement between the predicted and observed shifts between S_0 and S_1, we assign this band to the $2A_u + 3A_u$ combination.

Figure 3. 6b shows the emission spectrum obtained for excitation into the 0+174 cm^{-1} band. The spectrum is dominated by one prominent origin doublet at 166/170 cm^{-1}. This band is absent in the origin-excited dispersed fluorescence spectrum. Based on calculations and the agreement between computed and observed frequency changes between S_0 and S_1, we assign it to the first overtone of the $3A_u$ vibration.

Figure3. 6c shows the fluorescence emission spectrum obtained for excitation into the 0+220 cm^{-1} band in the LIF excitation spectrum. The spectrum is dominated by one prominent origin at 239 cm^{-1}. Although small in intensity, this band is also observed in the fluorescence emission recorded for origin band excitation. We assign this transition to $2\times1B_g$, in excellent agreement

with the calculated frequency and S_1-S_0 shift. This band forms the origin for transitions involving $2A_g$, $3A_g$, and $4A_g$ modes.

Excitation of the 0+394/398 cm^{-1} features (Figure 3.6 d) gives a similar spectrum to that of 0+220 cm^{-1} excitation. Now, however, the intensities of the peaks corresponding to $2x1B_g$ and $2A_g$ are similar. We therefore assign the 0+398 cm^{-1} band in the LIF excitation spectrum as the combination of $2A_g+2\times1B_g$.

3.2. C 0_0^0 *+184, 362, 364, and 541 cm^{-1} excitations*

Figure 3.7 shows dispersed fluorescence spectra obtained following the excitation of 0+184, 362, 364, and 541 cm^{-1} bands in the LIF spectrum, respectively.

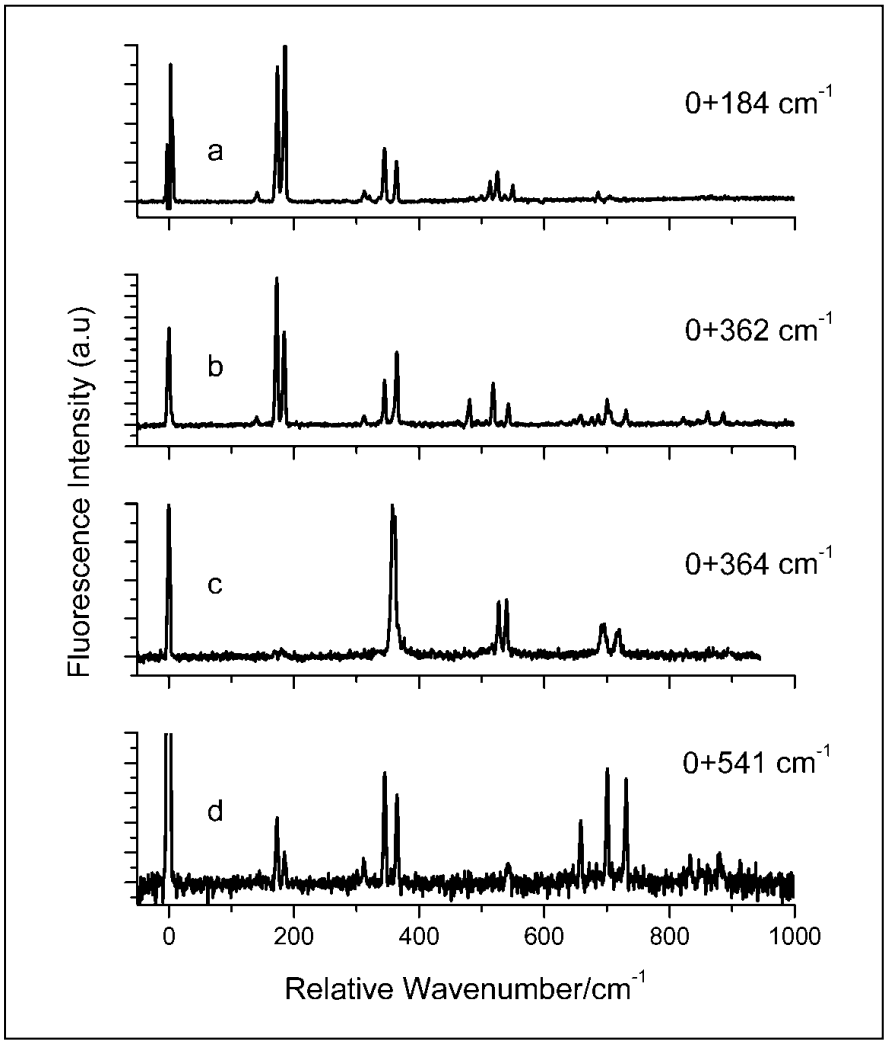

Figure 3.7. Dispersed fluorescence spectrum obtained via excitation of (a) 0+184, (b) 0+362, (c) 0+364, and (d) 0+541 cm^{-1} bands.

Even a cursory glance at the spectra reveals that the spectra in Figures 3.7a, b, and d form a group with a similar pattern, while that presented in Figure 3.7c is different.

The spectrum shown in Figure 3.7a is dominated by two bands at 174 and 186 cm^{-1} acting as pseudo origin, belonging to the tunneling doublet of the $2A_g$ mode. Therefore the band at 0+184cm^{-1} in the LIF excitation spectrum is assigned as $2A_g$. The bands at 143, 324, 514/526 and 538/551 cm^{-1} are also observed in the fluorescence emission spectrum obtained via excitation into the origin and are already assigned to $1A_g$, $1A_g$+$2A_g$, $2A_g$+$3A_g$ and $2A_g$+$4A_g$, respectively. Two medium intensity bands are located at 345 and 365 cm^{-1}. These frequencies are close to those corresponding to $3A_g$ and $4A_g$ modes, respectively. However, these bands are narrow and do not reveal splitting into doublets, expected for both $3A_g$ and $4A_g$ modes. Therefore, we assign these bands as the overtones of the $2A_g$ mode doublet. Similarly, the bands observed at 525 and 549 cm^{-1} are assigned to the third harmonic progression of the $2A_g$ mode. Of the remaining bands, the 501 cm^{-1} can be assigned to $6B_g$. This transition has been previously observed in the Raman spectrum, [97] but not in fluorescence.

Figure 3.7b shows the emission spectrum following excitation of the 0+362 cm^{-1} band in the LIF excitation spectrum. The spectrum exhibits features very similar to those observed in the emission obtained for 0+184 cm^{-1} excitation. Therefore, from the similarities of the spectra in Figures 3.7a and b, we assign the 0+362 cm^{-1} band in the LIF spectra as the second harmonic of the $2A_g$ mode. One can notice that the number of harmonic progressions of the $2A_g$ mode observed in Figure 3.7b is greater than that in Figure 3.7a. Such an increase in intensity and number of vibronic progressions with increasing excitation quanta is observed e.g, in tolanes. [186] The increase in intensity and number of vibronic progressions can be exploited for modeling the potential energy surface along the mode in consideration. The pairs of bands at 345 and 364 cm^{-1}, 518 and 543 cm^{-1}, 700 and 731 cm^{-1}, and 861 and 886 cm^{-1} are assigned as $2x2A_g$, $3x2A_g$, $4x2A_g$ and $5x2A_g$ progressions, respectively. It is remarkable that the pattern of the intensities of the doublet components is reversed for 184 and 362 cm^{-1} excitations.

Shifting the excitation by merely 2 cm^{-1}, to 0+364 cm^{-1} results in a dramatic change in the SVL spectrum (Figure 3.7c). It is now dominated by the $4A_g$ band. The features around 170/180 cm^{-1} are barely detected, but the $2A_g$ mode is readily observed at 527/540 cm^{-1}: this band doublet corresponds to the $4A_{g_1}^{1}2A_{g_1}^{0}$ transition. Contributions from $3A_g$ and $4A_g$ are also observed at 696 and 720 cm^{-1}. Comparison of two completely different spectra obtained for very similar excitation energies reveals the power of SVL experiments in disentangling complicated spectral patterns.

Figure 3.7d shows the fluorescence emission spectrum obtained for excitation of the 0+541 cm^{-1} band in the LIF excitation spectrum. The emission reveals features similar to those of Figures 3.7a and 3.7b, but is relatively simpler. Interestingly, while the vibronic activity in the vicinity of $3x2A_g$ is extremely weak, all the other vibronic progressions of the $2A_g$ mode are observed.

Therefore, we assign the band at 0+541 cm^{-1} in the LIF excitation spectra to $3x2A_g$. The low intensity of the $2A_{g_3}^3$ transition can be due to the interaction between nearly isoenergetic $3x2A_g$ and $2A_g+4A_g$ levels in the ground electronic state.

3.2. D 0_0^0 *+339, 364, 400, 481, and 518 cm^{-1} excitations*

Figure 3.8a-d presents dispersed fluorescence emission recorded for excitation into the 0+339, 364, 400, and 481 cm^{-1} bands in the LIF excitation spectrum. The corresponding pseudo-origins are observed in the emission spectra at 337, 361, 398, and 481 cm^{-1}.

All bands except 398 cm^{-1} are already observed in the origin-excited dispersed fluorescence spectrum. The Raman spectra yielded a feature at 399 cm^{-1}, assigned to $5B_g$. [97] All the spectra show similar features in that all are dominated by one prominent pseudo origin, while the rest of the bands belong to vibrations observed also for excitation into the origin. Thus the bands at 0+339, 364, 400, and 481 cm^{-1} in the LIF excitation spectrum are assigned as $3A_g$, $4A_g$, $5B_g$, and $5A_g$, respectively.

Figure 3.8e shows the emission spectrum for excitation into the 0+518 cm^{-1} band in the LIF spectrum. This spectrum looks different from the others in that there is no dominant band. However, the doublet at 343/348 cm^{-1} belonging to $3A_g$ and its combination with $2A_g$ at 514 and 526 cm^{-1} seems to compete for origin. Such competition was also observed in Figure 3.6d when exciting a combination mode. The analysis of the bands in this spectrum leads to the assignment of the band at 518 cm^{-1} in the LIF spectrum as the combination of $2A_g+3A_g$.

3.2. E 0_0^0 *+826 and 909 cm^{-1} excitations*

The corresponding spectra are shown in Figures 3.9a and b. All the spectra show similar features among themselves, but very different from the rest of the emission spectra discussed so far. They are characterized by broad emissions, a characteristic signature of IVR. [154] It has already been pointed out that the LIF excitation spectrum already showed additional excited state dynamics for excitation beyond 800 cm^{-1} above the 0-0 transition. The single vibronic level fluorescence emission spectra presented in this section confirm this conjecture. In Figure 3.9a, one can see a few discrete vibronic bands which could suggest a restricted IVR, while Figure 3.9b shows very broad emissions, characteristic of dissipative IVR. Due to spectral broadening and congestion of porphycene spectrum when excited with energy above 800 cm^{-1}, it was not possible to clearly assign the vibronic bands in the LIF excitation spectrum in this case.

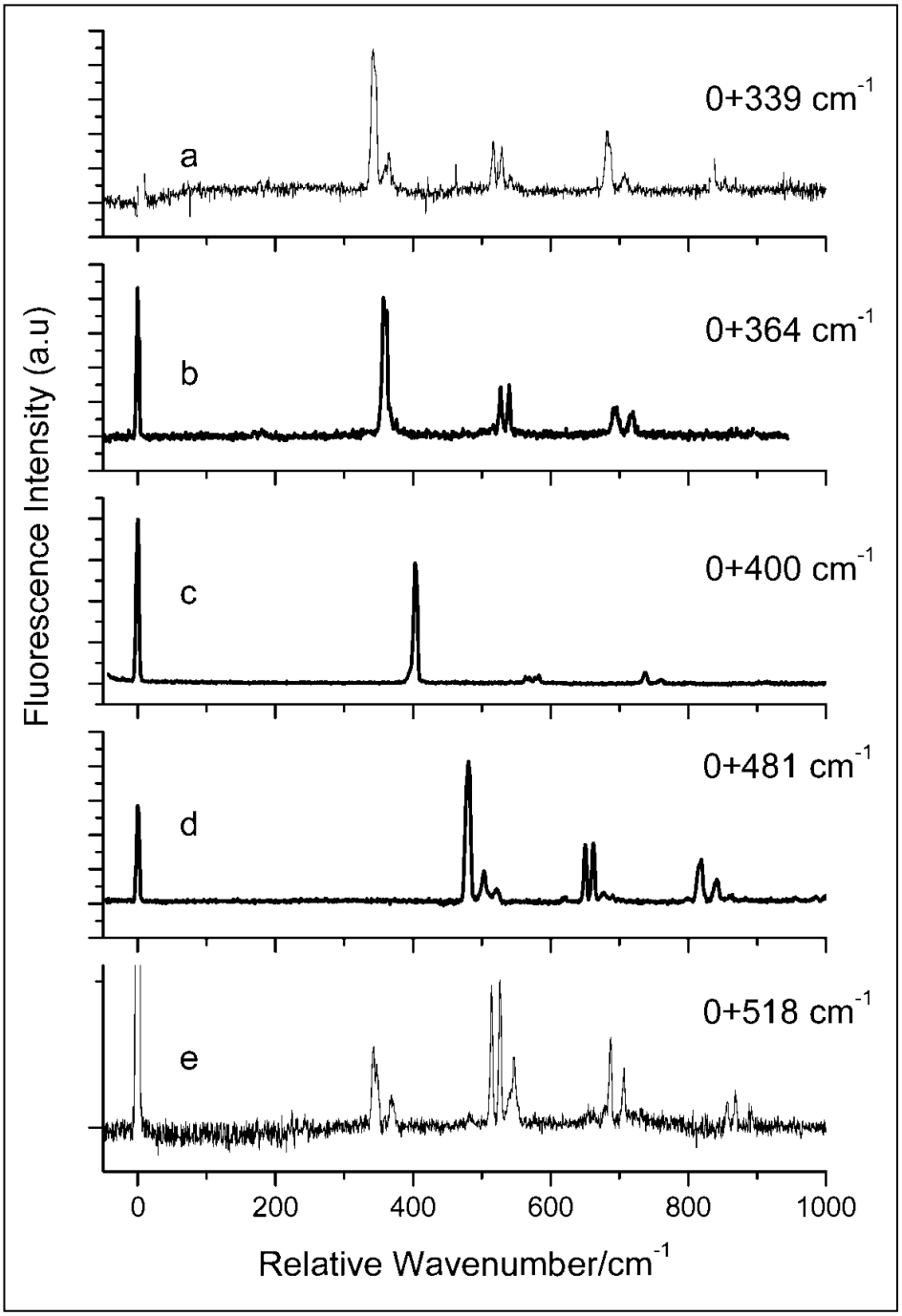

Figure 3.8 Dispersed fluorescence spectrum obtained for excitation into (a) 0+339, (b) 0+364, (c) 0+400, (d) 0+481, and (e) 0+518 cm^{-1} bands.

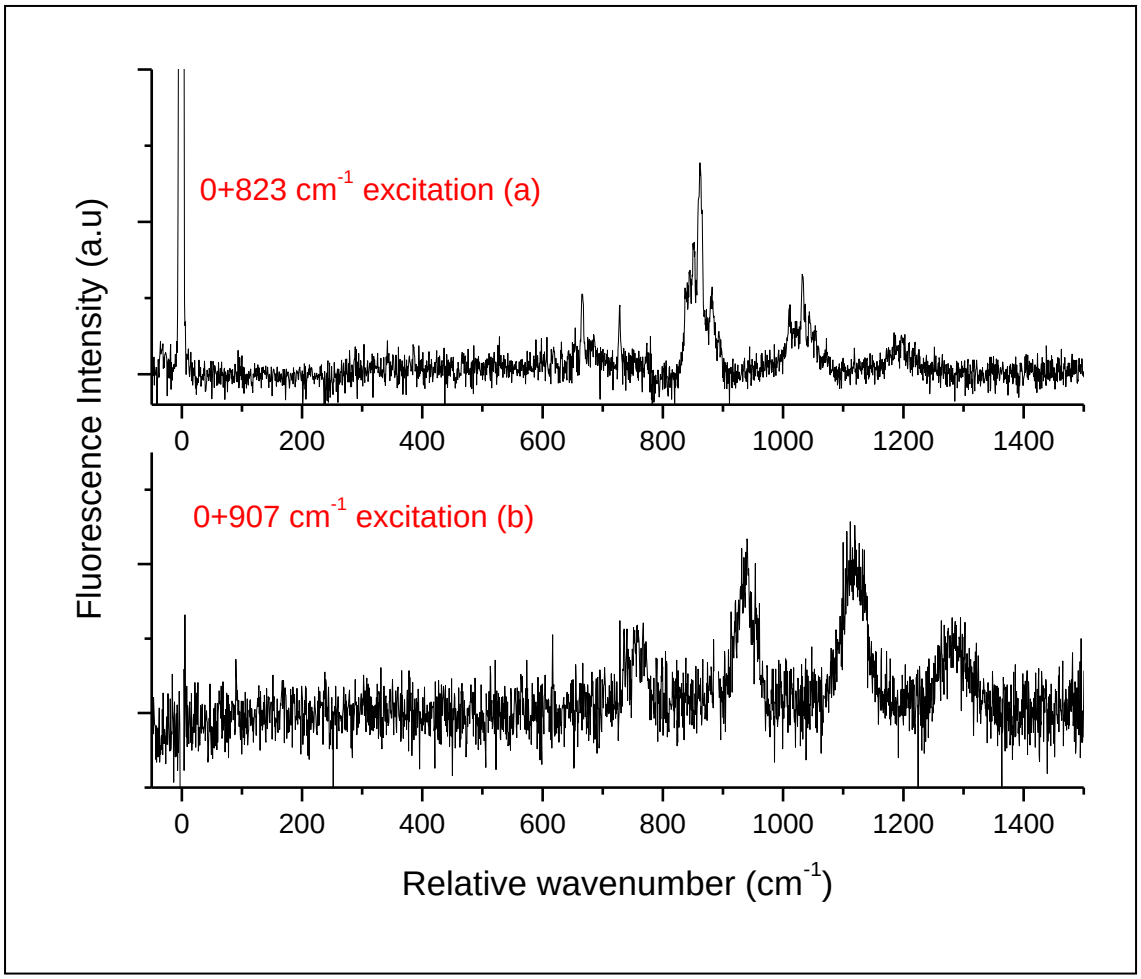

Figure 3.9 Dispersed fluorescence spectra obtained via excitation of (a) 0+ 826 cm^{-1} and (b) 0+909 cm^{-1} bands.

3.3 Comparison between experimental and calculated frequencies

Porphycene has 108 fundamental vibrations. The $\mathbf{C_{2h}}$ symmetry of the planar trans tautomeric forms dictate that eighteen A_u and thirty six B_u modes should be IR-active, whereas in the Raman and fluorescence, transitions involving thirty seven A_g and seventeen B_g modes are allowed. Inspection of IR and Raman spectra shows that the mutual exclusion principle is strictly obeyed, which provides a strong argument for the trans structure of porphycene. This finding also allowed a separate analysis of *gerade* and *ungerade* symmetry [97].

The analysis of SVL spectra allowed us to assign the origin of vibronic bands observed in the excitation and emission spectra of porphycene. Table 3.1 presented the assignment of over a hundred peaks (fifty doublets) observed in the LIF excitation spectrum in the range up to 850 cm^{-1} above the 0-0 transition. The analysis reveals the dominant role of totally symmetric modes, of which $2A_g$ is particularly active. Among the non-totally symmetric modes, $1B_g$ and $2B_g$ are present as fundamentals, combinations and overtones. A previously non-observed $3B_g$ mode was detected, both in LIF (combination with $2B_g$) and in emission (as a fundamental). Other modes observed for the first time are $1A_u$, $2A_u$, and $3A_u$; they were detected as combinations or overtones.

Optimization of geometry, followed by calculation of vibrational frequencies was performed for porphycene in both S_0 and S_1 electronic states. Figure 3.10 and Table 3.2 present the comparison between theory and experiment. Except for one mode in the S_1 state ($5B_g$) the agreement between theory and experiment is perfect. Practically the same fit quality is obtained for 6-31G(d,p) and 6-311++G(d,p) basis sets. For the ground state calculations, the double-zeta/triple zeta basis sets yield the scaling factor of 0.9802/0.9863, correlation coefficient r = 0.99983/0.99980, and the root mean square error of 8/9 cm^{-1}. For the S_1 calculations the corresponding values are 0.9902/0.9960, 0.99944/0.9993, and 12/13 cm^{-1}. Closer analysis reveals that not only the $5B_g$ mode in S_1, but in general, other out-of-plane vibrational transitions are calculated with worse accuracy than the in-plane modes, both for S_0 and S_1. This finding was recently discussed in another planar aromatic molecule, 1H-pyrrolo[3,2-*h*] quinoline. [187]

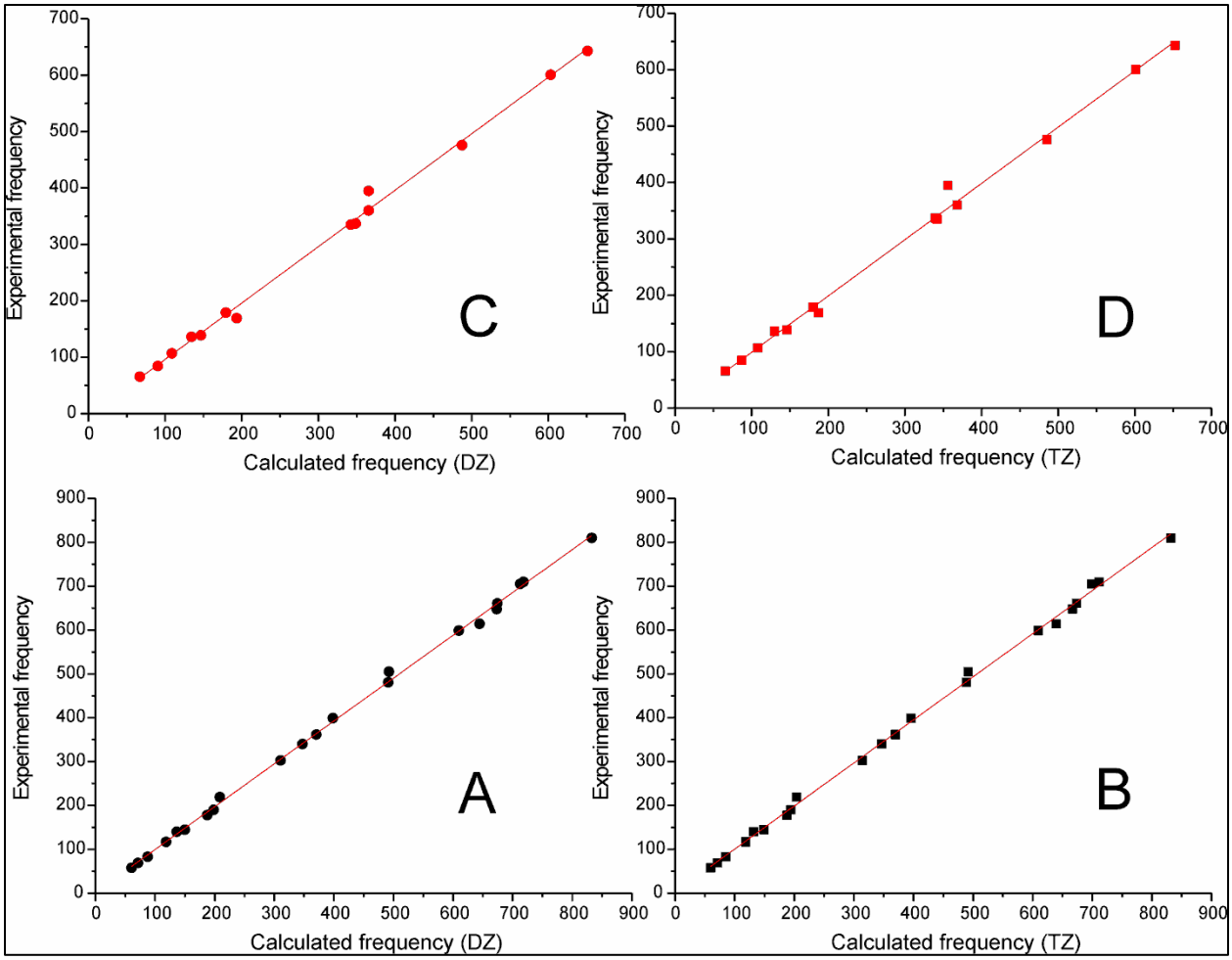

Figure 3.10 Comparison of experimental and calculated vibrational modes of porphycene in the ground (bottom) and the lowest excited singlet state (top). A and C are calculated frequencies using B3LYP/6-31G (d, p), B and D are calculated frequencies using B3LYP/6-311++G (d, p) calculations. The plots for S_0 include also the $8A_g$ mode at 810 cm^{-1}, [97] not observed in the present work.

Table. 3.2. Comparison of experimental and calculated low frequency modes of porphycene in S_0 and S_1 electronic states. The calculated values include scaling factors (see text).

S_0			S_1			Ass
Exp	6-31G(d,p)	6-311++G(d,p)	Exp	6-31G(d,p)	6-311++G(d,p)	
58	60	59	--	55	54	$1A_u$
69	71	70	65,5	66	65	$2A_u$
83	87	84	84,5	90	87	$3A_u$
117	116	117	107	108	107	$1B_g$
140	133	130	136	133	129	$2B_g$
145	147	147	139	145	146	$1A_g$
178	184	185	179	177	179	$2A_g$
190	194	191	169	191	186	$3B_g$
219	204	201	--	-	-	$4B_g$
303	311	310	283 [a]	284	290	$5A_u$
340	340	342	335	339	340	$3A_g$
362	363	365	360	362	367	$4A_g$
399	390	390	395	362	355	$5B_g$
481	482	482	476	483	483	$5A_g$
505	483	485	-	-	-	$6B_g$
614	632	630	-	-	-	$7B_g$
599	598	601	601	597	599	$6A_g$
648	660	658	-	-	-	$8B_g$
661	661	664	643	645	650	$7A_g$
705	699	690	-	-	-	$9B_g$
710	704	702	-	-	-	$10B_g$
810	816	820	--	--	--	$8A_g$

[a] estimated assuming 54 cm^{-1} for the frequency of $1A_u$.

3.4 Dynamics of intramolecular energy flow

The fact that the vibronic levels are split due to tunneling provides an opportunity to trace the relaxation of the initially excited levels by looking at the relative intensities of the doublet components. In most cases, selective excitation into either component of a tunneling doublet results in the emission from both (+) and (-) levels, demonstrating efficient equilibration on the time scale of S_1 lifetime. It should be recalled that the tunneling splitting in S_1 are small, of the order of a fraction of a wavenumber. [101] In order to evaluate the rate constant for equilibration in S_1, we carried out time-resolved experiments, searching for a possible delay between the onset of two emissions. No such delay could be determined while exciting into the origin. The time resolution of our oscilloscope is about 1ns, implying that the relaxation rate is above 10^9 s^{-1}.

Assuming tunneling splitting of 0.02 cm^{-1} in the S_1 state, the tunneling time would be about 1 ns Since the expected fluorescence lifetime is above 10 ns, the molecules excited into the origin can fully relax before emission. The situation may be different for excitation into higher vibronic levels. As already discussed, the emission spectra change significantly for the excess energy above 800 cm^{-1}.

For lower frequency vibrations the relaxation seems to be efficient. However, closer inspection of the spectra reveals remarkable exceptions, in particular for low-frequency modes. For the $2A_g$ pair, the relative intensities are practically the same no matter whether lower (179 cm^{-1}) or upper (184 cm^{-1}) tunneling pair is excited. This is not the case for $1B_g$ and $2B_g$ doublets (107/112 and 136/141 cm^{-1}, respectively) for which the emission occurs from the initially excited levels (Figure 3.5).

An interesting alternation of relative intensities is observed for the progressions of the $2A_g$ vibration, the mode which exhibits the largest splitting. It is also the most active mode in the fluorescence spectra. Because of considerable spectral separation of the doublet components of this mode and its activity, this vibration can be analyzed in detail by inspection of the SVL spectra, discussed in the next Section.

3.5. Mode-selective and vibrational-level-dependent tunneling splittings

Both supersonic jet [72] and helium nanodroplets [101] studies demonstrated that tunneling splitting in porphycene is mode-selective. The largest value of the splitting, 12 cm^{-1}, is observed for the $2A_g$ mode and its combinations with $3A_g$ and $4A_g$, for the $1A_g$ and $7A_g$ vibrations the splitting is negligibly low, whereas for other modes ($3A_g$, $4A_g$, $2x3A_g$, $3A_g+4A_g$) the values are similar to that observed for the zero-point energy level, 4.4 cm^{-1}. Our present results allow us to determine the values of tunneling splitting for the states in which two ground state vibrations are simultaneously excited, as well as to observe the values for different excitation levels of a particular mode. Due to the spectral resolution of our instrument, we could reliably monitor the changes in the $2A_g$ mode, the one that exhibits the largest splitting. Table 3.3 shows the values obtained for coexcitation of different S_0 vibrational levels. Two important features are evident. The first is the lowering of tunneling splitting of $2A_g$ for states in which, in addition to this mode, another vibration is excited. This was found for $1A_g$, $1B_g$, and $2B_g$ modes. The forms of these modes are shown in figure 3.11 below.

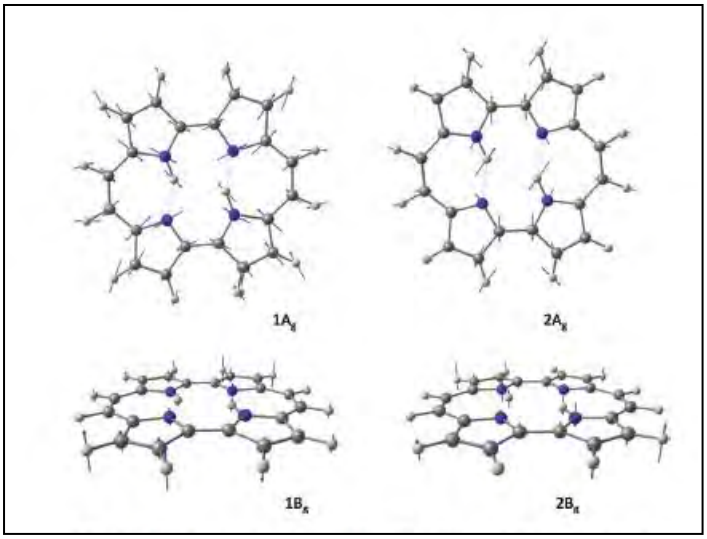

Figure 3.11 Displacement vectors of $1A_g$, $2A_g$, $1B_g$ and $2B_g$ normal modes obtained using B3LYP/6-311++G (d, p) calculation.

In Car-Parrinello molecular dynamics study of tautomerism in porphycene, simulation of simultaneous excitation was performed for $1A_g$, the "inhibiting" mode which reveals no tunneling splitting and $2A_g$, the "enhancing" mode with a large splitting. [70] The results indicated that the enhancing nature of $2A_g$ prevails over the inhibiting character of $1A_g$. This is in line with the present finding, since the tunneling splitting of 8 cm^{-1} measured for the $1A_{g_1}^{1}2A_{g_1}^{0}$ transition is almost twice higher than the value of 4.4 cm^{-1} observed for the vibrationless level. Regarding $1B_g$, and $2B_g$ modes, their out-of-plane character could suggests weakening of intramolecular hydrogen bonds during vibrational motion, which should result in a smaller splitting. Our spectral resolution is too small to verify this by looking directly at these modes, not at combinations, but a splitting somewhat smaller than 5 cm^{-1} and the lack of splitting observed for $1B_g$ and $2\times1B_g$ excitations, respectively, suggests it may be the case.

The second characteristic feature is a substantial increase of tunneling splitting for the overtones of $2A_g$. The values of 12, 19, and 24 cm^{-1} have been obtained for v=1, 2, and 3, levels respectively, which shows the crucial character played by this mode in the tautomerization path. Moreover, large values of the splitting allow us to hope that reliable splitting values could also be obtained for porphycene with one or perhaps even two internal protons exchanged for deuterons.

Table 3.3 also shows that the relative intensities of the bands forming tunneling doublets vary quite strongly. In particular, observation of S_0 overtones of $2A_g$ (Figure 3.7a-b) reveals the reversal of intensities for transitions ending on v=1 and v=2. Moreover, the reversal is also observed for a particular ground state vibrational levels when the excited state level changes from v=1 to v=2. These findings may be interpreted as indicating different energy order of (+) and (-) levels for even and odd vibrational quantum numbers.

Table 3.3. Ground state tunneling splitting of the $2A_g$ mode obtained from SVL spectra for different vibrationally excited levels.

Excitation [a]	Transition	Tunneling splitting [cm^{-1}]	Relative intensities [b] I_{low}/I_{high}
0^-_-	$2A_{g_1}^{\ 0}$	12	1.3
0^+_+	$2A_{g_1}^{\ 0}$	12	1.2
136	$2A_{g_1}^{\ 0}2B_{g_1}^{\ 1}$	7	2.1
141	$2A_{g_1}^{\ 0}2B_{g_1}^{\ 1}$	7	2.0
144	$1A_{g_1}^{\ 1}2A_{g_1}^{\ 0}$	8	0.9
155	$2A_{g_1}^{\ 0}2A_{u1}^{\ 1}3A_{u1}^{\ 1}$	13	0.8
179	$2A_{g_1}^{\ 1}$	12	0.9
184	$2A_{g_1}^{\ 1}$	12	0.8
220	$2A_{g_1}^{\ 0}1B_{g_1}^{\ 2}$	6	1.8
335	$2A_{g_1}^{\ 0}3A_{g_1}^{\ 1}$	12	1.2
339	$2A_{g_1}^{\ 0}3A_{g_1}^{\ 1}$	13	1.2
360	$2A_{g_1}^{\ 0}4A_{g_1}^{\ 1}$	13	1.1
362	$2A_{g_1}^{\ 2}$	12	1.6
362	$2A_{g_2}^{\ 2}$	20	0.5
362	$2A_{g_3}^{\ 2}$	24	2.0

364	$2A_{g_1}^{\ 0}4A_{g_1}^{\ 1}$	12	1.2
476	$2A_{g_1}^{\ 0}5A_{g_1}^{\ 1}$	11	1.2
481	$2A_{g_1}^{\ 0}5A_{g_1}^{\ 1}$	12	0.9
514	$2A_{g_1}^{\ 1}3A_{g_1}^{\ 1}$	13	0.6
514	$2A_{g_2}^{\ 1}3A_{g_1}^{\ 1}$	20	0.9
518	$2A_{g_1}^{\ 1}3A_{g_1}^{\ 1}$	12	0.9
518	$2A_{g_2}^{\ 1}3A_{g_1}^{\ 1}$	20	1.2
521	$2A_{g_1}^{\ 1}1A_{u_1}^{\ 1}5A_{u_1}^{\ 1}$	15	2.1
532	$2A_{g_1}^{\ 1}1B_{g_2}^{\ 2}2B_{g_1}^{\ 1}$	15	1.7
532	$2A_{g_2}^{\ 1}1B_{g_2}^{\ 2}2B_{g_1}^{\ 1}$	20	1.8
541	$2A_{g_1}^{\ 3}$	12	2.0
541	$2A_{g_2}^{\ 3}$	20	1.2

[a] Excess energy [cm^{-1}] counted from 0_-^-; [b] indices low/high correspond to the transition energy of $2A_g$ doublet components; estimated maximum error: ±30%.

3.6. Double proton tunneling in the S_1 state

We have noticed an "anomaly" that selective excitation of one of the components of the tunneling doublet ($0_+^+ \; or \; 0_-^- \; excitation \; for \; example$) shows fluorescence from both tunneling states. Such observation would have been expected either both $0_+^+ \; and \; 0_+^-$ excitations are allowed or if the second state is produced due to population after selective excitation of the first state as shown in the figures 3.12 a and b below.

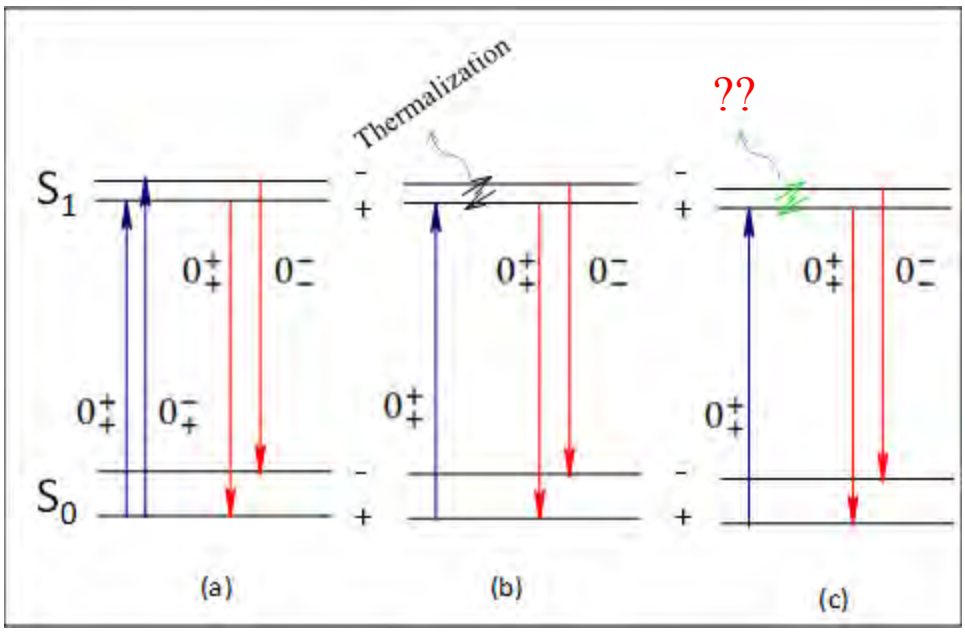

Figure 3.12 Simplified Jablonski diagrams to explain dual emission following selective excitation. (a) explains the direct access of two emitting states from a single ground state while (b) shows population of the second emitting state following thermalization. (c) Shows excited state population of the second state via a mechanism by which double emission is observed following selective excitation. At this stage, it was not possible to clearly propose a possible phenomena for the population of the second state.

However, spectroscopic transition selection rule dictates transition between states of the same parity (i.e, either 0_+^+ *or* 0_-^- transitions) are allowed hence the mechanism in Figure 3.12 a cannot be the reason. The explanation in Figure 3.12 b would be possible if there is effective collision between the molecules under investigation. However, such precondition is not allowed in supersonic-jet condition where effective collisions are negligible. At this stage, it was not possible to give specific mechanism for the population of the second state.

3.7 *Single vibronic level life time measurements of porphycene and Pc-d_{12}*

Additional information about excited state dynamics of porphycene comes from single vibronic level fluorescence lifetime measurement. Fluorescence decay from excitation of a single vibronic level was measured as an average of three sets of measurements; each set accumulating 512 decays (see Table 3.4).

Table 3.4 shows the measured fluorescence life times of porphycene from various vibronic levels.

Excitation energy (cm^{-1})	Assignment	Fluorescence lifetime, τ (ns)	$\Delta\tau$ = (+/+)-(-/-)
0-0 (-/-)		27.4	1.78
0-0 (+/+)		29.2	
136	$2B_{g\,0}^{1}$ (-/-)	26.1	0.81
141	$2B_{g\,0}^{1}$ (+/+)	26.9	
179	$2A_{g\,0}^{1}$ (-/-)	26.5	-0.83
184	$2A_{g\,0}^{1}$ (+/+)	25.7	
215	$1B_{g\,0}^{2}$ (-/-)	22.42	3.11
220	$1B_{g\,0}^{2}$ (+/+)	25.53	
238	$1B_{g\,0}^{1}$ (-/-) $2A_{u\,0}^{2}$ (-/-)	25.37	-1.98
242	$1B_{g\,0}^{1}$ (+/+) $2A_{u\,0}^{2}$ (+/+)	23.39	
305	$2B_{g\,0}^{1}$ (-/-) $3B_{g\,0}^{1}$ (-/-)	22.09	2.88
309	$2B_{g\,0}^{1}$ (+/+) $3B_{g\,0}^{1}$ (+/+)	24.97	
315	$2A_{g\,0}^{1}$ (-/-) $2B_{g\,0}^{1}$ (-/-)	24.02	1.12
320	$2A_{g\,0}^{1}$ (+/+) $2B_{g\,0}^{1}$ (+/+)	25.14	
318	$1A_{g\,0}^{1}$ (-/-) $2A_{g\,0}^{1}$ (-/-)	25.14	-2.55
323	$1A_{g\,0}^{1}$ (+/+) $2A_{g\,0}^{1}$ (+/+)	22.59	
335	$3A_{g\,0}^{1}$ (-/-)	26.07	0.45
339	$3A_{g\,0}^{1}$ (+/+)	26.52	
337	$1A_{u\,0}^{1}$ (-/-) $5A_{u\,0}^{1}$ (-/-)	-	----------
342	$1A_{u\,0}^{1}$ (+/+) $5A_{u\,0}^{1}$ (+/+)	26.32	
358	$2A_{g\,0}^{2}$ (-/-)	24.37	1.25
362	$2A_{g\,0}^{2}$ (+/+)	25.62	
360	$4A_{g\,0}^{1}$ (-/-)	25.16	-3.15
364	$4A_{g\,0}^{1}$ (+/+)	22.01	
371	$1B_{g\,0}^{1}$ (-/-) $2B_{g\,0}^{1}$ (-/-) $2A_{u\,0}^{2}$ (-/-)	-	----------
375	$1B_{g\,0}^{1}$ (+/+) $2B_{g\,0}^{1}$ (+/+) $2A_{u\,0}^{2}$ (+/+)	24.03	
394	$2A_{g\,0}^{1}$ (-/-) $1B_{g\,0}^{2}$ (-/-)	11.9	0.2
398	$2A_{g\,0}^{1}$ (+/+) $1B_{g\,0}^{2}$ (+/+)	12.1	
476	$5A_{g\,0}^{1}$ (-/-)	11.3	1.9
481	$5A_{g\,0}^{1}$ (+/+)	13.2	

The fluorescence lifetime generally tends to decrease with increasing excitation energy and does not show any significant dependence on the symmetry of vibrational levels in the S_1 state, as it was observed for Pc-d_{12} (see Figure 3.13). Interestingly, a sudden decrease (almost twofold) in the fluorescence life time was found for porphycene itself for vibratios above c.a 390cm^{-1}.

More detailed investigations are needed, however, to explain this interesting behavior, having in mind a regular behavior for Pc-d_{12}.

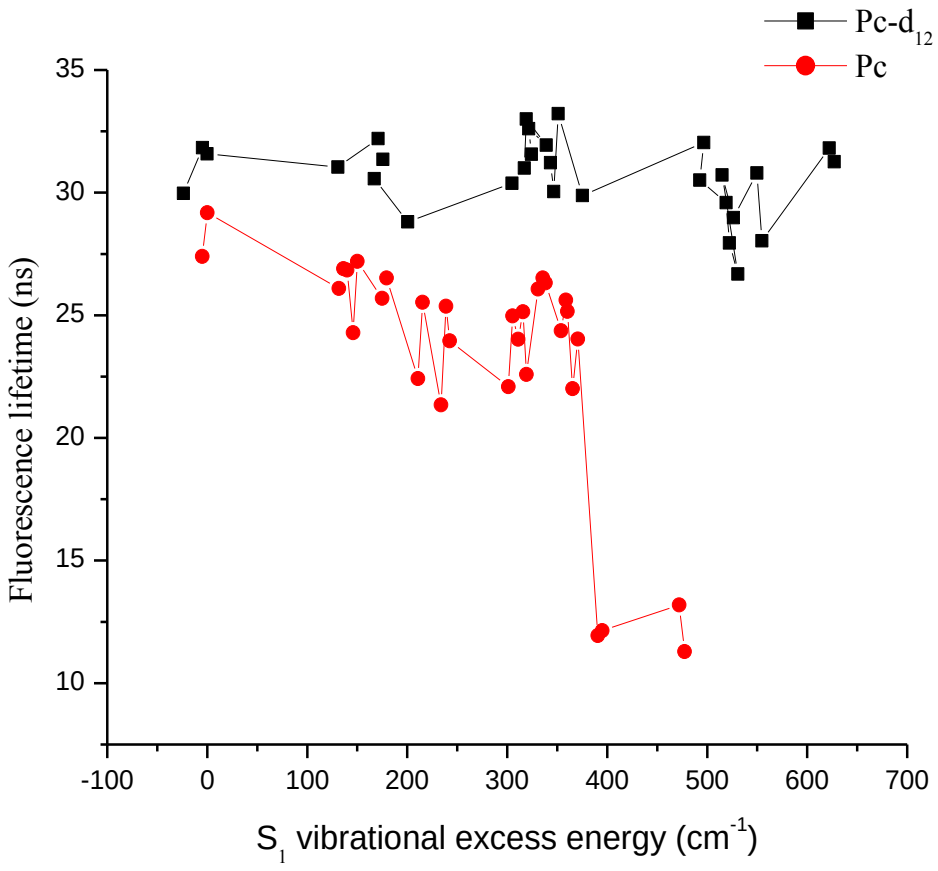

Figure 3.13 A plot of fluorescence life time versus excitation energy of porphycene and Pc-d_{12}.

3.8 Conclusions

LIF excitation spectra in combination with hole burning spectroscopy have revealed several transitions of porphycene which have never been reported so far. Combined with quantum chemical calculations, this procedure led to the precise assignment of low frequency vibrations of porphycene in the S_1 state. Almost all the single vibronic level fluorescence spectra give a simple pattern dominated by one sequence origin band, which makes the assignment and correlation of the vibronic bands in the S_0 and S_1 states pretty straightforward. Comparison of the spectroscopic characteristics of the tunneldoublets of the origin band has also been made. In most cases, the DF spectra of the doublets are similar. Single vibronic level fluorescence study also shows that the excited state dynamics is dominated by IVR for excitation energy exceeding c.a 800 cm^{-1}. Based on single vibronic level fluorescence study in combination with quantum chemical calculations, unambiguous assignment of the S_0 and the S_1 vibrations of porphycene were made. Moreover, our results demonstrate that the low frequency vibration in the electronically excited S_1 state can now be computed with the accuracy comparable to that of the ground state.

It turned out that the excitation into each of the two tunneling doublets gives similar spectral features in the DF spectra. Guided by the spectroscopic similarity, we were able to identify and compare the spectroscopic characteristics of various pairs of tunneling doublets, using selective excitation into the bands observed in the LIF excitation spectrum. For several cases, coupling of the $2A_g$ mode with other vibrations was observed, resulting in the lowering of tunneling splitting. Most interesting, the tunneling splitting of the $2A_g$ mode progressions were found to strongly increase in the S_0 state. Since the $2A_g$ mode is considered crucial for the promotion of tautomerization in porphycene, more detailed investigations are presented in chapter four. These studies lead to a better understanding of the multidimensional character of doubly hydrogen transfer in porphycene.

Chapter four

Low frequency assisted double proton tunneling in porphycene: Experiment and Theory

As stated in the previous chapters, knowledge of proton tunneling reactions needs detailed understanding of the potential barrier and its dependence on different vibrational modes. An additional question when dealing with double proton transfer is the notion of "concerted " versus "stepwise" mechanisms [24,70,88,101] . In concerted mechanism, the most stable trans isomer of porphycene involves a "simultaneous" hydrogen transfer leading to equivalent isomer while in stepwise mechanism, one hydrogen is first transferred to form an intermediate cis-isomer followed by the second hydrogen transfer to form the second equivalent trans isomer or back hydrogen transfer to restore the original isomer. Results from fluorescence anisotropic study of porphycene in polymer films [88, 95, 102, 188] are in agreement with the concerted proton transfer mechanism.

Concerning vibrational mode dependence of tunneling splitting, Vdovin et.al [88,101] have shown different tunneling splittings for different vibrations of porphycene in the ground state. Based on the extent of tunneling splitting three types of vibrational modes, promoting (those splitted by 12 cm^{-1} or more), neutral (mode splitted by 4.4 cm^{-1}) and hindering (modes which do not show splitting within the experimental resolution) modes have been identified. The differences in tunneling splitting in different vibrational modes show coupling of proton transfer coordinate with other modes and hence multidimensional character of the potential energy surface (PES) for proton transfer. This observation has also been strengthened by the experimental results (Chapter 3) from LIF excitation near a saturation regime, hole burning spectroscopy, and extensive single vibronic level (SVL) dispersed fluorescence measurements of supersonic jet-isolated porphycene, along with quantum chemical calculations. It was also possible to demonstrate the multidimensional nature of proton tunneling and the importance of mode coupling in influencing the process, for we have seen different values of tunneling splittings for different fundamentals, progressions and combinations of vibronic transitions. This picture was confirmed by theoretical studies, based on Car-Parinello molecular dynamics simulations. [97]

When vibrational motion couple to proton transfer , the tunneling splitting in the vibrationally excited level may increase (promoting) or decrease (hindering) due to the change in the tunneling potential energy surface. [189]

In this chapter the results from LIF excitation and single vibronic level dispersed fluorescence (SVLF) spectral measurements via selective excitation of a totally symmetric low frequency mode (**$2A_g$**) and its harmonic progressions (**$2x2A_g$** and **$3x2A_g$**) in porphycene (Pc), mono-deuterated porphycene (Pc-d_1) and doubly deuterated porphycene (Pc-d_2) are presented. In this case the deuterations are performed in the internal nitrogen cavity of porphycene. Coupling between this mode and the tunneling coordinate has been observed. Then the calculated energy split were fitted to the experimental ones using two-dimensional symmetric mode coupling (SMC) and V-parabola model. [147, 150]

4.1. Laser induced fluorescence (LIF) excitation spectra

Because pure samples of Pc-d_1 and Pc-d_2 are not available in pure forms, they were produced from pure porphycene by seeding a deuterating agent (Methanol (MeOD) in this case) in the carrier gas. This procedure results in the formation of Pc-d_1 from partial deuteration, Pc-d_2 from complete deuteration and unsubstituted pure porphycene. For convenience the name Pc-mix is adopted for the mixture. LIF excitation spectra of Pc-mix (black) and pure Pc (red) isolated in supersonic jet are presented in Figure 4.1.

Comparison of the spectra in Figure 4.1 shows the appearance of new bands around 16139.4 and 16119 cm^{-1}. The first band is red-shifted by about 24 cm^{-1} from the 0-0 transition of Pc (16163.44 cm^{-1}). A similar red shift (about 24 cm^{-1}) was observed for parent porphycene when one of the internal NH hydrogens had been exchanged by deuterium showing the reproducibility of the result[45,101,147]. Therefore, we assign the band at 16139.4 cm^{-1} as the 0-0 transition of Pc-d_1, where one of the cavity NH hydrogens in Pc is replaced by deuterium. The second band at 16119 cm^{-1} is red-shifted by about 44 cm^{-1} relative to the origin of Pc and it is assigned as the 0-0 transition of Pc-d_2 where both internal NH hydrogens are exchanged by deuterons.

Identification of $2A_g$ mode and its second harmonic, $2x2A_g$ in Pc-d_1 and Pc-d_2 requires comparison of the LIF excitation spectrum of Pc-mix with that of parent porphycene. The identification of especially $2x2A_g$ mode in Pc-d_1 and Pc-d_2 is further complicated by the method of deuteration of parent porphycene in supersonic-jet. After preparation of Pc-d_1 and Pc-d_2 there is still plenty of pure porphycene sample left in the molecular beam sample. Therefore, the resulting LIF excitation spectrum is actually a contribution from the three species. Fortunately, the relative position of $2A_g$ mode is not affected by deuteration. So it is expected that the relative positions of $2A_g$ and its harmonic progressions in Pc-d_1 and Pc-d_2 are more or less at the same relative position as that of parent porphycene.

$2A_g$ mode is found at 179.6, 180 and 180.5 cm^{-1} for Pc, Pc-d_1 and Pc-d_2, relative to the origin of the respective species. As shown in Figure 4.1, this mode is splitted by 4.4 cm^{-1} in Pc while splitting is not observed for the deuterated porphycenes indicating suppression of proton tunneling in the deuterated isotopomers. Comparison of LIF excitation spectrum of the mixture

with that of pure porphycene in wavelength scale shows that $2A_g$ modes of Pc and Pc-d_1 are relatively isolated. Therefore selective excitation of these modes give a fluorescence spectra corresponding to the respective "pure" species. On the other hand, the position of $2A_g$ mode of Pc-d_2 overlap with the other vibration of porphycene which is already assigned as $2B_g$ mode (Table 3.1). Therefore, fluorescence from selective excitation of this mode is expected to show contributions from both Pc and Pc-d_2 and hence a careful comparison of the mixed spectrum with spectrum of pure porphycene at the same excitation wavelength is necessary. Similarly, the second harmonic $2A_g$ mode ($2A_{g\,0}^2$) is observed at 360.3, 359.8 and 359 cm^{-1} for Pc, Pc-d_1 and Pc-d_2 relative to the origins of the respective isotopologues.

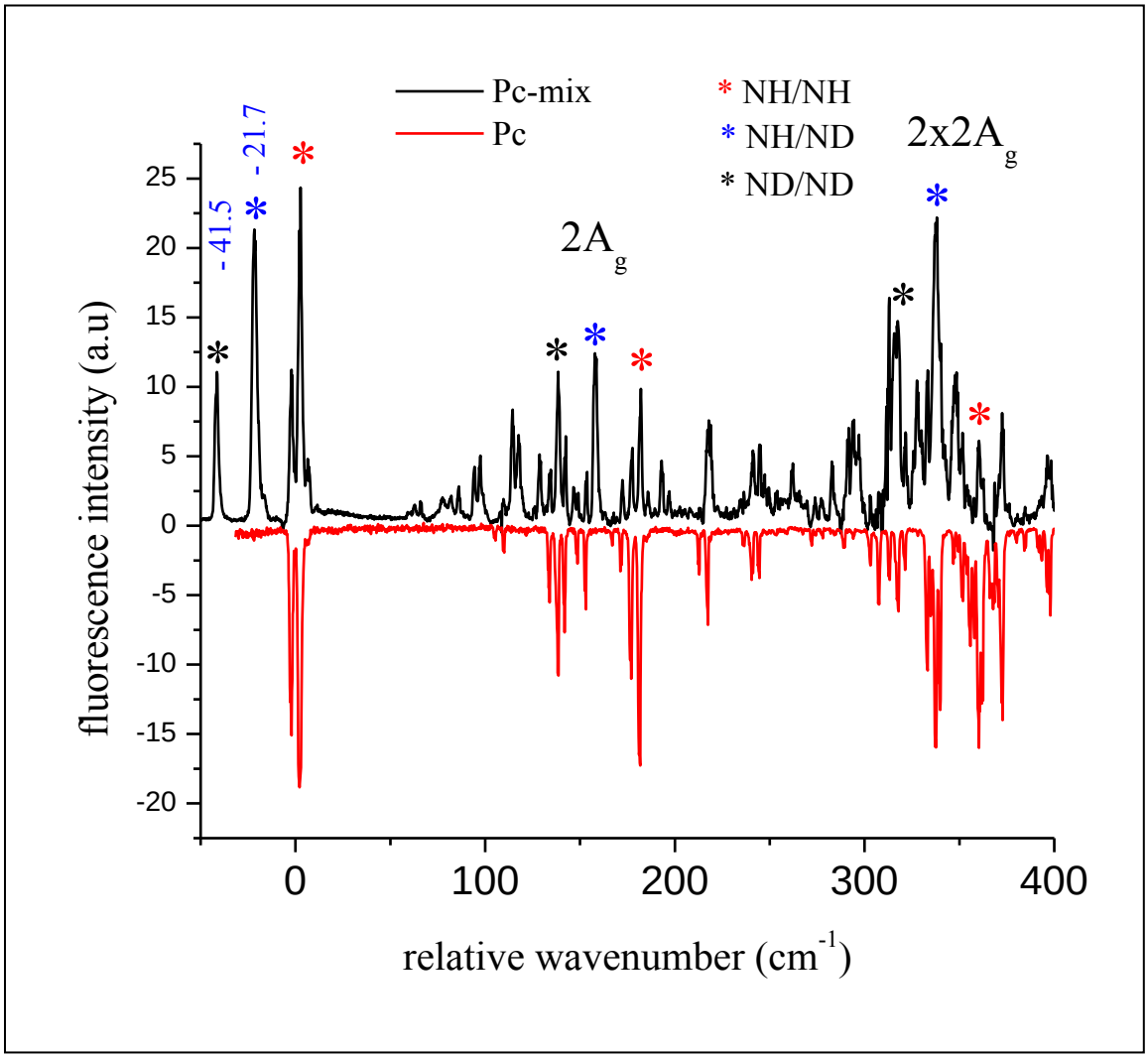

Figure 4.1 Laser-induced fluorescence excitation spectra of Pc-mix (black) and pure Pc (red) in a supersonic jet. The spectrum of pure Pc is mirror reflected for easier comparison.

4.2 Single Vibronic level dispersed fluorescence spectra

4.2.A 0-0 Excitation

Dispersed fluorescence spectra of Pc, Pc-d_1 and Pc-d_2 via excitations of the respective origin bands are presented in Figure 4.2 a, b and c.

The results show that the tunneling splitting observed in $2A_g$ mode of Pc disappears when one or both inner NH hydrogen atoms of porphycene are exchanged with deuterons indicating lower proton tunneling rate in the deuterated isotopomers. A decrease in the value of tunneling splitting is also observed for other modes. For example 3Ag and 4Ag modes observed at about 340 and 365 cm^{-1}, respectively, show tunneling splitting of about 4.4 cm^{-1} in Pc while the splitting disappears in the deuterated isotopomers. Similar studies had been carried out in He nanodroplets which essentially showed the same results [101]. However, the experimental resolution in the droplets was high enough to see the tunneling splitting of 2.3 cm^{-1} in $2A_g{}^0{}_1$ mode of Pc-d_1 which is below the resolution of our set-up (about 4 cm^{-1}). In the spectra presented, we do not observe the harmonic progressions of $2A_g$ mode and associated tunneling splitting.

4.2.B 0 +180 cm^{-1} Excitation

Fluorescence spectrum from a single vibronic level of a molecular vapour is proved to be important in many cases in detecting the high vibrational levels of the ground state [190,191]. Fig.4.3 a, b and c shows fluorescence spectra after 0+180 cm^{-1} excitation of Pc, Pc-d_1 and Pc-d_2, respectively.

As expected, selective excitation of 0+180 cm^{-1} mode helps to see progressions of $2A_g$ mode up to n=3. It was found that tunneling splitting in $2A_{g1}{}^1$ mode is increasing from 12 cm^{-1} to 19 cm^{-1} in $2A_{g\,2}{}^1$ and to 25 cm^{-1} in $2A_{g\,3}{}^1$ progressions, respectively. This result is in line with earlier suggestions that the mode is promoting. Tunneling splittings in $2A_{g1}{}^1$ modes of Pc-d_1 and Pc-d_2 were not observed in our experiment. This might be because the splittings are too small to be resolved in our experiment (< 4 cm^{-1}). Results from high resolution spectroscopy of porphycene in helium nanodroplets showed tunneling splitting of 2.3 cm^{-1} for $2A_g$ mode of Pc-d_1 in the ground state. On the other hand, it was possible to observe a tunneling splitting of 5.6 cm^{-1} for $2A_{g\,2}{}^1$ transition (n=2 level) of Pc-d_1. The tunneling splitting for $2A_{g\,2}{}^1$ transition (n=2 level) of Pc-d_2 is not observed probably because it is still below the experimental resolution.

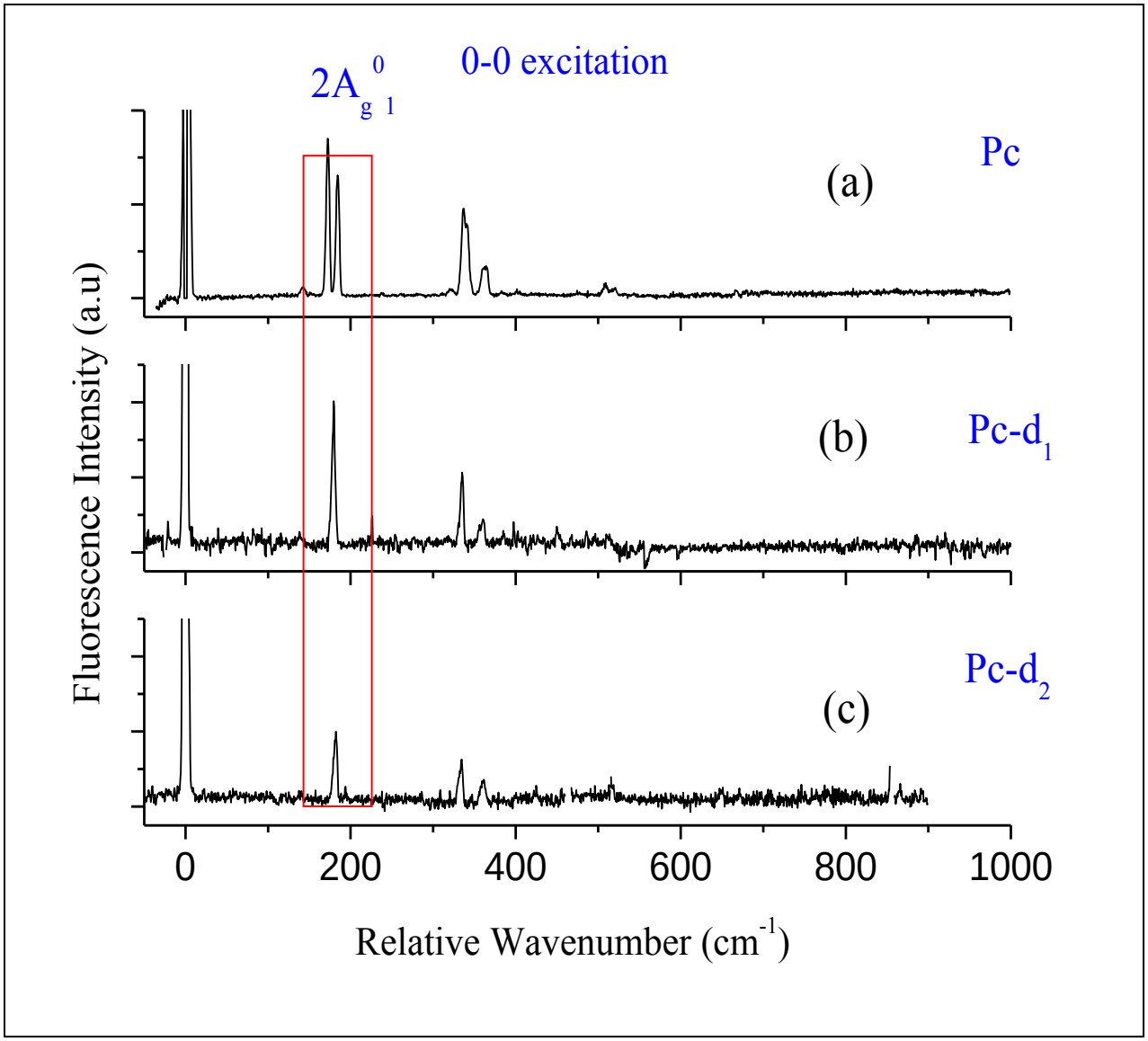

Fig. 4.2 Dispersed fluorescence spectra of (a) Pc, (b) Pc-d_1 and (c) Pc-d_2 via origin band excitation in supersonic jet.

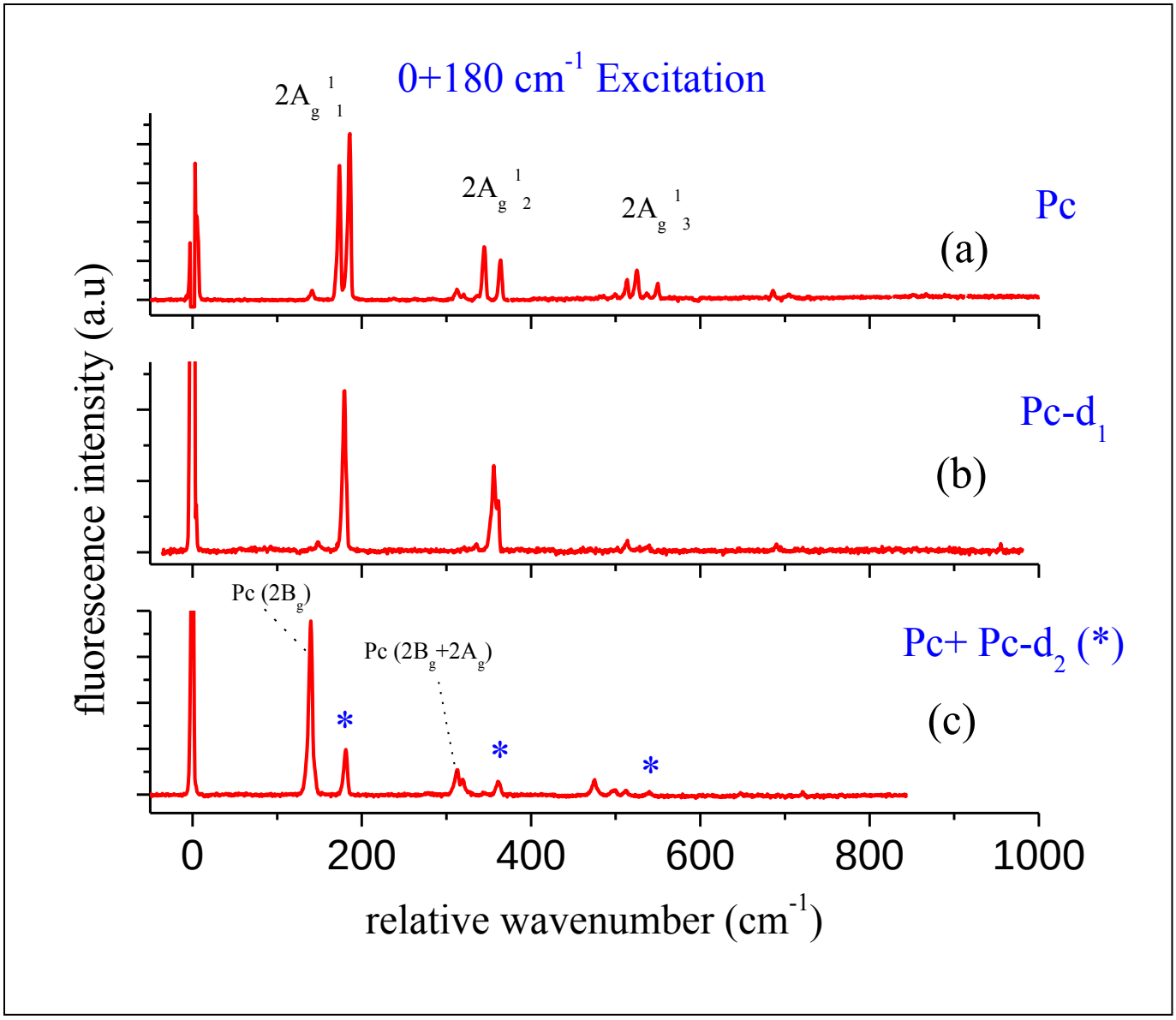

Figure 4.3 Dispersed fluorescence spectrum of obtained by excitation into $2A_{g_0}^1$ *transition of (a) Pc, (b) Pc-d$_1$ and (c) Pc-d$_2$ isotopomers in supersonic jet. The asterisks in (c) show transitions belonging to Pc-d$_2$.*

Another distinct feature in Figure 4.3 is that the dispersed fluorescence spectrum of Pc-d_2 (Figure 4.3.c) is different from the other two spectra. As explained earlier, the spectrum is found to be a contribution of dispersed fluorescence from pure porphycene (via $2B_g$ mode excitation) and Pc-d_2 (via $2A_{g0}^1$ excitation) (see Figure 4.4).

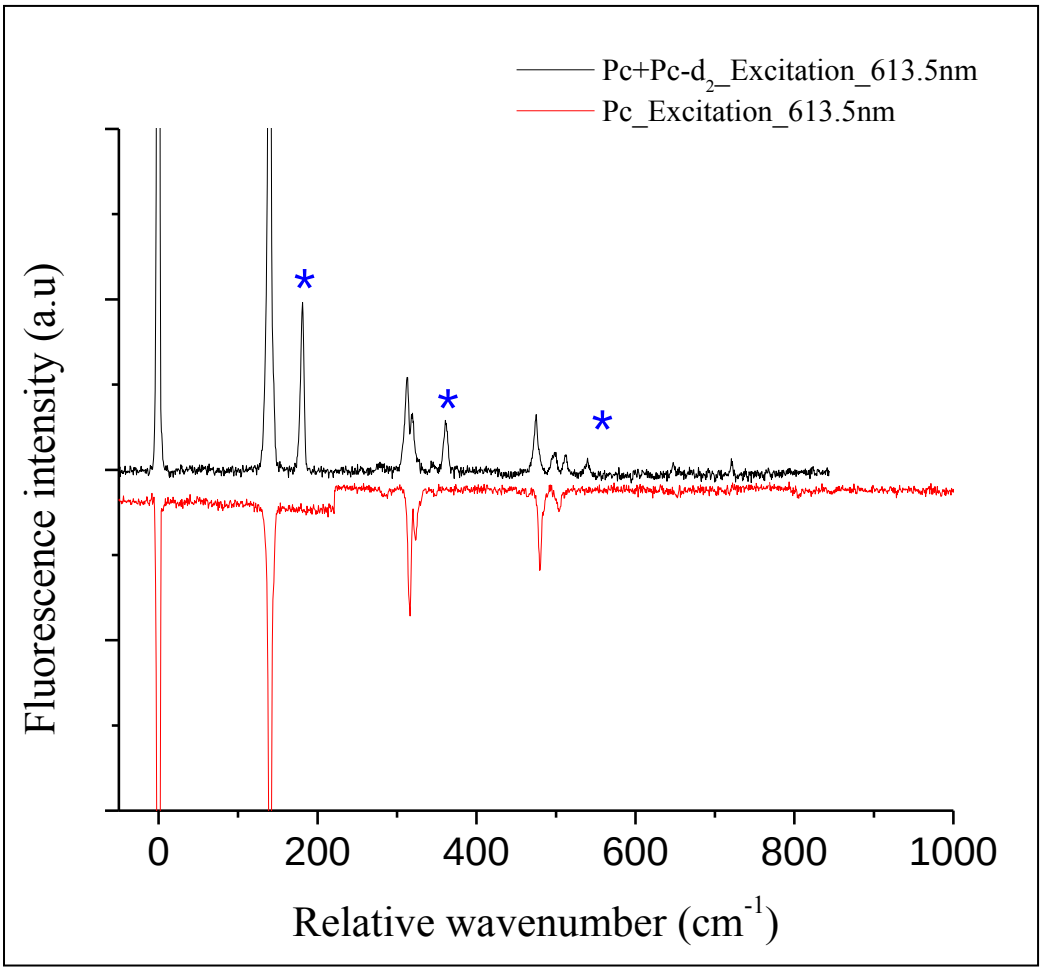

Figure 4.4 Dispersed fluorescence spectra of Pc-mix (black) and pure Pc (red) via excitation of the band at 0+141 cm^{-1} (613.5 nm) in a supersonic jet. The spectrum of pure Pc is mirror reflected for easier comparison.

Comparison of the spectra in Figure 4.4 with fluorescence spectrum from $2B_g$ mode (0+141cm^{-1}) excitation of pure porphycene was helpful to identify vibrations belonging to pure Pc-d_2 (marked with asterisks). Observation of tunneling splittings for both Pc and Pc-d_1 is an important result which gives a powerful insight while modeling the potential energy surface for proton tunneling

and even to predict tunneling splitting which are not observed in the experiment, especially for Pc-d_2. Summary of experimental and theoretical values of tunneling splitting in the 0 level, $2A_g$ and its progressions is summarized in Table 4.1.

4.2.C 0 +360 cm^{-1} ($2A_{g\,0}^{2}$) excitation

Inspired by the results above, we excited $2x2A_g$ level expecting to see a greater number of vibronic progressions in $2A_g$ mode in the ground state [191]. Dispersed fluorescence spectra of Pc, Pc-d_1 and Pc-d_2 via excitation of 0+360 cm^{-1} are presented in figure 4.5 a, b and c, respectively.

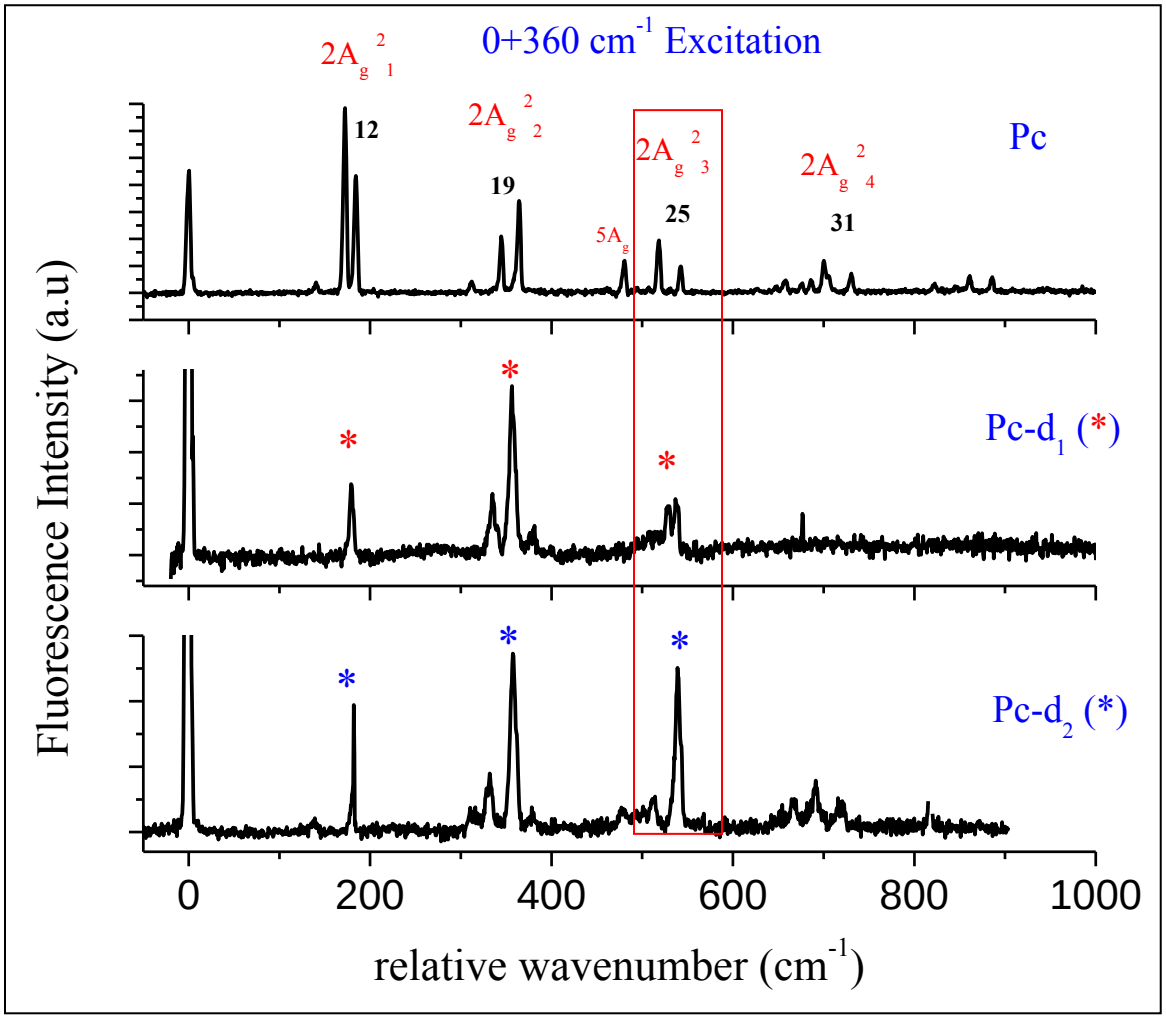

Figure 4.5 Dispersed fluorescence spectra of porphycene and isotopomers via excitation of $2A_{g0}^{2}$ mode in the respective species.

As shown in Figure 4.5, indeed progressions of $2A_g$ mode up to n=4 level are observed in the ground state. Tunneling splittings are found to be 12, 19, 25 and 31 cm^{-1} for n=1, n=2, n=3 and n=4 levels of $2A_g$ mode for Pc, respectively. It was also possible to observe tunneling splitting value of 9 cm^{-1} in n=3 level of $2A_g$ mode in Pc-d_1. Once again we found additional experimental values of tunneling splitting for Pc and Pc-d_1 in n=3 level of 2Ag mode that could be used as an input for modeling the proton transfer coordinate.

4.3 Two dimensional modeling of the potential energy surface

The modeling of intra-molecular proton tunneling in porphycene requires the knowledge of the local behavior (force constants) of the 108-dimensional potential energy surface (PES) obtained from ab initio studies. One could try to fit two-dimensional analytical approximation to this surface and investigate the dependence of the high frequency and low frequency oscillatory modes under consideration and then followed by comparison of the calculated energy splittings (the tunneling effect) with the observed ones from the single level dispersed fluorescence spectra. SMC model [147,150] was used as analytical functions to map the ground state PES.

4.3.1 SMC model

In the symmetric mode coupling (SMC) method we assume that the approximate potential is quartic along the high frequency mode (tunneling coordinate) and quadratic along the low frequency mode (promoting $2A_g$ mode). The dimensionless form of this potential has three independent parameters: g, ω, α, where g can be related to the average kinetic energy of the mode, ω – to the ratio of the frequencies and α – to the coupling strength between the modes.

$$H_{SMC} = T + V_{SCM} = -\frac{g^2}{2}\left(\frac{\partial^2}{\partial x^2} + \frac{\partial^2}{\partial y^2}\right) + \frac{1}{8}(x-1)^2(x+1)^2 + \frac{1}{2}\omega^2(\alpha(x^2-1)+y)^2$$

The fitting is done in such a way that the experimental 0 level tunneling splitting in the ground state was kept fixed and the parameters in the analytic function are varied until the 0 level splitting is reproduced. Then after, the tunneling splitting in $2A_g$ mode and its progressions are predicted. The results of fitting (Table 4.1) shows good correspondence for the calculated and observed tunneling splitting in the low frequency mode for porphycene (a) and monodeuterated isotopologue (Pc-d_1) (b).

Table 4.1 Calculated and observed tunneling splitting in the low frequency modes for porphycene (a) and monodeuterated isotopologue (Pc-d_1) (b) using SMC model.

a) The results of fitting parameters **ω, α** and **g** (**Pc**)

		$2A_g$	**$2x2A_g$**	**$3x2A_g$**
Frequency (experimental)	0	176.8	352.3	528.3
Frequency (Calculated)	0	176.2	352.0	527.5
Tunneling splitting (Expt)	**4.4**	**12**	**19**	**25**
Tunneling splitting (Calcul)	4.4	9.3	16.2	25.2
Parameters	ω → 0.092 ; α→ 6.4 ; g→0.0932			

For $\tilde{\omega}_x = 3080\ cm^{-1}$, $\tilde{x}_0 = 0.72$ Å , $m_x = 1.41$ and $\tilde{\omega}_y = 283.36\ cm^{-1}$

b) The results of fitting parameters **ω, α** and **g** (**Pc-d_1**)

		$2A_g$	**$2x2A_g$**	**$3x2A_g$**
Frequency (experimental)	0	176.8	358.7	533.5
Frequency (Calculated)	0	175.3	349.9	524.0
Tunneling splitting (Expt)	**0.58**[a]	**2.2** [a]	**5.6**	**9.8**
Tunneling splitting (Calcul)	0.58	2.2	5.7	11.9
Parameters	ω → 0.15 ; α→ 6.4 ; g→0.0932			

For $\tilde{\omega}_x = 2240\ cm^{-1}$, $\tilde{x}_0 = 0.72$ Å , $m_x = 2.23$ and $\tilde{\omega}_y = 336\ cm^{-1}$

[a] Experimental values are obtained from helium nanodroplet experiments.

One interesting result is that the experimental tunneling splittings in $2x2A_g$ and $3x2A_g$ transitions are well predicted by the SMC model. However, the model overestimates the frequency of the assisting mode, ($\tilde{\omega}_y$) both in Pc and Pc-d_1 predicting a frequency of 283 and 336 cm^{-1} in the former and the latter species while the experimental value of this mode is about 180 cm^{-1} in both species.

Figures 4.6 a and b show the three dimensional potential fitted and contour plot of the SMC model for porphycene, respectively.

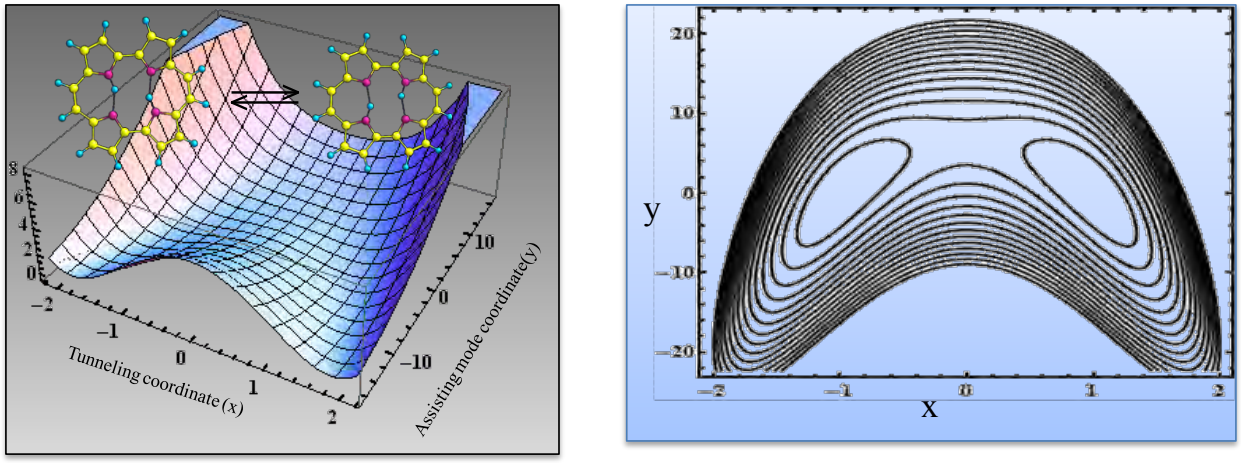

(a) (b)

Figure 4.6 (a) Three dimensional SMC potential fitted for porphycene and (b) Contour plot of the SMC model for porphycene, respectively.

Based on SMC model, the value of the potential barrier corresponding to the saddle point is predicted to be 4131 cm^{-1}. On the other hand, Vdovin et.al [72] had estimated a potential barrier in the range of 217-1360 cm^{-1} using one dimensional symmetric double minimum potential [192]. This value is by far much less than the value found in this work. Gawinkowski et.al [97] have shown that the average value of the N-H stretching frequency (which most probably be the tunneling coordinate) has an average value of 2500 cm^{-1}. This implies that the vibrationless level will have a frequency of about 1250 cm^{-1} which makes the proton transfer process almost barrier less and hence the role of tunneling should be insignificant if one assumes the results of the one dimensional model considered above is true. However, all experimental results show that the process is extremely sensitive to isotopic substitution. Besides, the fact that there are modes which promote or inhibit whithout being the reaction coordinate and the sensitivity of the process to substitution even when it is far from the reaction coordinate proves that the effect is not one dimensional.

4.4 Conclusions

Dispersed fluorescence spectra received from selective excitation of progression levels (n=1, 2) of a low frequency totally symmetric in plane mode, $2A_g$ clearly revealed corresponding vibronic progressions of this mode in the ground state. The values of tunneling splittings are found to increase with vibrational quantum number in the ground state along the assisting $2A_g$ mode both in Pc and Pc-d_1. On the other hand, no tunneling splitting is observed for Pc-d_2.

SMC model was applied to map two dimensional potential surface of porphycene. Using this model, the experimental tunneling splittings were well reproduced. Base on the model, the potential barrier for double proton tunneling is predicted to be about 4000 cm^{-1}. The results of the study show that $2A_g$ mode is indeed a promoting mode assisting proton tunneling in porphycene by decreasing the potential barrier.

Chapter five

Spectroscopic study of jet-cooled deuterated porphycenes: Unusual isotopic effects on proton tunneling

Proton tunneling is an extremely sensitive phenomenon that could respond to both electronic and geometrical perturbation of the reaction center. It has been shown that both substitution of the inner tunneling N-H hydrogens by deuterons or alkyl substitution of external C-H hydrogens have dramatic effects on the tunneling rate and/or mechanism, as mentioned in the previous chapters. However, the effects of the alkyl substitution are twofold. It first modifies the electronic distribution within Pc, which in turn alters the NH···N distance. Second, the substitution lowers the overall symmetry of the system and introduces additional frequency modes. To disentangle the electronic from nuclear effects in the consequences of outer rim substitution on proton tunneling, the effect of weak perturbations brought about by hydrogen/deuterium substitution on the outer rim of the porphycene macrocycle has been studied and is reported in this chapter . Full substitution of the outer rim results in Pc-d_{12}, which retains the C_{2h} symmetry of Pc. However, vibrational modifications due to deuteration may lead to a change in the coupling schemes between the reaction coordinates and the other modes. Partial deuteration of the outer rim results in various Pc-d_{11} or Pc-d_{10} species. Most of them undergo small deviations from the symmetrical double minimum character of the potential that governs tautomerization in Pc.

The main purpose of this work was to study the effects of these weak structural changes on double hydrogen tunneling, a phenomenon which can be extremely sensitive even to weak perturbations. We show that the replacement of peripheral protons by deuterons does not significantly affect the tunneling splitting values observed for the 0-0 transition and for the progression of the tautomerization-promoting $2A_g$ mode. On the other hand, a change in the form of another mode, $4A_g$, caused by deuteration, transforms this vibration from being neutral to tautomerization-enhancing.

5. 1 Computational results

The assignment of the bands observed in the LIF excitation spectrum near the 0-0 transition of Pc-d_{mix} is challenging (section 5.2), due to the possibility of partial deuteration at different positions and the associated slight shifts in absorption. Therefore, except for Pc-d_{12}, it is not an easy task to attribute the bands to specific isotopologues. In order to tackle this challenge, S_0 and S_1 geometry optimizations and frequency calculations have been carried out for (i) Pc and Pc-d_{12}, where all the rim hydrogens are substituted with deuterium, (ii) x-Pc-d_{11}, where all the outer rim hydrogens except at position x (x= m/m1/ e/e1/ ee or ee1, see scheme 1, chapter 1) are exchanged by deuteriums, and (iii) Pc-d_8, where all skeletal hydrogens except those at the *meso*-positions are deuterated.

The calculated harmonic frequencies have been used to determine the Zero-Point-Energy (ZPE) values in S_0 and S_1, denoted as ZPE (S_0) and ZPE(S_1) in Table 5.1. The isotopic shift $\Delta E_{0\text{-}0}$ of the electronic transition is the modification of the difference between ZPE(S_0) and ZPE(S_1) by deuteration. For the sake of comparison with the experimental results, Table 5.1 also gives the isotopic shift relative to Pc-d_{12}. The experimentally determined position of the 0-0 transition of Pc-d_{12} (section 5.2) was used to find a common vibrational scaling factor for the S_1 state of various isotopologuess in such a way that the calculations reproduce the experimental shift for Pc-d_{12} relative to parent Pc. Then, the same scaling factor was applied to the other isotopologues.

Table 5.1 shows that different x-Pc-d_{11} species introduce different shifts relative to Pc. Comparison of the 0-0 transition energies of x-Pc-d_{11} and Pc-d_{12} provides a more clearcut picture regarding the contribution of each x position to the shift (column 5). The structures m/m1, e/e1, and ee/ee1 of the Pc-d_{11} species can be treated as tunneling tautomeric pairs and the expected shift of the 0-0 transition can be considered as the average of each pair. Therefore, deuteration in the m/m1 position is expected to introduce an average experimental shift of 3.9 cm^{-1}, while deuteration at e/e1 and ee/ee1 positions introduce an average shift of 2.45 and 1.8 cm^{-1} relative to Pc-d_{12}, respectively. It is also evident from the calculations that each tunneling tautomer of Pc-d_{11} has asymmetric zero-point energies in a symmetric double minimum potential (within BO approximation) which is also a critical parameter in affecting tunneling splitting. The asymmetry is the largest (5.6 cm^{-1}) for the ee/ee1 pair and the smallest (1.5 cm^{-1}) for the m/m1 pair in the ground electronic state.

Exchange of the cavity NH hydrogens with deuterium is predicted to cause a red shift of about 1.6 and 3.3 cm^{-1} for single and double deuteration both in Pc and Pc-d_{12}. Although in the right direction, the calculations underestimate the experimental red shifts of about 24 and 44 cm^{-1} for single and double internal NH/ND hydrogen/deuterium exchange in Pc, respectively. [45,101]

Table 5.1 Zero-point energies ZPE (S_0) ZPE (S_1) and 0-0 electronic transition shifts relative to that of Pc ($\Delta E_{0\text{-}0}$) or Pc-d_{12} ($\Delta E_{0\text{-}0}$ vs Pc-d_{12}) of porphycene isotopomers calculated using TD (DFT)/B3LYP/6-31+G(d, p). The S_0 and S_1 scaling factors amount to 0.964 and 0.9633, respectively.

	ZPE (S_0) kcal/mol	ZPE (S_1) kcal/mol	$\Delta E_{0\text{-}0}$ [cm^{-1}]	$\Delta E_{0\text{-}0}$ vs Pc-d_{12} [cm^{-1}]
Pc				
NHNH	185.27691	183.31200		
NHND	183.17890	181.20757	-1.6	
NDND	181.08082	179.10307	-3.3	
Pc-d_{12}				
NHNH	160.77122	158.88555	32.7	
NHND	158.67261	156.78049	31.0	-1.7
NDND	156.57393	154.67537	29.4	-3.3
Pc-d_8				
	169.11128	167.18513	17.0	-15.7
Pc-d_{11}				
m	162.85452	160.96242	30.0	-2.7
m1	162.85893	160.96970	27.6	-5.1
e	162.79820	160.90704	30.4	-2.3
e1	162.78547	160.89350	30.0	-2.7
ee	162.80146	160.91125	30.7	-2.0
ee1	162.78473	160.89585	31.1	-1.6

5.2 LIF excitation spectrum

LIF excitation spectra of pure Pc and Pc-d_{mix} isolated in supersonic jet using laser desorption are presented in Figures 5.2 a and 5.2 b, respectively. Comparison of the two spectra shows that they generally exhibit a similar pattern in the low frequency region. The absence of bands due to undeuterated Pc in the spectrum of Pc-d_{mix} is in accordance with mass spectrometry analysis and

confirms the efficiency of the procedure used here. The narrow and most blue-shifted intense band at 16210.2 cm^{-1} was assigned to the transition origin of Pc-d_{12} where all peripheral hydrogens of porphycene are substituted by deuterons. The blue-shift amounts to 32.7 cm^{-1} relative to the origin of Pc, indicating that lowering of the zero-point energy due to deuteration is larger in the ground electronic state than in the excited electronic state.

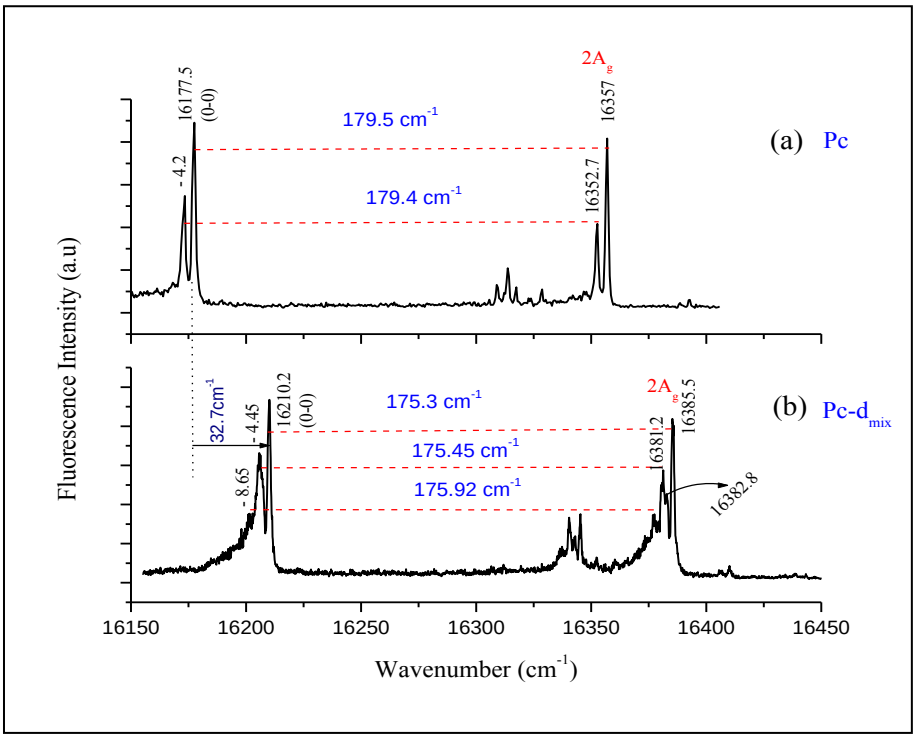

Figure 5.2 Laser-induced fluorescence excitation spectra of Pc (a) and Pc-d_{mix} (b) in supersonic jet conditions using laser desorption.

Another strong feature is observed with the maximum at 16205.8 cm^{-1} (-4.5 cm^{-1} from the origin of Pc-d_{12}). The band profile is asymmetric due to the expected heterogeneity of the sample. It is probably composed not only of the "hot" tunneling component of Pc-d_{12}, but also of significant contributions from various isotopic species with smaller mass, such as Pc-d_{11} and Pc-d_{10}. An additional complication is introduced by the presence of tunneling splitting leading to "hot bands" of electronic transitions belonging to various Pc-d_{11} and Pc-d_{10} species. The analysis of dispersed fluorescence spectra (Section 3.3) measured by excitation at different positions of the asymmetric feature allowed assigning the positions of the 0-0 transition of Pc-d_{11} and Pc-d_{10} at 16205.8 (-4.5 cm^{-1} from the intense band) and 16201.55cm^{-1} (-8.65 cm^{-1} from the intense band), respectively. Such shifts correlate well with the calculated average shift (-3.9 cm^{-1}) caused by the

lack of deuterium at the m/m1 positions in the rim of Pc-d_{11}. Similar study on perdeuteration of porphyrin showed that the hydrogens in the meso positions are facile [193].

A slightly better resolved feature is observed ca. 175 cm^{-1} above the origin. Per analogy to Pc spectrum, it could be assigned to the $2A_g$ mode. Again, respective assignment of the contributing isotopic species to the spectral features could be made by a systematic analysis of dispersed fluorescence spectra obtained by selective excitations, as presented in the next section. Anticipating these results, the marked positions at 16385.5, 16381.2, and 16377.5 cm^{-1} (where the latter two bands are located -4.3 cm^{-1} and -8.0 cm^{-1} from the former band, respectively) were assigned as $2A_g$ mode analogs of Pc-d_{12}, Pc-d_{11} and Pc-d_{10}, respectively. The shifts and assignments correspond very well to those drawn earlier from the spectral features around 16210 cm^{-1}.

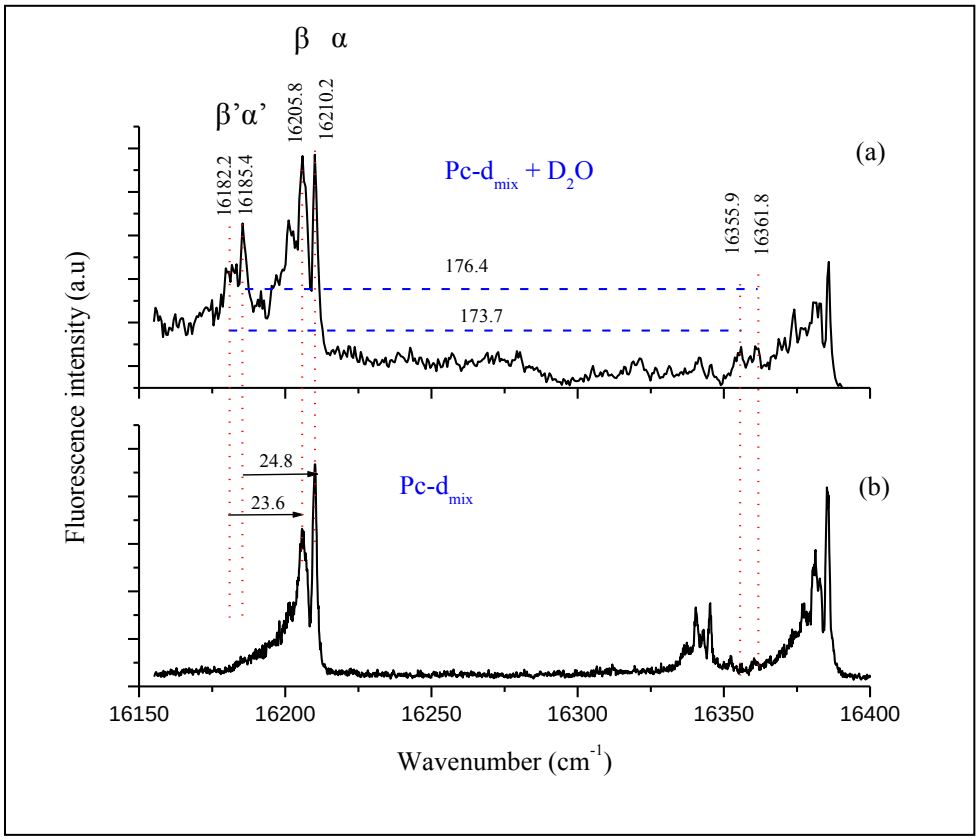

Figure 5.3 LIF excitation spectrum of jet-cooled Pc-d_{mix} using Ne seeded with D_2O as a carrier gas (a) and pure Ne without D_2O (b). The partial vapor pressure of D_2O in Ne was determined by thermostated bath kept at 0^0 C.

It was also very interesting to check the spectral response of the laser-desorbed sample cooled by Ne carrier gas with heavy water (D_2O) contamination. Figure 5.3a shows the LIF excitation spectrum of the desorbed sample (Pc-d_{mix}) with heavy water in Ne buffer gas. For comparison, the LIF spectrum of Pc-d_{mix} in pure Ne gas is shown in Figure 5.3b.

The optimum signal for spectrum (a) is found at a relatively closer laser-to-nozzle distance than for spectrum (b), which explains a relatively lower signal to noise ratio and a higher background in spectrum (a). The new transitions around the origin of (a) are marked by Greek letters for further discussion.

Comparison of Figures 5.3a and b shows the appearance of new bands around 16185 (α'and β') and 16360 cm^{-1}. The first band (α') is red-shifted by about 25 cm^{-1} from the 0-0 transition of Pc-d_{12}. A similar red shift (about 24 cm^{-1}) was observed for parent porphycene when one of the internal NH hydrogen had been exchanged by deuterium. [45,101] Therefore, we assign the band at 16185.4 cm^{-1} (α') to the 0-0 transition of Pc-d_{12+1}, where one of the cavity NH hydrogens in Pc-d_{12} is replaced by deuterium. It is worth noticing that only a single replacement of deuteron manifests itself in the spectrum, contrary to the effective single and double deuterium exchange observed after conventional heating of porphycene sample in an oven before expansion. [45] This observation can be explained in terms of significantly reduced probability of effective secondary collisions between D_2O and Pc-d_{12+1} due to a limited time in the collision zone before gas expansion in the laser desorption regime.

A weaker intensity red shoulder centred at 16182.2 cm^{-1} (β') was assigned to an overlap of 0-0 transition of various Pc-d_{11+1}, where one of the internal NH hydrogens of Pc-d_{11} is substituted by deuterium. Similar to Pc-d_{12+1}, this band is red-shifted by about 24 cm^{-1} from the 0-0 transition of Pc-d_{11}. An interesting and expected effect of deuteration of the internal NH hydrogens is a significant change (by a factor of 2) of the relative intensities of the bands: α/β vs α'/β'. It is mainly caused by the reduction of tunnelling splitting in Pc-d_{12+1}, which reduces the contribution of the "hot band" overlapping with the band of Pc-d_{11}.

Two other low intensity bands were also observed at 16355.9 and 16361.8 cm^{-1} (Figure 5.3a) and shifted by about 175 cm^{-1} relative to the bands at 16182.2 and 16185.4 cm^{-1}, respectively. These bands were assigned as $2A_g$ mode analogues of Pc-d_{11+1} and Pc-d_{12+1} isotopomers, respectively. One should notice that the notation $2A_g$ is correct only for Pc and Pc-d_{12}, as both molecules belong to the C_{2h} point groups, but not quite correct for the other isotopologues, since they have lower symmetries. The notation is adopted for corresponding modes between parent porphycene and its isotopologues. The LIF spectrum of Pc-d_{mix} shows close similarity with that of Pc.

Another important result worth noticing is that the LIF spectrum of Pc-d_{mix} in Figure 5.3a is collected at closer laser-to-nozzle distance relative to that of Figure 5.3b. Comparison of the two

spectra shows that the intensity ratio α/β in Figure 5.3a is larger than that of Figure 5.3b. The results shows that the intensity of band β increases with decreasing laser-to-nozzle distance indicating its hot nature. Therefore, based on the fact that band β is "hot" and red shifted, along with the information gathered from dispersed fluorescence studies (section 5.3.1), it is possible to conclude that the tunneling splitting of the zero level of ground state (S_0) of Pc-d_{12} is larger than the tunneling splitting of the zero level of the first excited (S_1). Similar behavior was reported for parent porphycene by Sepioł et.al [45].

LIF spectrum of Pc-d_{mix} was also measured in an extended region (Figure 5.4). The spectrum shows a more complicated structure around 350 cm^{-1} and assignments of the marked vibronic bands are given based on single vibronic level fluorescence and theoretical calculations in the next section.

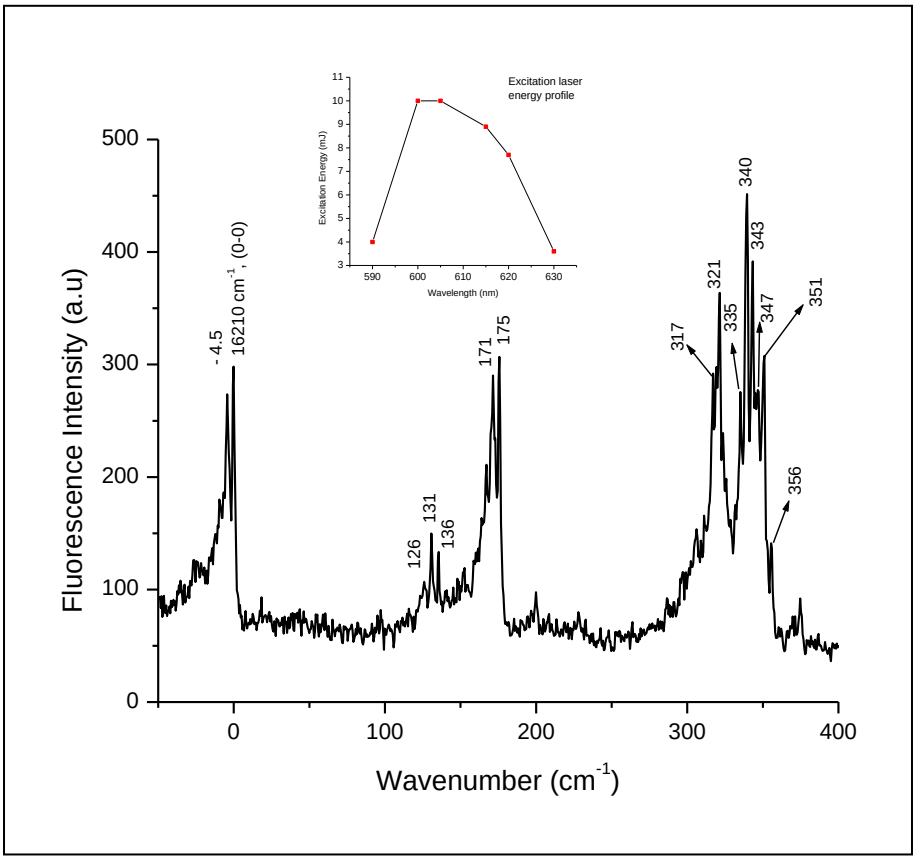

Figure 5.4 LIF excitation spectrum of jet-cooled Pc-d_{mix}. The inset shows the energy profile of the excitation laser. Note that the LIF excitation spectrum is not normalized with respect to the laser power.

5.3 Single vibronic level fluorescence (SVLF) spectra

In this section we present SVLF spectra of porphycene isotopologues obtained for 0-0 band and higher frequency excitations. Since the $2A_g$ mode is the most tautomerization-promoting mode for which the largest tunnelling splitting of 12 cm^{-1} is found in the ground state, we exploit this mode as a probe to see subtle effects brought about by deuteration of outer rim hydrogens. Deatailed assignment and analysis of SVLF spectra of porphycene isotopologues is presented in this section.

5.3.1 0-0 Excitation

Dispersed fluorescence spectra resulting from the excitation at 16207.2, 16210.2, 16205.75, and 16201.15 cm^{-1} bands of the LIF excitation spectrum of Pc-d_{mix} are presented in Figures 5.5 a-d, respectively. As a reference, dispersed fluorescence spectrum of porphycene obtained for 0_+^+ excitation is also shown in Figure 5.5e.

A glimpse at the spectra recorded for excitation into the bands at 16210.2 and 16207.2 cm^{-1} (Figures 5.5 a and b) shows that they are identical and typical of the excitation of the two components of tunnelling doublets. The spectra also exhibit a pattern similar to that of parent porphycene shown in Figure 5.5e. The 0-0 transition of Pc-d_{12} is split by the same amount as that of parent Pc, despite the fact that the zero-point energy is decreased in the former isotopologue. On the other hand, comparison of the tunnelling splittings for the corresponding $2A_g$ modes shows only a slight decrease in Pc-d_{12} (10.7 cm^{-1}) compared to parent porphycene (12 cm^{-1}). Therefore, it is possible to deduce that the low frequency $2A_g$ mode, involving the motion of the internal cavity, is only weakly coupled to the motion of external rim hydrogens. In this respect, Gawinkowski *et. al.* [97] have also shown for Pc that the C-H stretching modes of the external hydrogens are unaffected by deuteration of the cavity NH hydrogens, showing that the motion of cavity hydrogens is also decoupled from the motion of the external hydrogens. Thus, it is not surprising to see a similar behaviour for Pc and Pc-d_{12} with respect to proton tunnelling.

In contrast, the spectra shown in Figures 5.5c and d are different from each other and from the rest of the spectra, confirming excitation of different species. This observation is in line with the assignment we presented earlier, that the transitions at 16205.75 and 16201.5 cm^{-1} in the LIF excitation spectrum of Pc-d_{mix} (Figure 2b) belong to the 0-0 transitions of Pc-d_{11} and a set of Pc-d_{10} isotopomers, respectively. It also appears from the spectra in Figures 5.5c and d that the 0-0 transitions are broader, with no signature of tunnelling splitting, indicating the effects of smearing due to the presence of various contributing structures.

A closer look at Figure 5.5c shows an interesting feature. The bands at about 170 cm^{-1} appear as doublets of doublets, contrary to the features observed in Pc and Pc-d_{12} in which simple doublets were seen. This result is in line with our earlier assignment that the band at 16205.75 cm^{-1} in

Figure 5.2b is actually an overlap of two transitions: 0-0 transition of Pc-d_{11} and the "hot" tunnelling counterpart of the origin of Pc-d_{12}. Deconvolution of the peaks at about 170 cm^{-1} of the dispersed fluorescence spectrum (see Figure 5.6) shows that there are four distinct transitions. The tunnelling pairs belonging to Pc-d_{12} are indicated by red arrows, while the blue arrows indicate the tunnelling pairs belonging to Pc-d_{11} species.

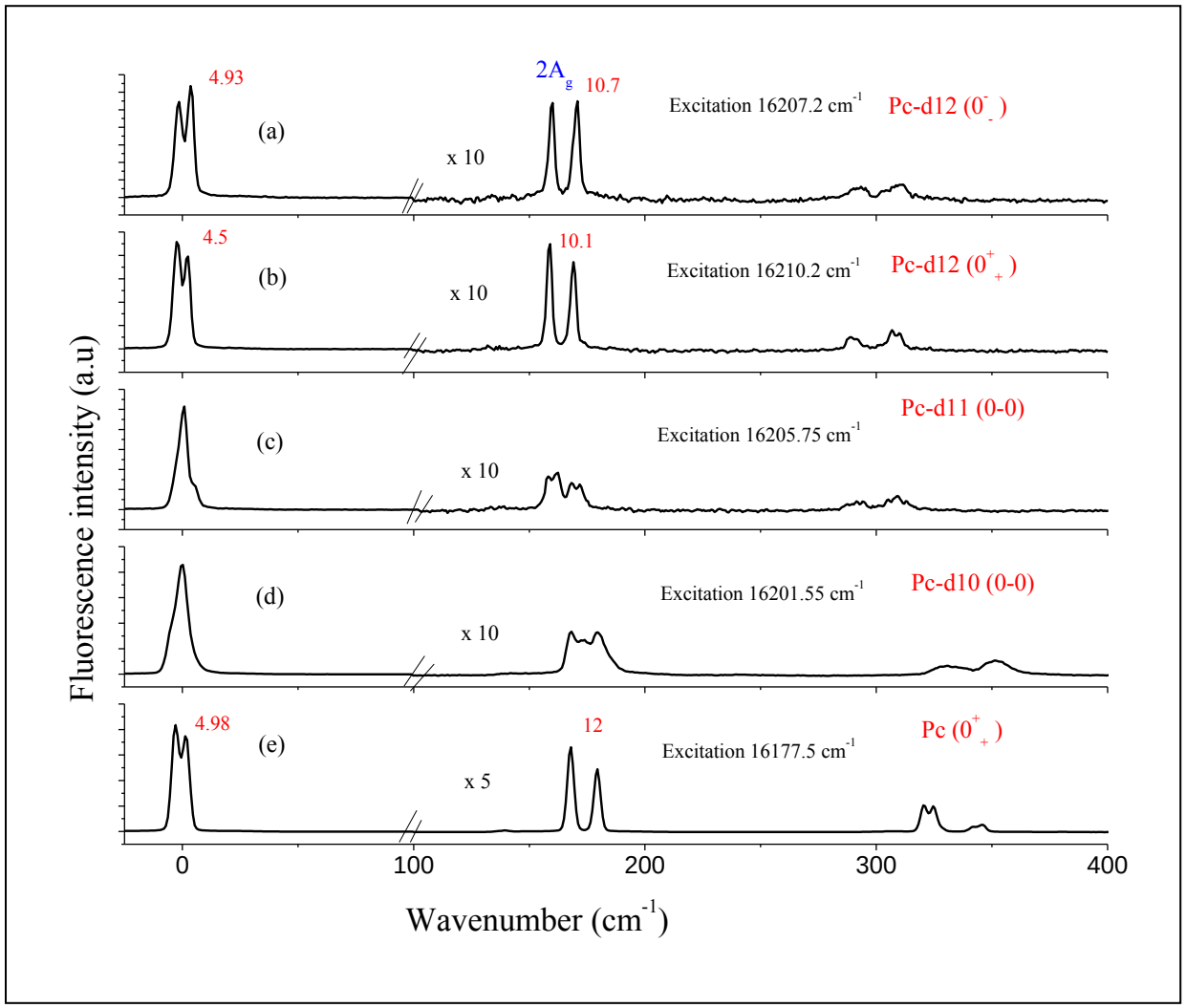

Figure 5.5 Dispersed fluorescence spectra of jet-cooled porphycene isotopologues. For clarity, the intensities of the spectra in the range 100-400 cm^{-1} are magnified 10 times (a-d), while the spectrum of Pc is magnified 5 times (e).

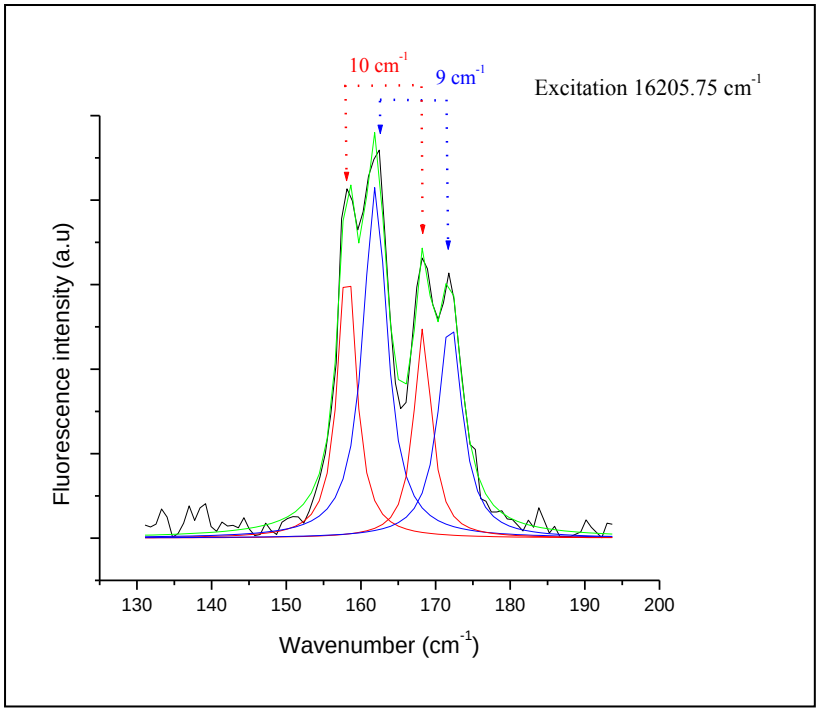

Figure 5.6 Portion of dispersed fluorescence emission spectrum resulting from excitation at 16205.75 cm^{-1}. Deconvolution of the peaks into bands with Lorentzian line shape shows four distinct transitions. The pair at 158.1/168.2 cm^{-1} (red) belongs to a tunnelling multiplet of the $2A_g$ mode of Pc-d_{12}, while the doublet at 162/171.3 cm^{-1} (blue) belongs to a tunnelling multiplet in the corresponding transition of Pc-d_{11}.

The results presented in Figure 5.6 show that proton tunnelling is operating in both Pc-d_{11} and Pc-d_{12} isotopomers along this mode. A slight decrease of the tunnelling rate in the former can tentatively be explained by the lower symmetry of the molecule (C_s).

Figure 5.5d presents dispersed fluorescence (DF) spectrum obtained for excitation at the 16201.55 cm^{-1} peak in the LIF spectrum of Pc-d_{mix}. Even though the resulting DF spectrum exhibits a crude similarity to the other spectra, one can notice a broad band with some structure at about 175 cm^{-1}. This band is interpreted as the $2A_g$ analog of various Pc-d_{10} species. The mode which appears as a tunnelling multiplet in Pc, Pc-d_{12} and Pc-d_{11} now appears as a congested feature due to overlap of many bands belonging to several Pc-d_{10} species. This can be understood if one considers the large number of possible Pc-d_{10} species formed during the synthesis (see the experimental section). Thus, it is not surprising to see a broad band with some details. However, at this point it is not possible to specify which Pc-d_{10} species are responsible for the spectrum.

5.3.2 (0-0) + 126, 131 and 136 cm^{-1} excitation.

Figure 5.7 shows the dispersed fluorescence spectra resulting from the excitation of the low frequency bands observed at 126, 131 and 136 cm^{-1} from the origin (see Figure 5.4). The spectra show very simple patterns. They are dominated by a prominent $\boldsymbol{\nu_1^1}$ band acting as a pseudo origin for a 0-0 type emission.

Figure 5.7 (a) shows the dispersed fluorescence resulting from the excitation of the band at 126 cm^{-1}. The fluorescence spectrum is dominated by the $\boldsymbol{\nu_1^1}$ transition at 131 cm^{-1}. Theoretical calculations (see Table 5.2) for Pc-d_{12} predict vibrational frequencies at 124 and 126 cm^{-1} in the S_1 and S_0 states, respectively, for a mode of B_g symmetry. Therefore the band at 126 cm^{-1} in the LIF spectrum and the band at 131cm^{-1} in the dispersed fluorescence are assigned to this $2B_g$ mode in the S_1 and S_0 states, respectively. It is to be noted that $2B_g$ mode is not active in the dispersed fluorescence spectrum resulting from the excitation of the origin bands of any of Pc-d_{mix} species.

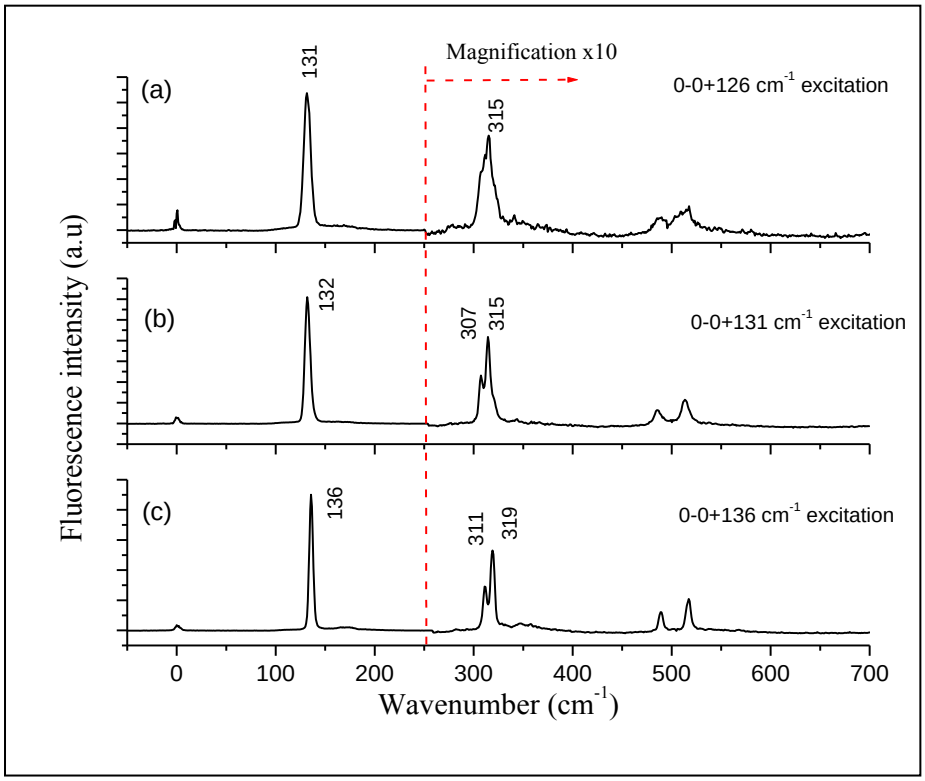

Figure 5.7 Dispersed fluorescence spectra obtained via excitation of low frequency bands: (a) 126 cm^{-1}, (b) 131 cm^{-1} and (c) 136cm^{-1}. Note that the intensity of the bands above 300 cm^{-1} are magnified ten times.

Figure 5.7 (b) and (c) show dispersed fluorescence spectra resulting from the excitation of the band at 131 and 136 cm^{-1}. The spectra are dominated by a $\boldsymbol{\nu_1^1}$ transition at 132 and 136 cm^{-1}, respectively. As described for the spectrum shown in Figure 5.7 (a), the $\boldsymbol{\nu_1^1}$ acts as an origin for a vibrational progression built on the $2A_g$ mode. The first member of this progression is split by 8 cm^{-1}. By analyzing the spectra in Figure 5.7 (b) and (c) in the same way as before, we conclude that the bands at 131 and 136 cm^{-1} in the LIF spectrum of Pc-d_{mix} are the two members of a tunneling doublet. Due to the larger population of the lower (+) level, which results in higher emission intensity, we will base our assignment on the spectrum of Figure 5.7 (c).

The spectrum of Figure 5.7 (c) is dominated by the $\boldsymbol{\nu_1^1}$ transition at 136 cm^{-1}. Theoretical calculations (see Table 5.2) for Pc-d_{12} predict a mode of A_g symmetry with vibrational frequencies of 139 and 142 cm^{-1} in the S_1 and S_0 states, respectively. Therefore the band at 136 cm^{-1} both in the LIF and the dispersed fluorescence spectra is assigned to the $1A_g$ mode in the S_1 and S_0 electronic states, respectively. The doublet at 311/319 cm^{-1} is assigned to the $1A_g + 2A_g$ combination mode.

From the perspective of ground state proton tunneling dynamics in Pc-d_{12}, the $1A_g{}_1^1$ and $2B_g{}_1^1$ transitions do not show tunneling splitting. Moreover, the $1A_g{}_1^1\,2A_g{}_1^0$ or $2B_g{}_1^1\,2A_g{}_1^0$ transitions show a decrease of the tunneling splitting relative to the $2A_g{}_1^0$ transition from about 12 cm^{-1} to about 8 cm^{-1}. This shows the proton tunneling inhibiting nature of the modes. Similar inhibiting characteristics for these modes is also reported for parent porphycene [70, 101].

5.3.3 (0-0) + $2A_g$ excitation

Dispersed fluorescence spectra of porphycene and its isotopomers obtained by excitation of the $2A_g$ mode (0+175cm^{-1}) are presented in Figures 5.8 a-e. The spectra are dominated by progressions of the $2A_g$ mode in the ground state.

Figure 5.8a shows the DF spectrum of the parent porphycene. Two high intensity pairs of doublets are observed at 164/177 cm^{-1} and 351/373 cm^{-1}. These pairs were already assigned [100] as $2A_{g_1}^1$ and $2A_{g_2}^1$ modes. Dispersed fluorescence spectrum of Pc-d_{12} obtained by excitation of $2A_g$ is presented in Figure 5.8b. Similar to porphycene, two pairs of doublets are observed at 158.5/170 cm^{-1} and 342.5/364 cm^{-1}, with tunnelling splittings of 11.5 and 21.5 cm^{-1}, respectively. These pairs of bands are assigned as $2A_{g_1}^1$ and $2A_{g_2}^1$ transitions of Pc-d_{12}. It will be shown below that each of these multiplets is found to respond to deuteration of cavity NH hydrogens. Apart from a slight difference in the tunnelling splitting value in Pc-d_{12}, the spectrum shows a pattern similar to that of parent porphycene. Comparison of Figures 5.8 b and c shows that the spectra

are identical, typical of excitation of tunnelling doublets. Therefore the bands at 16385.5 and 16382.8 cm^{-1} belong to $2A_{g\,0+}^{1+}$ and $2A_{g\,0-}^{1-}$ transitions in the LIF spectrum of Pc-d_{12} (Figure 5.2b). The results also show that tunnelling splitting increases with vibronic progressions of $2A_g$ mode both in Pc-d_{12} and Pc-d_{11} in the ground state, however not linearly. A similar result was already reported for Pc. [100] Further, there is no significant difference in tunnelling splitting between the two isotopomers along this mode.

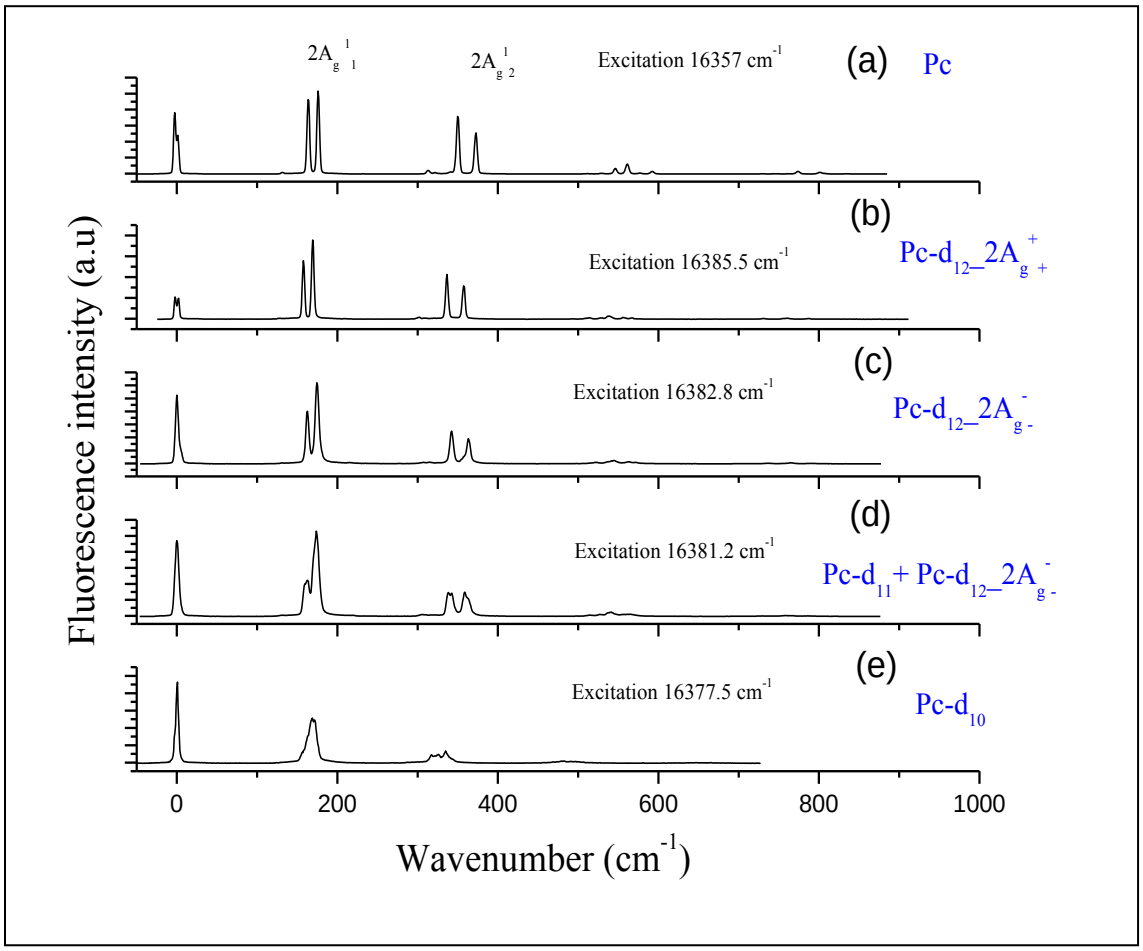

Figure 5.8 Dispersed fluorescence spectrum of Pc-d_{mix} obtained by excitation into $2A_{g\,0}^{1}$ transition of respective isotopomers in supersonic jet.

On the other hand, the DF spectrum resulting from the excitation at 16381.2cm^{-1} (Figure 5.8 d) shows a dramatic difference with respect to both Pc and Pc-d$_{12}$. Around 170 cm^{-1}, doublets of doublets are observed instead of a single doublet, similarly to the case we have seen earlier (Figure 5.8 c). Additional doublets of doublets are also observed centered at 350 cm^{-1}, again with a dramatic increase in tunnelling splitting. Deconvolution of the transitions around 170 and 350 cm^{-1} shows four distinct transitions in each position (Figure 5.9).

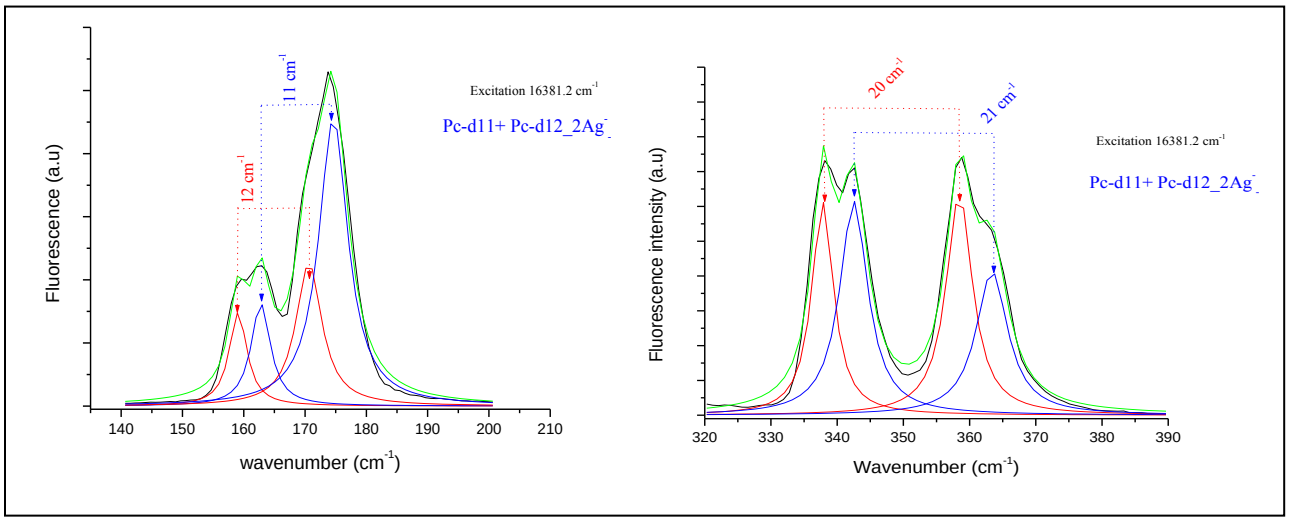

Figure 5.9 Portions of DF fluorescence spectrum of Pc-d$_{mix}$ obtained by excitation at 16381.2 cm^{-1} and respective multiple Lorentzian fits.

It can be deduced from the results that the excitation at 16381.2 cm^{-1} reveals an overlap of two transitions, one corresponding to the $2A_{g_0}^1$ transition of Pc-d$_{11}$ and the other to the "hot" tunnelling counterpart of the $2A_{g_0}^1$ transition of Pc-d$_{12}$.

More dramatic spectral change is observed for excitation at 16377.5 cm^{-1} (Figure 5.8 e). A single broad peak appears around 170 cm^{-1}, while a broad band occurs around 330 cm^{-1} with some structural details. The band broadening and lack of tunnelling splitting features could be explained by the presence of several Pc-d$_{10}$ species formed during the synthesis.

5.3.4 (0-0) +2A_g excitation: response to NH /ND exchange in the internal cavity

As the decrease of the splitting of vibronic levels due to internal NH/ND exchange was delivering a direct proof of hydrogen tunnelling in porphycene, [45, 101] we present in Figures 5.10 a-d the dispersed fluorescence spectra of Pc-d_{12} / Pc-d_{12+1}, and Pc-d_{11} /Pc-d_{11+1} pairs obtained via $2A_{g_0}^1$ excitation of the respective isotopologues.

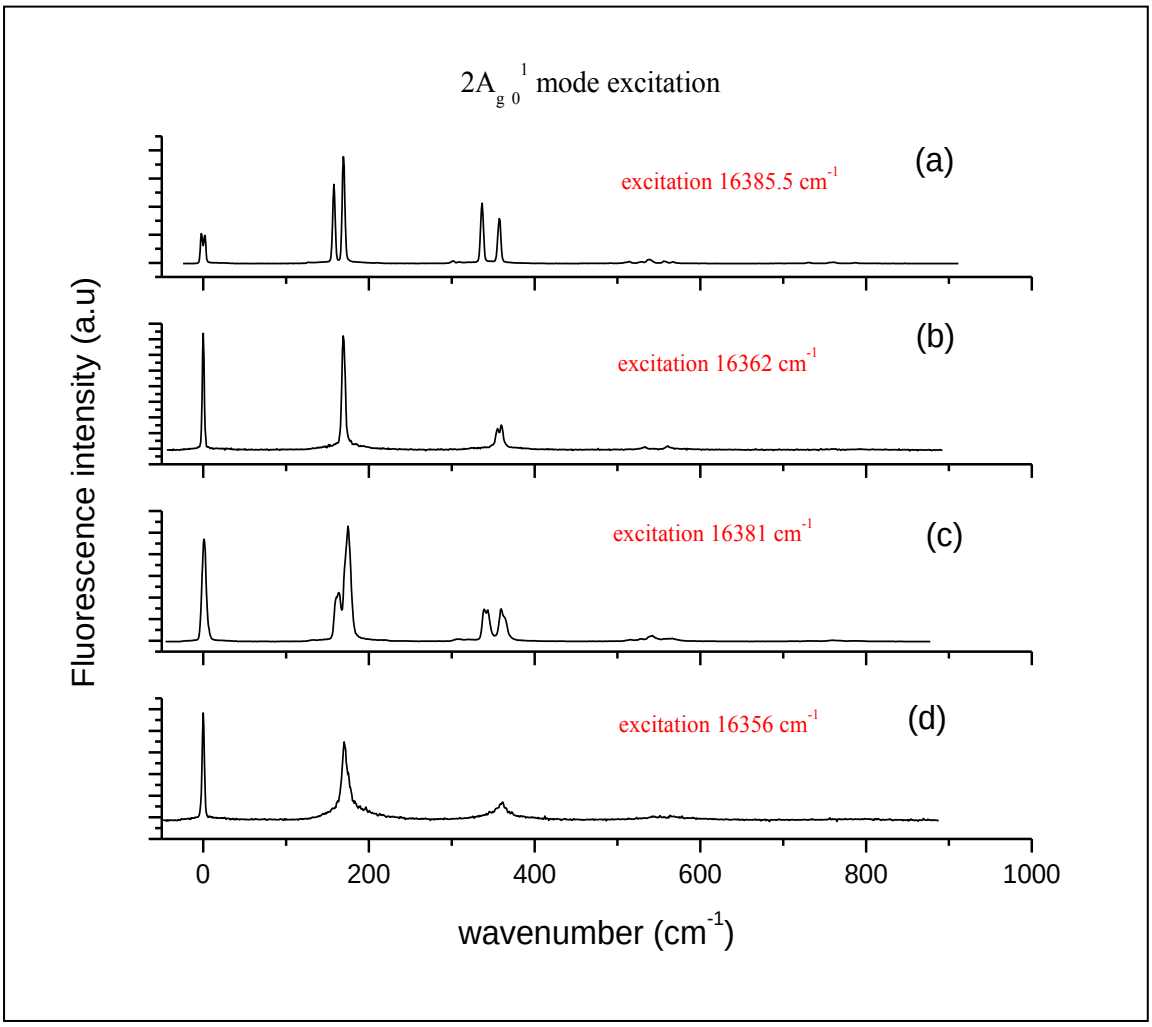

Figure 5.10 Dispersed fluorescence spectrum of Pc-d_{12} (a), Pc-d_{12+1} (b), Pc-d_{11} (c) and Pc-d_{11+1} (d) via excitation of the 2A_g modes.

Comparison of Figure 5.10a and b shows that the splitting of the $2A_{g_1}^1$ transition vanishes upon deuteration of one of the exchangeable NH hydrogens in Pc-d_{12}, whereas for the $2A_{g_2}^1$ transition the value of tunnelling splitting decreases from about 20 cm^{-1} in Pc-d_{12} to 4.5 cm^{-1} in Pc-d_{12+1},

confirming that the origin of the doublets is tunnelling. On the other hand, comparison of Figures 5.10 c and d shows that the doublets in Pc-d_{11} are collapsed to a single broad band as a result of deuteration of one of the internal hydrogens in Pc-d_{11+1}. The results of this experiment clearly confirm proton tunnelling both in Pc-d_{12} and Pc-d_{11} isotopologues.

5.3.5 *(0-0) + 317 and 321 cm^{-1} excitations*

Figure 5.11 shows dispersed fluorescence spectra resulting from the excitation of the low frequency bands at 317 and 321 cm^{-1} from the LIF excitation spectrum of Pc-d_{mix}.

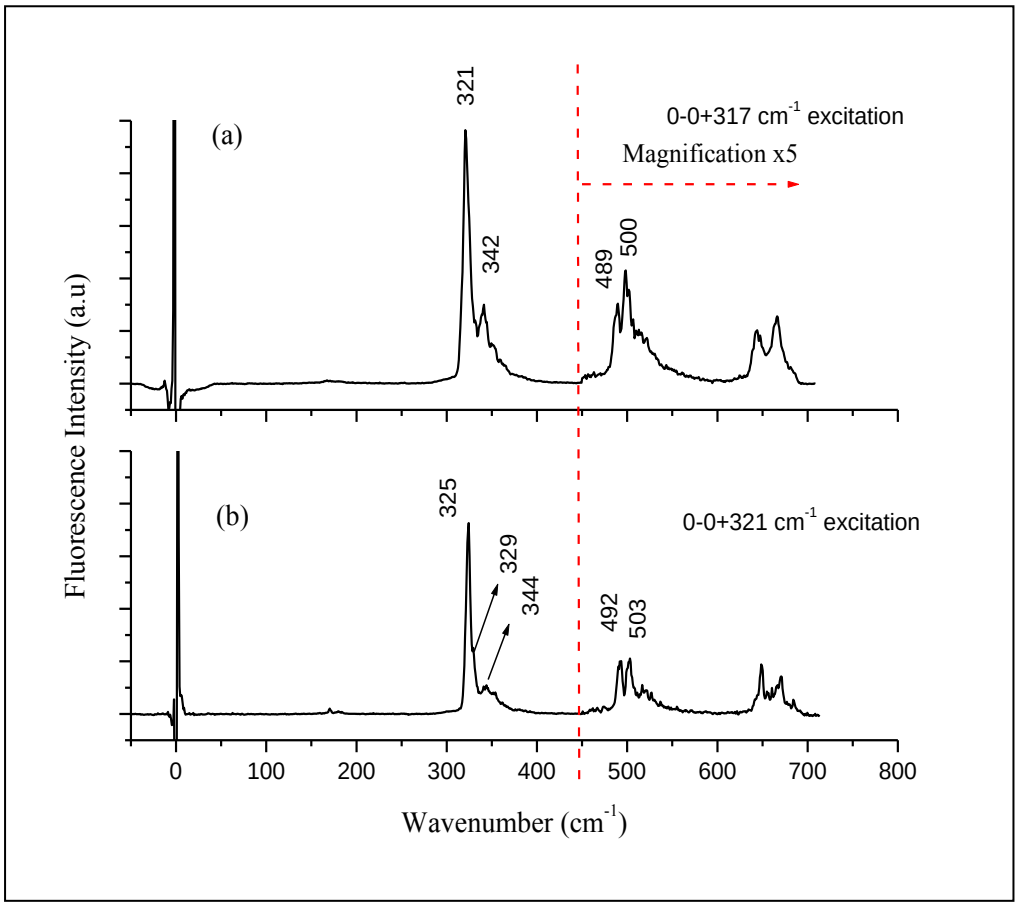

Figure 5.11 Dispersed fluorescence spectra obtained via excitation of low frequency bands: (a) 317 cm^{-1} and (b) 321cm^{-} . Note that the intensity of the bands above 450 cm^{-1} are magnified five times.

The spectra shown in Figure 5.11 (a) and (b) have similar patterns, except a shoulder in the low-energy part of the vibronic bands in Figure 5.11 (a). This shoulder could result from co-excitation of the close-lying vibronic band at 319 cm^{-1}. The fluorescence spectrum in Figure 5.11 (b) shows better resolution and the assignment of the observed vibronic transitions will be based on the latter. The spectrum is dominated by an asymmetric vibronic transition at

325 cm^{-1} with a shoulder at 329 cm^{-1}. Theoretical calculations predict an A_g mode with frequencies of 316 and 319 cm^{-1} in the S_1 and S_0 states, respectively. Therefore, the bands at 321 cm^{-1} in the LIF spectrum and at 325 cm^{-1} in the dispersed fluorescence spectrum are assigned to the $3A_g$ modes in the S_1 and S_0 states of Pc-d_{12}, respectively. The doublets at 492 and 503 cm^{-1} are assigned to the $3A_{g1}^1\ 2A_{g1}^0$ transition. Similarly, the band at 321 cm^{-1} in figure 5.11 (a) is assigned to the $3A_{g1}^1$ transition while the doublets at 489 and 500 cm^{-1} are assigned to $3A_{g1}^1\ 2A_{g1}^0$ combination.

The $3A_g$ mode is split by about 4 cm^{-1} in the ground state. However, the doublets are barely resolved because of the limited resolution of our spectrometer (about 3 cm^{-1}); instead the splitting is estimated from the asymmetry of the band at 325 cm^{-1} in Figure 5.11 (b). The splitting of this band is comparable to that observed for the origin transition. Moreover, the $3A_{g1}^1\ 2A_{g1}^0$ transition shows tunneling splitting (11 cm^{-1}) similar to that of the promoting $2A_g$ mode (12 cm^{-1}). These observations suggest that $3A_g$ mode is a neutral mode, in a sense that it is neither proton tunneling inhibiting nor promoting mode. This mode is also reported to be neutral in parent porphycene [101] .

5.3.6 *(0-0) + 335, 340, 343, 346, 351 and 356 cm^{-1} excitations*

The LIF excitation spectrum of Pc-d_{mix} shows a complicated structure at about 340 cm^{-1} above the 0-0 transition (see Figure 5.4). There are at least six vibronic transitions in the range between 335 and 360 cm^{-1}, which makes the assignment difficult from the LIF excitation spectrum alone. Therefore, we have measured the single vibronic level fluorescence spectra resulting from the excitation of each band in the specified region. The results are presented in Figure 5.12 (a)-(f).

Figure 5.12 (a) shows the dispersed fluorescence spectrum resulting from the excitation of the band at 335 cm^{-1} in the LIF spectrum. The dispersed fluorescence spectrum is dominated by the $\boldsymbol{\nu_1^1}$ transition at about 350 cm^{-1}, which is split by 9 cm^{-1}. Theoretical calculations for Pc-d_{12} predict vibrational frequencies of A_g symmetries at 335 and 339 cm^{-1} in the S_1 and S_0 states, respectively. Moreover, the experimental and calculated frequency shifts of the mode between the excited state and the ground state, *i.e.* $\nu(S_1\text{-}S_0)_{expt}$ and $\nu(S_1\text{-}S_0)_{calcul}$ agree with the assignment (see Table 5.2). Further, comparison of the isotopic shifts of the modes between parent porphycene and Pc-d_{12} show a good agreement both in the S_0 and S_1 states (see Table 5.3). Based on the analysis given, the band at 335 cm^{-1} in the LIF excitation spectrum and the doublets around 350 cm^{-1} in the dispersed fluorescence spectrum are assigned to the $4A_g$ modes of Pc-d_{12} in the S_1 and S_0 states, respectively.

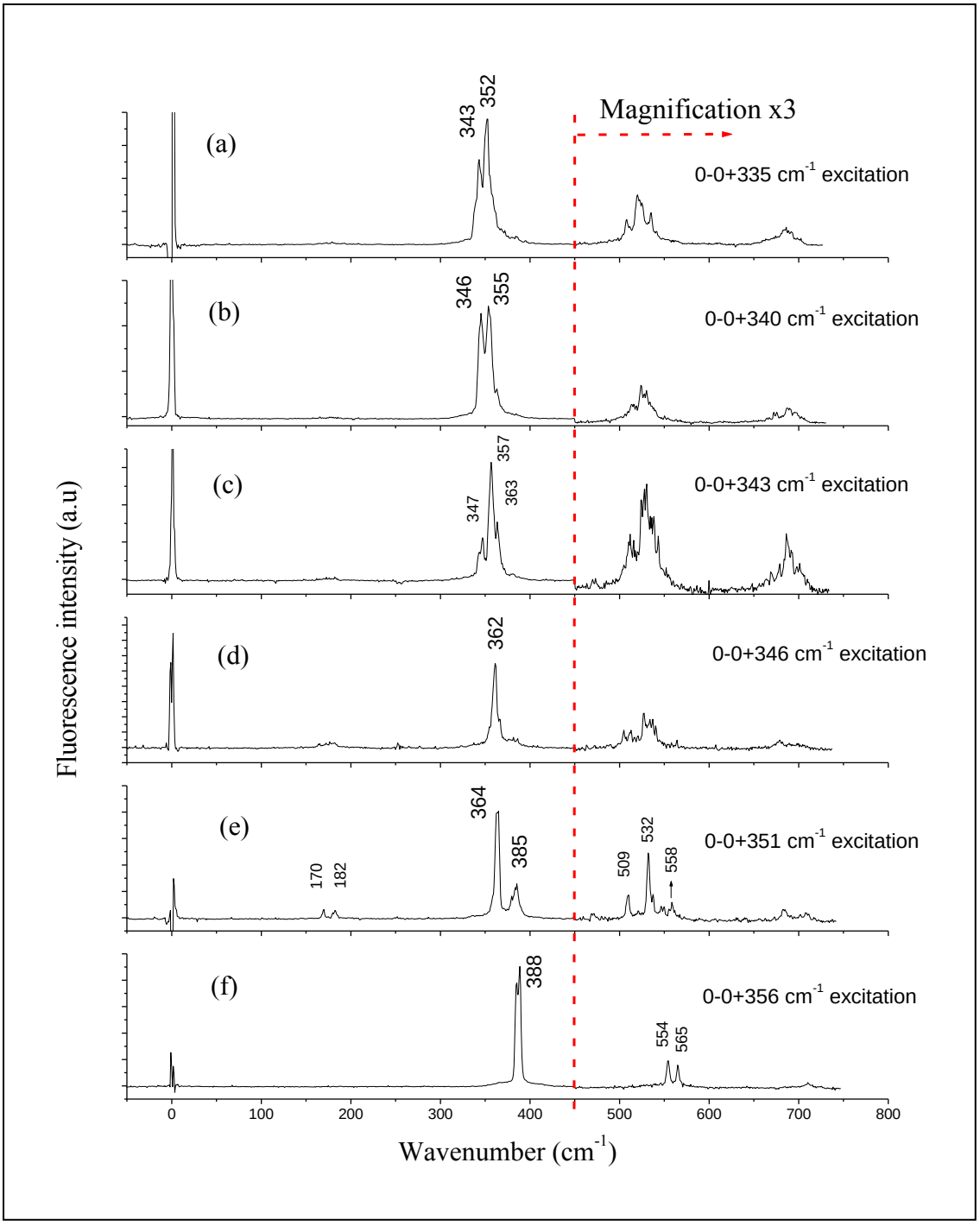

Figure 5.12 Dispersed fluorescence spectra obtained via excitation of low frequency bands around 340 cm^{-1} in the LIF excitation spectrum of Pc-d_{mix}; the excitation positions are indicated for each spectrum. Note that the intensity of the bands above 450 cm^{-1} are magnified three times.

A glimpse at Figure 5.12 shows that the spectra (a) and (b) have similar patterns, including splitting and band widths of their $\boldsymbol{\nu_1^1}$ transition. Therefore, we can anticipate that the bands at 335 and 340 cm^{-1} are the two members of a tunneling doublet. Hence, the band at 335 cm^{-1} is assigned to the $4A_{g\_}^{-}$ transition while the band at 340 cm^{-1} corresponds to $4A_{g+}^{+}$.

Figure 5.12 (c) shows the dispersed fluorescence spectrum resulting from the excitation of the band at 343 cm^{-1} in the LIF spectrum. It shows a more complicated pattern in the region of the $\boldsymbol{\nu_1^1}$ transition. One possible reason for that could arise from the excitation of two different overlapping transitions. Comparison of Figures 5.12 (b), (c) and (d) shows that the complicated pattern in (c) can be explained by a superposition of (b) and (d) spectra. A "(b)" like spectrum is expected if one considers the possible excitation of $4A_g$ mode of Pc-d_{11} at about 343 cm^{-1} in the LIF spectrum. This consideration is plausible, as we have already seen contribution of Pc-d_{11} isotopologue near the 0-0 transition and more active $2A_g$ mode in the LIF excitation spectrum. The assignment of the second "(d)" like spectrum is differed for the time being until the assignment of the spectrum in Figure 5.12 (d).

Figure 5.12 (d) shows the dispersed fluorescence resulting from the excitation of the band at 346 cm^{-1}. The spectrum is dominated by the $\boldsymbol{\nu_1^1}$ transition at 362 cm^{-1}. Calculations for Pc-d_{12} predict a B_g vibrational mode with frequencies of 320 and 350 cm^{-1} in the S_1 and S_0 states, respectively. Therefore, we assign this band to $5B_g$. The experimental and calculated frequency shifts of the mode between the excited state and the ground state, *i.e.* $\nu(S_1\text{-}S_0)_{expt}$ and $\nu(S_1\text{-}S_0)_{calcul}$ agree with the assignment (see Table 5.1). Moreover, comparison of the isotopic shifts of the modes between parent porphycene and Pc-d_{12} show a good agreement both in the S_0 and S_1 states (see Table 5.3).

One has to remember that all the vibronic transitions of Pc-d_{12} appear as doublets in the LIF spectrum, with tunneling splitting of about 4 cm^{-1}. Therefore, one expects to find the other tunneling component of the $5B_g$ mode of Pc-d_{12} in the LIF spectrum within ± 4 cm^{-1} of the 346 cm^{-1} band. Figure 5.12 (e) shows dispersed fluorescence spectrum resulting from the excitation of the band at 351 cm^{-1} (+5 cm^{-1} from the 346 cm^{-1} band). Comparison of Figures 5.12 (d) and (e) shows the spectra are due to excitation of different vibrations. Therefore, the band at 351 cm^{-1} cannot be the tunneling counterpart of that at 346 cm^{-1}. This will lead us to the conclusion that the band at 346 cm^{-1} in the LIF excitation spectrum is the $5B_{g+}^{+}$ transition of Pc-d_{12}. Consequently, the $5B_{g\_}^{-}$ transition of Pc-d_{12} should be found at 342 cm^{-1}. This will lead us to the reexamination of the fluorescence spectrum shown in Figure 5.12 (c), which contains a contribution from excitation of the "hot" tunneling component of $5B_g$ mode of Pc-d_{12}. This assignment therefore explains the nature of the complicated spectral feature in Figure 5.12 (c), which results from co-excitation of the $4A_g$ mode of Pc-d_{11} and $5B_{g\_}^{-}$ mode of Pc-d_{12}.

Figure 5.12 (f) shows the dispersed fluorescence resulting from the excitation of the band at 356 cm^{-1}. It is dominated by the $\boldsymbol{\nu_1^1}$ transition origin at 388 cm^{-1}. Theoretical calculations for Pc-d_{12} do not predict any fundamental transition of A_g or B_g symmetry at 356 cm^{-1} in the excited S_1 state and at 388 cm^{-1} in the S_0 state. However, two weak intensity doublets separated by 11cm^{-1} are also observed. These doublets are found at about 180 cm^{-1} from the origin. This observation leads us to suppose that the spectrum origin might be a $2A_g + 2x1B_g$ combination band. As shown in Table 5.2, the experimental and calculated frequency shifts of the mode between the excited state and the ground state, *i.e.* $\nu(S_1\text{-}S_0)_{expt}$ and $\nu(S_1\text{-}S_0)_{calcul}$ agree well with this assignment.

TABLE 5.2. Ground (S_0) and excited state (S_1) vibrational frequencies of Pc-d_{12} obtained from LIF and SVL fluorescence spectra.

ν (S_1) expt Pc-d_{12}	ν (S_1) calc Pc-d_{12}	ν (S_1) calc Pc-d_{12} scaled (*)	ν (S_0) expt Pc-d_{12}	ν (S_0) calc Pc-d_{12}	ν (S_0) calc Pc-d_{12} *scaled* (**)	ν (S_1 -S_0) $_{expt}$	ν (S_1 -S_0) calc	ν (S_1 -S_0) $_{calc}$ scaled	Assignment
126	129	124	131	131	126	-5	-2	-2	$2B_g$
131	144	139	132	147	142	-1	-3	-3	$1A_g$ --
136	144	139	136	147	142	0	-3	-3	$1A_g$ ++
171	172	166	163/175 (mean=169)	180	174	+2	-8	-8	$2A_g$ --
175	172	166	158/170 (mean=164)	180	174	+11	-8	-8	$2A_g$++
317	328	316	321	331	319	-4	-4	-3	$3A_g$ --
321	328	316	325	331	319	-4	-4	-3	$3A_g$ ++
335	348	335	343/352 (mean=347.5)	352	339	-12.5	-4	-4	$4A_g$ --
340	348	335	345/353 (mean=349)	352	339	-9	-4	-4	$4A_g$ ++
343	332	320	347/357 363	363	350	-20	-31	-20	($5B_g$ --) + "$4A_g$" of Pc-d_{11}
346	332	320	362	363	350	-16	-31	-20	$5B_g$ ++
351	345	332	364	361	348	-13	-16	-16	2 x$2A_g$ (??)
356	378	364	388	405	390	-32	-27	-26	$2A_g$ +2x$1B_g$

(*) TD-B3LYP/6-31+G (d, p), Scaling factor 0.9633

(**) B3LYP/6-31+G (d, p), Scaling factor 0.9640

$\nu(S_1\text{-}S_0)_{expt}$: the experimental frequency shift of a mode between the excited (S_1) and ground (S_0) electronic states.

$\nu(S_1\text{-}S_0)_{calc}$: Calculated frequency shift of a mode between the excited (S_1) and ground (S_0) electronic states.

TABLE 5.3. Experimental and calculated isotopic shifts of the low frequency vibrations of Pc and Pc-d_{12}

ν (S_1) expt Pc-d12	ν (S_1) calc scaled Pc-d12	ν (S_1) expt Pc	ν (S_1) calc scaled Pc	*Δν (S_1) expt*	*Δν (S_1) Calc scaled*	*ν* (S_0) expt Pc-d12	*ν* (S_0) calc scaled Pc-d12	*ν* (S_0) expt Pc	*ν* (S_0) calc scaled Pc	*Δν (S_0) expt*	*Δν (S_0) Calc scaled*	Assignment
91	99	112	107	-21	-8	112	108	117/121 (mean= 119)	117	-7	-9	1Bg++
126	124	136	130	-10	-6	131	126	135/140 (mean= 138)	131	-7	-5	$2B_g$
131	139	139	141	-8	-2	132	142	145	145	-13	-3	1Ag --
136	139	144	141	-8	-2	136	142	145	145	-9	-3	1Ag ++
171	166	179	170	-8	-4	163/175 (mean=169)	174	169/181 (mean=175)	177	-6	-3	2Ag --
175	166	184	170	-9	-4	158/170 (mean=164)	174	174/186 (mean=180)	177	-16	-3	2Ag++
317	316	335	328	-18	-12	321	319	335/340 (mean=338)	334	-17	-15	3Ag --
321	316	339	328	-18	-12	325	319	337/341 (mean=339)	334	-14	-15	3Ag ++
335	335	360	354	-25	-19	343/352 (mean=348)	339	357/362 (mean=360)	357	-12	-18	4Ag --
340	335	364	354	-24	-19	345/353 (mean=349)	339	361/364 (mean=363)	357	-14	-18	4Ag ++
343	320	395	349	-52	-29	347/357 363	350	399	386	-36	-36	(5Bg --) +4Ag pcd11
346	320	400	349	-54	-29	362	350	398	386	-36	-36	5Bg ++
351	332	362	339	-11	-7	364	348	345/364 (mean=355)	355	+9	-7	2 x2Ag ++
356	364	398	383	-42	-19	388	390	411/418 (mean=415)	411	-27	-21	$2A_g$ +2x1B_g++

Δν (S_1) denotes the isotopic shift between analogous modes of Pc-d_{12} and Pc in the excited S_1 state.

Δν (S_0) denotes the isotopic shift between analogous modes of Pc-d_{12} and Pc in the ground state.

Experimental data from Single Molecule Surface Enhanced Resonance Raman Spectroscopy (SM-SERRS) study (S.Gawinkowski, M. Pszona, S. Gorski and J. Waluk, Poster presentation) predict isotopic shifts of -4, -16 and -18 cm^{-1} between Pc-d_{12} and Pc for $2A_g$, $3A_g$ and $4A_g$ modes in the ground state.[3] The predictions are in good agreement with our results considering the differences in the techniques.

5.3.7 (0-0) +4A_g excitation: "Reversed" isotopic effect

Figures 5.13 a-c present the comparison of DF spectra of Pc-d_{mix} obtained by excitation of the bands at 16550 (a) and 16545.4 cm^{-1} (b) with that of Pc (c, $4A_{g_0}^{1}$ excitation).

An interesting isotopic effect is observed while comparing tunnelling splittings in Pc and Pc-d_{12} for the $4A_g$ mode in the ground state. This mode is identified as neutral, neither proton tunnelling promoting nor inhibiting in porphycene, [100,101] with the tunnelling splitting of 4.5 cm^{-1} similar to the splitting of the vibrationless level of the ground state. Surprisingly, however, the tunnelling splitting of this mode in Pc-d_{12} is found to be twice as large as in Pc in the ground state.

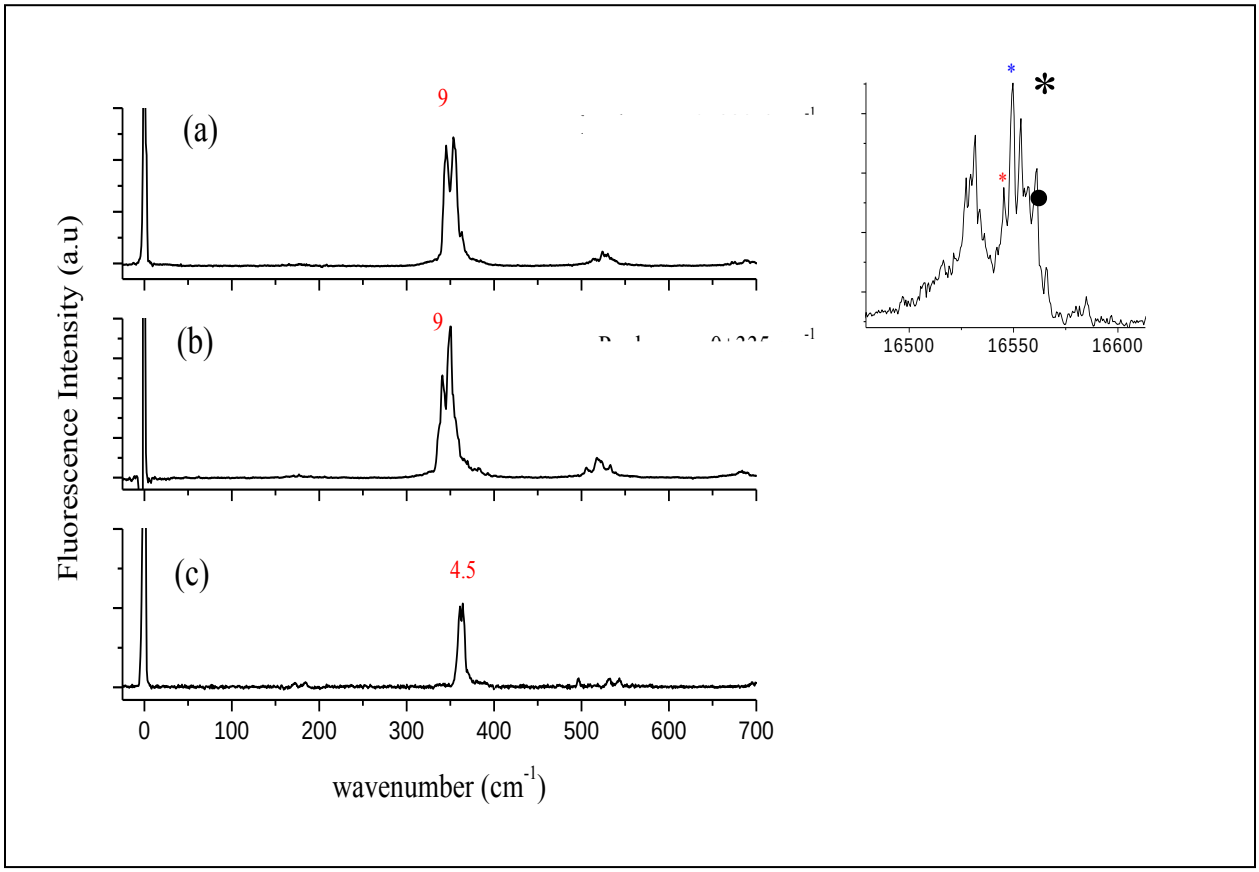

Figure 5.13 Dispersed fluorescence spectrum of (a) Pc-d_{12}, $4A_{g0+}^{1+}$ excitation at 16550 cm^{-1} (asterisk); (b) Pc-d_{12}, $4A_{g0-}^{1-}$ excitation at 16545.4 cm^{-1} (dot); (c) Pc, $4A_{g0+}^{1+}$ excitation. The inset shows part of the LIF spectrum of Pc-d_{mix} and the asterisk and the dot show the position of the tunnelling doublet of the $4A_g$ mode of Pc-d_{12}.

The increase in tunnelling splitting in Pc-d_{12}, at first surprising and contrary to the expectation, could be explained when analysing the displacement vectors of the mode in the deuterated species. Figures 5.14a and b show the displacement vectors of the $4A_g$ mode in Pc and Pc-d_{12} in the ground state.

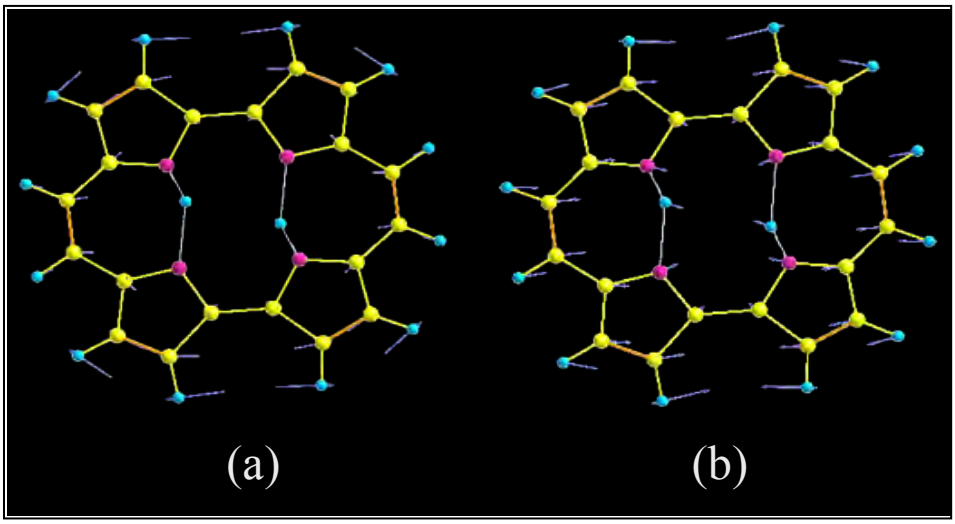

Fig 5.14 Displacement vectors of the $4A_g$ normal mode of Pc (a) and Pc-d_{12} (b) obtained using DFT B3LYP/6-31+G(d, p).

It is evident that in Pc only the skeletal hydrogens reveal significant displacement, while in Pc-d_{12} there is also a significant displacement of the cavity nitrogens and the inner hydrogens in addition to the skeletal hydrogens. This results in modification of the NH···N distance in Pc-d_{12}, but not in Pc upon excitation of the $4A_g$ mode. Therefore, the increase in the tunnelling splitting of the $4A_g$ mode in Pc-d_{12} can be ascribed to modification of the NH···N distance. This finding shows that deuteration affects not only the frequency of vibrations, but also the nature of displacement vectors of some modes, as already calculated for free base porphyrin. [194] Such an effect was also observed in deuterated tropolones (TRN), where the tunnelling splitting in mode ν_{13} of 5D-TRN is larger than the corresponding mode in the parent TRN. [195]

5.4 Conclusions

LIF and SVLF measurements, in combination with quantum chemical calculations were applied to investigate heterogenous, deuterated Pc samples (Pc-d_{mix}) with prevailing contribution of Pc-d_{12}. Comparison of Pc-d_{12} with parent undeuterated porphycene reveals similar spectroscopic features in the two isotopologues. Comparable tunneling splittings are observed both for 0-0 transition and for the most tautomerization-promoting $2A_g$ mode. Slightly smaller values of tunneling splitting are observed for $2A_g$ in Pc-d_{12}. One could thus conclude that the CH–involving vibrations do not effectively couple to the hydrogen transfer potential. Deuteration, however, can lead to a change in the form of other normal modes, as demonstrated by the interesting isotopic effect observed via comparison of $4A_g$ modes of Pc and Pc-d_{12}. The $4A_g$ mode is known to be a neutral one in Pc, i.e., exhibiting similar value of the splitting as the 0-0 transition. However, in Pc-d_{12}, this mode shows twice the value of the tunneling splitting in 0-0. This observation was explained in terms of the modification of the displacement vectors of the $4A_g$ mode upon deuteration, which, in turn, increases the coupling to the reaction coordinate. The $4A_g$ mode, neutral in undeuterated Pc, becomes tautomerization-promoting in Pc-d_{12}. This finding opens new perspectives for the studies of other porphycene isotopologues, e.g., those with ^{15}N.

Comparison of the spectra of Pc with those of x-Pc-d_{11} and Pc-d_{10} species revealed similarities as well as differences. Broadening instead of splitting in the 0-0 transitions of the latter two species, both in the LIF and DF spectra, can be a result of large heterogeneity of the isotopomers. On the other hand, similar tunneling splittings are found for Pc, Pc-d_{12} and x-Pc-d_{11} along the most promoting $2A_g$ mode.

Successful measurements of the LIF and DF spectra of Pc and its isotopologues isolated in supersonic jet using laser desorption shows that this technique is promising for the study of proton tunneling in derivatives of porphycene which were previously inaccessible with conventional heating techniques, either due to high melting points of the derivatives or to uncontrolled reactions in the furnace as a result of high temperature. Our results also demonstrate the potential of supersonic jet spectroscopy for the analysis of heterogeneous samples, consisting of isotopologues which are extremely difficult to separate by other methods.

Chapter Six

Spectroscopic study of jet-cooled selected porphycene derivatives

It has been shown in the previous chapters that proton tunneling in porphycene is sensitive for isotopic substitutions of the internal NH hydrogens. It has been also stated that alkyl substitution of external C-H hydrogens have dramatic effects on the tunneling rate and/or mechanism (chapter 1). In this chapter, the results of LIF and dispersed fluorescence spectra of 2,7,12,17-tetra-tert-butylporphycene (TTPC) (Scheme 6.1a) and 2,7,12,17-tetraphenylporphycene (TPP0) (scheme 6.1b) are presented. The effect of alkyl or aryl substitution is twofold: On one hand, it modifies the electronic distribution within porphycene which in turn alters the NH···N distance and on the other hand, the substitution lowers the overall symmetry of the system and introduces additional frequency modes. Therefore, such modifications represent more stringent electronic and structural perturbations.

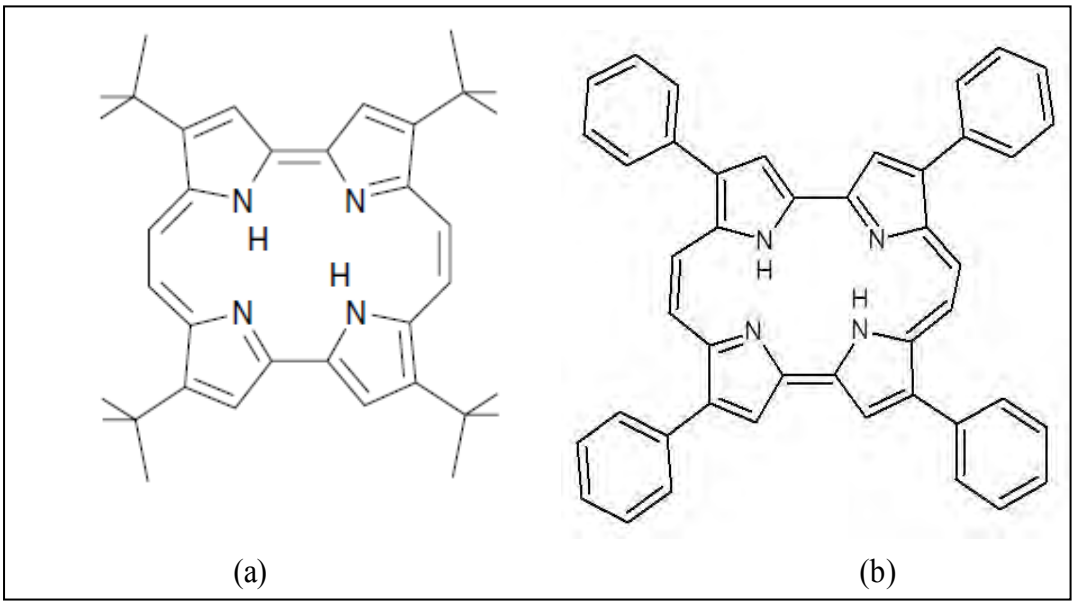

Scheme 6.1 Structural formula of 2,7,12,17-tetra-tert-butylporphycene (TTPC) (a) and 2,7,12,17-tetraphenylporphycene (TPP0).

6.1 LIF excitation and dispersed fluorescence spectra of TTPC

Although the LIF excitation spectrum of TTPC was first measured by Nosenko et.al [196] in a conventional supersonic-jet, the sample was measured again in a supersonic jet conditions using both conventional heating and laser desorption method in the low frequency region (Figure 6.1).

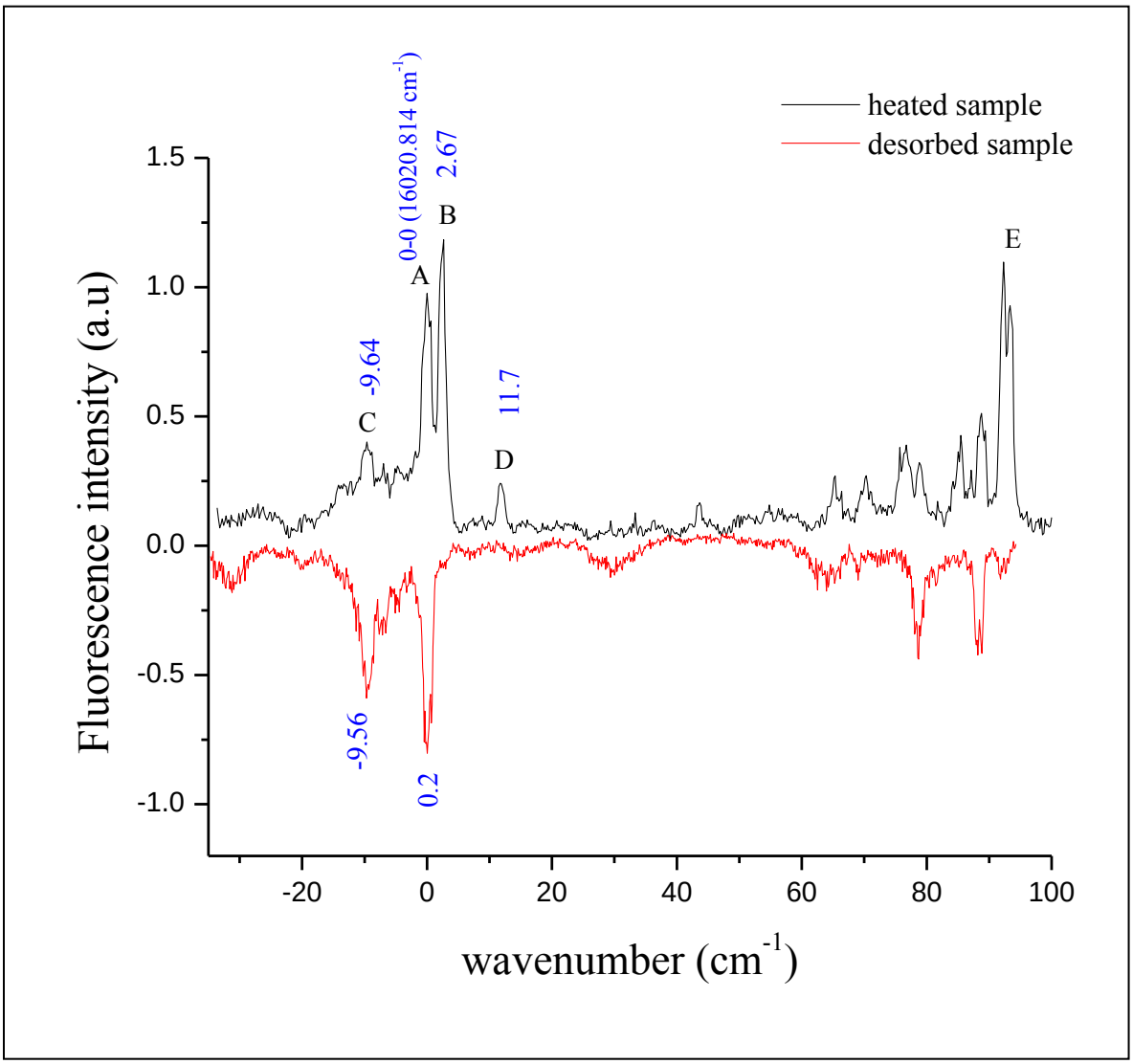

Figure 6.1 LIF excitation spectrum of TTPC in supersonic jet condition using conventional heating oven (black) and laser desorption (red) presented as mirror reflection for easier comparison. The position of band A was chosen as a reference position for other bands.

Comparison of the two spectra brought surprising results. Similar to the results of Nosenko et.al [196], four transitions were observed near the origin when using a sample in a heated oven while only two strong transitions were observed when using laser desorption technique. The most intense band (B) and smaller intensity band (D) were observed only in a heated oven. Notice that a strong vibronic band (E) which was shown to be related to band B via hole burning spectroscopy is also missing in the spectrum recorded with the laser ablation source. The difference in the two LIF spectra suggests the reduced number of species cooled by laser desorption, even though, the cooling process in both technique are equally effective as evidenced by the similar spectral widths of corresponding bands. It could be inferred from such an observation that there exist a preferential cooling in laser desorption technique where the selectivity depends on the relative stability of the structure of the analytes on the desorption surface. Nosenko et.al [196] deduced from hole burning experiment that the strong bands A and B belong to origin bands of different conformers. Further, they have demonstrated the "hot" nature of band C and suggested that this band might be the "hot" tunneling counterpart of species represented by A with tunneling splitting of 9.9 cm^{-1}. Their suggestion was, however, based on indirect methods. On the other hand, they did not suggest about the nature of band D. In order to learn more about these bands, dispersed fluorescence spectra were measured via selective excitation of the bands A, B, C and D (Figure 6.2).

Excitation of the bands A and C leads to well matched dispersed fluorescence spectra typical for excitation of tunneling multiplets of a single species. Similar results were found for porphycene by excitation of tunneling doublets[100]. Therefore, band C is assigned as "hot" transition belonging to tunneling doublet of species A. Emission spectrum from excitation of band A shows clear doublets in the resonance transition separated by about 10 cm^{-1}. This value is similar to the separation of the multiplets in the LIF excitation spectrum showing much greater tunneling splitting in the S_0 state than in the S_1 state as suggested by Nosenko et.al. On the other hand, the emission spectrum from excitation of the bands B and D are different from each other and from the multiplets. Therefore, one can postulate the presence of three stable conformers, especially at higher temperature in the oven. On the contrary, in the case of laser desorption, only species A was observed indicating one stable form in the solid prior to desorption.

Geometry optimization shows that the most stable is the C_{2h} symmetric trans isomer. The second most stable isomer is actually the cis-tautomer (marked by C_{2v}) which is less stable than the most stable trans form by 1.5 kcal/mol. There are also other trans isomers of TTPC of which two of them, marked as $C_{2h}(2)$ and C_{s1} are presented in figure 6.3. They are higher in energy by approximately 2.7 kcal/mol per every tertbutyl group rotated by 180 deg.

According to the above results, structure C_{2h} (2) lies higher in energy and hence it is less likely to be formed.

Assignment of the bands A, B, C and D to specific structures needs comparison of optimized structures both in the ground and the S_1 excited state. However, as the excited state calculation is not yet done, tentative assignment will be given based on indirect methods. The most intense band in the LIF spectrum (B) could be assigned as the most stable C_{2h} structure of TTPC. The lack of tunneling splitting in the origin transition of this species could be accounted by expansion of the NH…N distance in this isomer (2.667 Å) relative to unsubstituted porphycene (2.663 Å). On the other hand, the tunneling multiplets A and C could be assigned as tunneling tautomers of the second most stable cis-tautomer (C_{2v}). This assignment is based on the fact that the NH….N distance in the optimized structure of Cis-C_{2v} isomer is significantly smaller than the corresponding distance in unsubstituted porphycene (2.626 vs 2.667 Å). The decrease in NH…N distance is expected to result in faster proton tautomerization rate in the C_{2v} TTPC and hence greater tunneling splitting in the ground state as observed in the experiment (9.9 cm^{-1}). Therefore, the bands A and C in the LIF spectrum are assigned to the Cis-C_{2v} TTPC.

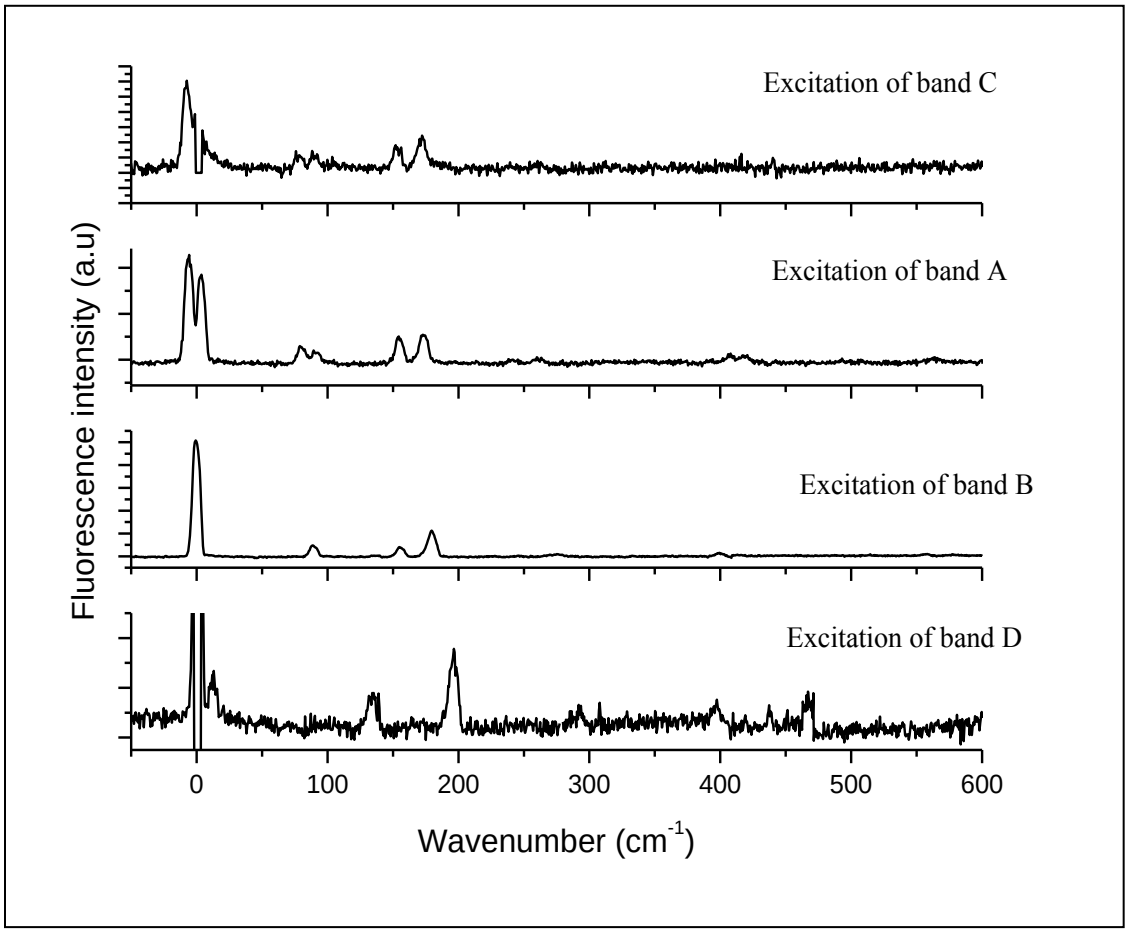

Figure 6.2 Single vibronic level dispersed fluorescence spectra of TTPC in supersonic jet from heated oven.

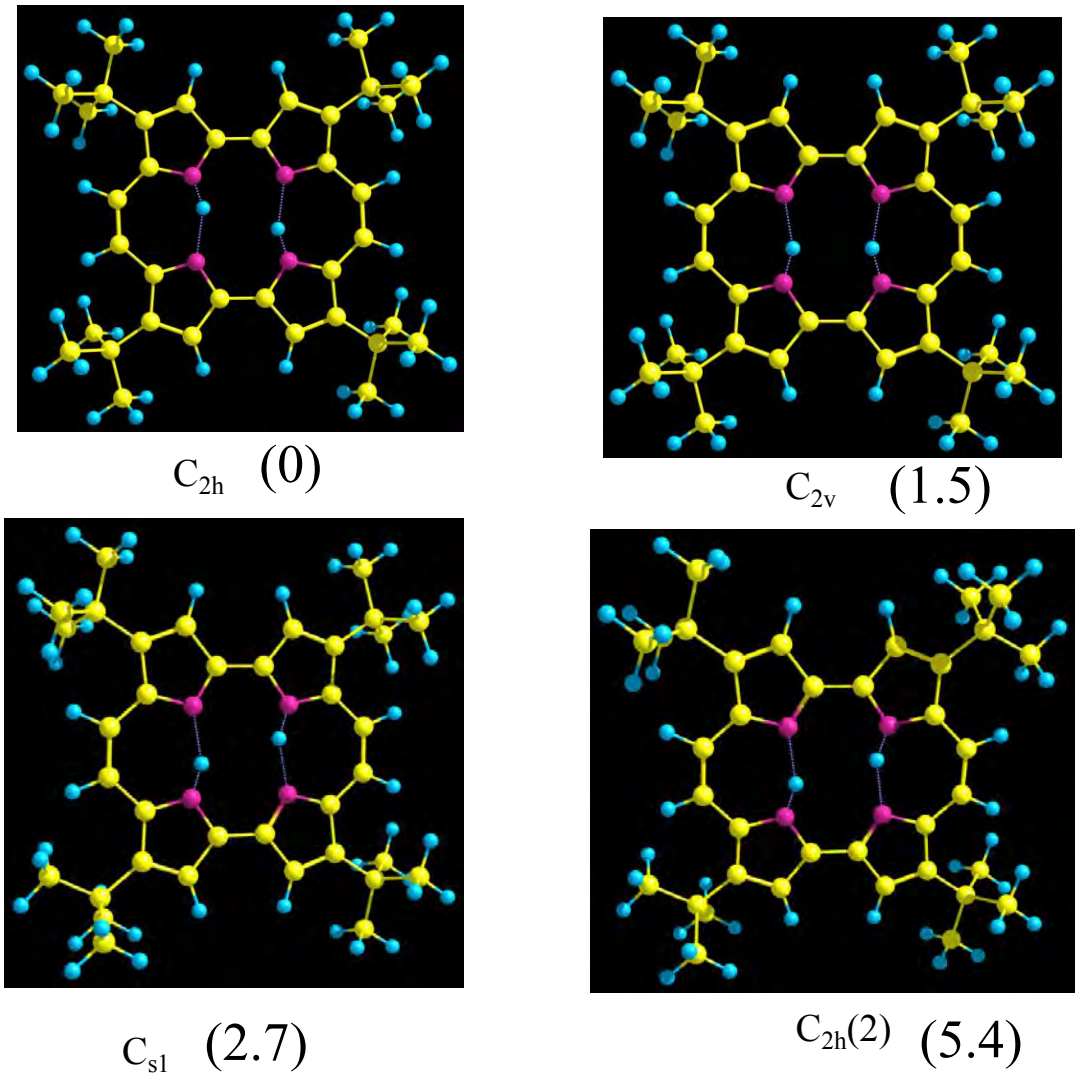

Figure 6.3. The most stable optimized structures of TTPC obtained using DFT B3LYP/6-31+G(d, p). The relative energies (in Kcal/ mole) of the isomers are given in parenthesis.

The remaining small intensity and blue shifted band (D) could be assigned as the less stable C_{s1} conformer of TTPC. Although this structure has comparable NH…N distance (2.6637 Å) to unsubstituted porphycene (2.6633 Å), it does not show any signature of tunneling splitting. This observation can be accounted by the decrease in the symmetry of the structure (C_s) which would result in non- equivalent tunneling tautomers. However, the assignment of band D should be

taken with care, as there is also a possibility to assign it as a low frequency mode of the other two stable structures of TTPC. Therefore, hole burning spectral analysis should be done for band D. Based on the interpretations given above, the following energy diagram is proposed.

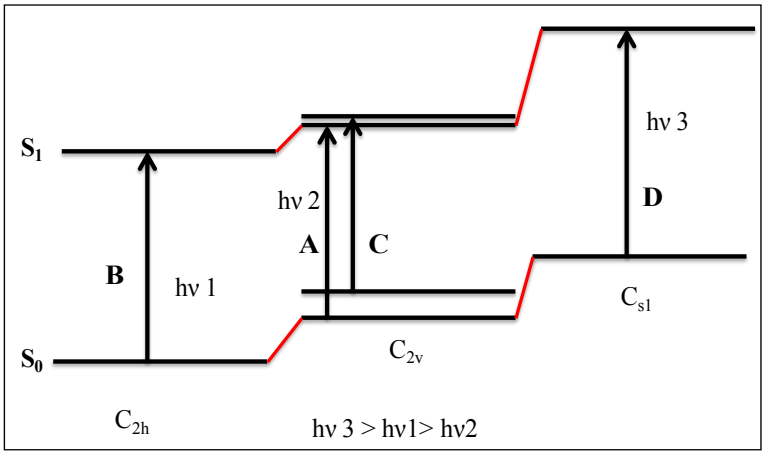

Figure 6.4 Qualitative representation of the relative energies of the most stable isomers of TTPC.

One could notice that the LIF excitation spectrum of TTPC using laser desorption method shows the presence of only one conformer, namely the Cis- C_{2v} structure. This shows that the C2v structure of TTPC is dominating in the solid sample.

6.2 LIF excitation spectrum of TPP0

As explained in the experimental section, measurement of LIF spectrum of TPP0 was not possible in supersonic-jet set up using conventional heat source because of high sublimation point (> 300^0C) of the sample. Therefore, laser desorption method was applied to vaporize the sample. Figure 6.5 shows the LIF spectrum of TPP0 using laser desorption method.

The LIF spectrum shows non resolved signal centered at about 641 nm, with rather poor signal to noise ratio. This signal is found to respond to the valve and the desorption laser. This shows that it was possible to get the sample in to a gas form. However, it was not possible to see discrete transitions. This might be due to relatively large background pressure (about 10^{-3} mbar) which might be too much to allow cooling of a floppy molecule like TPP0.

Measurement of the fluorescence lifetime (excitation laser fixed at 643 nm) shows a single exponential decay with life time of about 10 ns approximately twice shorter than that of porphycene.

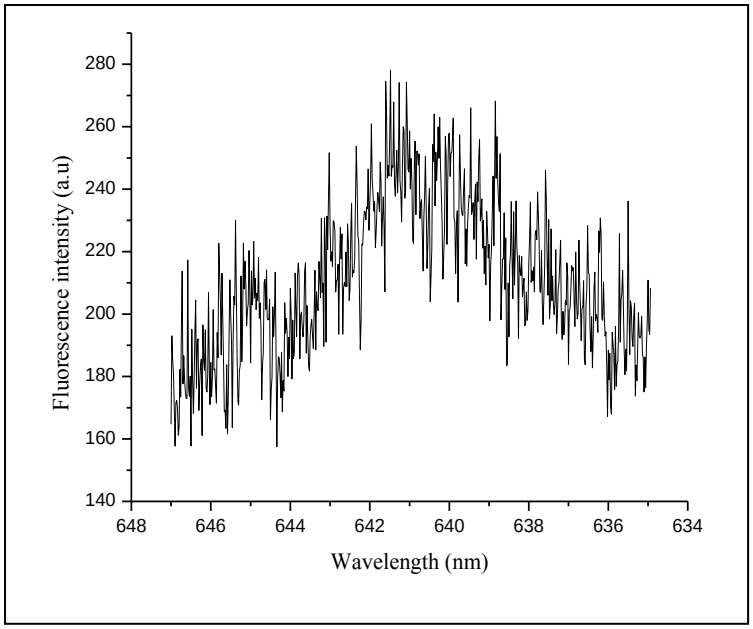

Figure 6.5 LIF excitation spectrum of TPP0 using laser desorption.

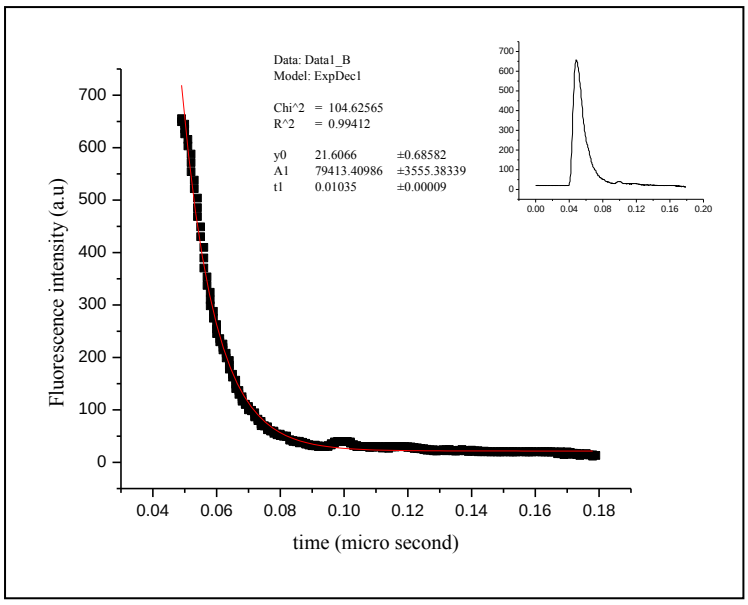

Figure 6.6 Fluorescence intensity decay profile of TPP0 (excitation 643nm). The inset shows the fluorescence intensity rise and decay time.

6.3 Conclusions

LIF and SVLF measurements, in combination with quantum chemical calculations shows the presence of two trans (of C_{2h} and C_{s1}) and one Cis (C_{2v}) isomers of TTPC in the supersonic jet condition. A tunneling splitting of about 10 cm^{-1} is found for the C_{2v} structure while no tunneling splitting is found for either of the trans isomers. This observation was explained by smaller NH….N distance in the cis isomer. Comparison of the LIF spectra of TTPC from an oven source and from ablation brought surprising results. Four transitions were observed near the origin when using a sample in a heated oven while only two strong transitions were observed when using laser desorption technique. Therefore, one can postulate the presence of three stable conformers, especially at higher temperature in the oven whereas in the case of laser desorption, only one stable form in the solid is transferred to the vapor and hence reduced number of species could be expected. Our attempt to obtain resolved LIF spectrum of TPP0 failed.

The data presented in this chapter are, however, only preliminary and it was not possible to "see" the nature and contribution of the substituents on the proton transfer dynamics. An extensive systematic study is required to confirm the tentative assignments and conclusions. Therefore, single vibronic level fluorescence study of the above derivatives is essential. For TPP0, it might be necessary to change the carrier gas to Ar to get a better cooling condition.

Chapter Seven

Summary and outlook

The investigations presented in this thesis, along with previous studies, represent an effort towards full and accurate characterization of the vibrational modes and proton tunneling dynamics of porphycene. Spectroscopic studies of porphycene isotopologues and some selected derivatives were also performed in supersonic-jet conditions.

Laser induced fluorescence (LIF) excitation near a saturation regime, hole burning spectroscopy, and extensive single vibronic level (SVL) dispersed fluorescence measurements of jet-cooled porphycene, along with quantum chemical calculations, were carried out. Consequently, precise assignments of the bands observed in the S_0 and S_1 states of porphycene have been proposed. It was also possible to demonstrate, explicitly, the multidimensional nature of proton tunneling and the importance of mode-coupling in influencing this process, for different fundamentals, progressions and combinations of vibronic transitions exhibit different values of tunneling splitting. The values of tunneling splitting along the progressions of $2A_g$ mode were found to increase with the vibrational quantum number in the S_0 state. For several cases, however, coupling of the $2A_g$ mode with other vibrations was observed, and led to the lowering of tunneling splitting. In most cases, the dispersed fluorescence spectra resultant from the excitation of tunneling doublets show similar features. Our single vibronic level fluorescence study also shows that intramolecular vibrational energy redistribution (IVR) contributes significantly in relaxation of the S_1 sublevels bearing the vibrational energy in excess of 800 cm^{-1}.

An analytical function based on symmetric mode coupling (SMC) model was applied to map a two-dimensional potential energy surface of porphycene, where N-H stretch is considered as the tunneling coordinate, while the low frequency $2A_g$ mode is an assisting mode. The measured values of tunneling splitting were well reproduced by this model. The results of the study show that $2A_g$ mode is indeed a promoting mode assisting proton tunneling in porphycene by decreasing the energy barrier.

The study was extended to investigate heterogeneous, perdeuterated Pc samples (Pc-d_{mix}) with prevailing contribution of Pc-d_{12}, in order to see the effect of a weak structural perturbation on the proton transfer dynamics. This study, performed using laser desorption as the conventional heating method, posed some difficulties for these delicate systems. Comparison of the DF spectrum of Pc-d_{12} with parent, undeuterated porphycene reveals similar spectroscopic features

in both isotopologues. One could thus conclude that the CH–involving vibrations do not effectively couple to the hydrogen transfer potential. The deuteration could, however, modify some modes, as demonstrated by the interesting isotopic effect observed via comparison of $4A_g$ modes of Pc and Pc-d_{12} (see Chapter 5). Consequently, the $4A_g$ mode, neutral in undeuterated Pc, becomes a promoting mode in Pc-d_{12}. This finding opens new perspectives for the studies of other porphycene isotopologues, e.g., the ^{15}N-substituted.

LIF and SVLF measurements of 2,7,12,17-tetra-tert-butylporphycene (TTPc) in the supersonic jet (with conventional heating) have pointed out, in combination with quantum chemical calculations, the presence of two Trans- (of C_{2h} and C_s symmetries) and one Cis- (C_{2v}) isomers. A tunneling splitting of about 10 cm^{-1} was observed and ascribed to the C_{2v} structure, while no tunneling splitting was observed for either of the trans isomers. This observation was tentatively explained by smaller NH----N distance in the Cis-isomer. Interestingly, presence of only the Cis-form of TTPc was manifested in the LIF spectrum measured in a supersonic jet using the laser desorption method (see Chapter 6).

Although most of the objectives presented in Section 1.4 were successfully addressed, there are still some questions (born also during the study) which deserve further investigations. Unexpected and still puzzling was the observation of the tunneling splitting in dispersed fluorescence spectra, in spite of the excitation of a selected (either +/+ or -/-) tunneling component known from the LIF excitation spectrum - implying fast relaxation between the states of different parities. Our attempt to see the NH stretch (30 B_u mode) band of porphycene by the IR/VIS hole-burning measurement in a supersonic jet failed. This is probably due to extensive coupling of the mode which results in band broadening, as was already suggested by condensed phase studies. Although we managed to detect fluorescence of 2,7,12,17-tetra-tert-phenylporphycene (TPP0), attempts to measure a well-resolved LIF spectrum have been unsuccessful.

The studies presented in this thesis shed light on understanding the double proton tunneling dynamics of porphycene and its isotopologues. Most importantly, the experimental values of tunneling splitting reported here for various fundamentals, progressions, and combination modes could be used as the benchmarks for theoretical modeling of the multidimensional double proton tunneling in porphycene systems.

List of references

1. D.Dolphin, The Porphyrins, Vol.2, university of Michibgan, Academic press, 1978.
2. Milgrom L. R. , The colors of life, Oxford University press: oxford; 1997
3. (a) James P. Collman,* John T. McDevitt,* Gordon T. Yee,* Charles R. Leidner,* Laughlin G. McCullough,* William A. Little,† and Jerry B. Torrance‡, Proc Natl Acad Sci U S A. Jul 1986; 83(13): 4581–4585.

   (b) "Efficient multistep photoinitiated electron transfer in a molecular pentad," Gust, D.; Moore, T. A.; Moore, A. L.; Lee, S. J.; Bittersmann, E.; Luttrull, D. K.; Rehms, A. A.; DeGraziano, J. M.; Ma, X. C.*Science* **1990**, *248*, 199-201.

   (c) Sirlin. C. 'Bosio, L., Simon, J. , J. Chem. Soc. , Chem. Commun. 1987, 379.

   (d) Wagner R.W. , Lindsey J. S. , Pure Appl. Chem. 1996,68, 1373.
   (e) Wagner R.W. , Lindsey J. S. , Seth J. , Palaniappan V. , Bocian D. F. , J. Am. Chem. Soc. 1996, 118, 3996.

4. (a) Kessel, D.; Dougherty, T., Eds. Porphyrin Photosensitization, Advances in Experimental Medicine and Biology 160; Plenum: New York, 1983. (b) Andreoni, A.; Cubeddo, R., Eds. Porphyrins in Tumor Phototherapy; Plenum: New York, 1984. (c) Fukuda, H.; Casas, A.; Chueke. F.; Paredes, S. Int. J. Biochem. 1993, 25, 1395. (d) Hamblin, M.; Newman, E. J. Photochem.Photobiol. B: Biol. 1994, 23,3.(e) Richert, C.; Wessels, J.; Muller, M.; Kisters, M.; Benninghaus, T.; Goetz, A. J. Med. Chem. 1994, 37, 2797. (f) Dolphin, D. Can. J. Chem. 1994, 72, 1005. (g) Meng, G. G.; James, B. R.; Skov, K. A.; Korbelik, M. Can. J. Chem. 1994, 72, 2447. (h) Bonnett, R. Chem. Soc. Rev. 1995, 19. (i) Boyle, R. W.; Dolphin, D. Photochem. Photobiol. 1996, 64, 469.

5. (a) Shaheen P Karimm and Ron A Adelmann, Clin Ophthalmol. 2013; 7: 1867–1875.

   (b) Scott L. J, Goa K. L., Verteporfin. *Drugs Aging*. 2000; 16:139-46.

6. Drabkin, D. L. (1963), Introduction: some historical highlights in knowledge of porphyrins and porphyrias. Annals of the New York Academy of Sciences, 104: 658–665. doi: 10.1111/j.1749-6632.1963.tb17699.x

7. E. D. Sternberg et at., Tetrahedron 54 (1998) 4151 -4202.

8. Leanne B. Josefsen and Ross W. Boyle, "Photodynamic Therapy and the Development of Metal-Based Photosensitisers," Metal-Based Drugs, vol. 2008, Article ID 276109, 23 pages, 2008. doi:10.1155/2008/276109

9. Meyer-Betz F. (1913) Wirkung des hamatoporhpyrins und anderer derivative des blut und gallenfarbestoffs. Dtsch Arch Klin Med. 112:476-503.

10. “Handbook of Porphyrins and Related Macrocycles. Volume 6, Applications: Past, Present and Future”, Karl M. Kadish, Kevin Smith and Roger Guilard, Eds., Academic Press: Burlington, MA, (2000), 346 pages

11. Biesaga, M., Pyrzyńska, K., & Trojanowicz, M. (2000). Porphyrins in analytical chemistry. A review. *Talanta*, *51*(2), 209-224.

12. Sánchez-García, David, Jose I. Borrell, and Santi Nonell. "One-Pot Synthesis of Substituted 2, 2′-Bipyrroles. A Straightforward Route to Aryl Porphycenes†."*Organic letters* 11.1 (2008): 77-79.

13. (a) Franck, B. Angew. Chem., Int. Ed. Engl. 1982, 21, 343. (b) Gosmann, M.; Franck, B. Angew. Chem., Int. Ed. Engl. 1986, 25, 1100. (c) Knubel, G.; Franck, B. Angew. Chem., Int. Ed. Engl. 1988, 27, 1170. (d) Franck, B.; Nonn, A. Angew. Chem., Int. Ed. Engl. 1995, 34, 179.

14. Sessler, J.; Burrell, A. K. Top. Curr. Chem. 1991, 161, 177. (b) Sessler, J. L.; Weghorn, S. J.; Morishima, T.; Rosingana, M.; Lynch, V.; Lee, V. J. Am. Chem. Soc. 1992, 114, 8306. (c) Sessler, J. L.; Hemmi, G.; Mody, T. D.; Murai, T.; Burrell, A.; Young, S. W. Acc. Chem. Res. 1994, 27, 43. (d) Sessler, J. L.; Weghorn, S. J.; Hiseada, Y.; Lynch, V. Chem. Eur. J. 1995, 1, 56. (e) Rexhausen, H.; Gossauer, A. J. Chem. Soc., Chem. Commun. 1983, 275. (f) Gossauer, A. Chimia 1983, 37, 341.

15. (a) Vogel, E. Pure Appl. Chem. 1990, 62, 557. (b) Vogel, E. Pure Appl. Chem. 1993, 65, 143. (c) Vogel, E. Pure Appl. Chem. 1996, 68, 1355. (d) Vogel, E. J. Heterocycl. Chem. 1996, 33, 1461.

16. (a) Furuta, H.; Asano, T.; Ogawa, T. J. Am. Chem. Soc. 1994, 116, 767. (b) Chmielewski, P. J.; Latos-Grazynski, L.; Rachlewicz, K.; Glowiak, T. Angew. Chem., Int. Ed. Engl. 1994, 33, 779. (c) Chmielews- ki, P. J.; Latos-Grazynski, L.; Rachlewicz, K. Chem. Eur. J. 1995, 1, 68.

(d) Ghosh, A. Angew. Chem., Int. Ed. Engl. 1995, 34, 1028. (e) Chmielewski, P. J.; Latos-Grazynski, L.; Glowiak, T. J. Am. Chem. Soc. 1996, 118, 5690.

17. (a) Johnson, A. W. Pure Appl. Chem. 1971, 28, 195. (b) Grigg, R. In The Porphyrins, Vol. II, Dolphin, D., Ed.; Academic Press: New York, 1978; p 327. (c) Will, S.; Rahbar, A.; Schmickler, H.; Lex, J. Vogel, E. Angew. Chem., Int. Ed. Engl. 1990, 29, 1390. (d) Kadish, K. M.; Koh, W.; Tagliatesta, P.; Sazou, D.; Paolesse, R.; Licoccia, S.; Boschi, T. Inorg. Chem. 1992, 31, 2305. (e) Paolesse, R.; Licoccia, S.; Fanciullo, M.; Morgante, M.; Boschi, T. Inorg. Chim. Acta 1993, 203, 107. (f) Licoccia, S.; Paolesse, R. Structure and Bonding, 84; Buchler, J. W., Ed.; Springer-Verlag: Berlin, 1995; p 71.

18. Dicationic oxygen, sulfur, and selenium analogues of porphyrins: (a) Vogel, E.; Haas, W.; Knipp, B.; Lex, J.; Schmickler, H. Angew. Chem., Int. Ed. Engl. 1988, 27, 406. (b) Vogel, E.; Rohrig, P.; Sicken, M.; Knipp, B.; Herrmann, A.; Pohl, M.; Schmickler, H.; Lex, J. Angew. Chem., Int. Ed. Engl. 1989, 28, 1651. (c) Vogel, E.; Dorr, J.; Herrmann, A.; Lex, J.; Schmickler, H.; Walgenbach, P.; Gisselbrecht, J.; Gross, M. Angew. Chem., Int. Ed. Engl. 1993, 32, 1597. (d) Vogel, E.; Pohl, M.; Herrmann, A.; Wiss, T.; Konig, C.; Lex, J.; Gross, M.; Gisselbrecht, J. P. Angew. Chem., Int. Ed. Engl. 1996, (e) Markl, G.; Sauer, H.; Kreitmeier, P.; Burgemeister, T.; Kastner, F.; Adolin, G.; Noth, H.; Polborn, K. Angew. Chem., Int. Ed. Engl. 1994, 33, 1151. Carbapor- phyrin: (f) Berlin, K.; Steinbeck, C.; Breitmaier, E. Synthesis 1996, 336. Oxipyriporphyrin: (g) Lash, T. D.; Chaney, S. T. Chem. Eur. J. 1996, 2, 944. S0022-3263(97)01566-1.

19. Wu, Yun-Dong, et al. "Porphyrin isomers: geometry, tautomerism, geometrical isomerism, and stability." *The Journal of Organic Chemistry* 62.26 (1997): 9240-9250.

20. Hemiporphycene: (a) Callot, H. J.; Rohrer, A.; Tschamber, T.; Metz, B. New J. Chem. 1995, 19, 155. (b) Vogel, E.; Broring, M.; Weghorn, S. J.; Scholz, P.; Deponte, R.; Lex, J.; Schmickler, H.; Schaffner, K.; Braslarsky, S. E.; Muller, M.; Po ¨rting, S.; Fowler, C. J.; Sessler, J. L. Angew. Chem., Int. Ed. Engl. 1997, 36, 1651.

21. Corrphycene: (a) Sessler, J. L.; Brucker, E. A.; Weghorn, S. J.;Kisters, M.; Scha¨fer, M.; Lex, J.; Vogel, E. Angew. Chem., Int. Ed. Engl. 1994, 33, 2308. (b) Aukauloo, M. A.; Guilard, R. New. J. Chem. 1994, 18, 1205. (c) Falk, H.; Chen, Q., Q. Monatsh, Chem. 1996, 127, 69.

22. Vogel, Emanuel, et al. "Porphycene—a novel porphin isomer." *Angewandte Chemie International Edition in English* 25.3 (1986): 257-259.

23. (a) Porphyrins with various heteroatoms: A. W. Johnson in K. M. Smith (Ed.): Porphyrins and Metalloporphyrins. Elsevier, Amsterdam 1975, p. 729: (b) homoporphyrins: H. J. Callot, E. Schaeffer, J. Org. Chern. 42 (1977) 1567; (c) sapphyrins: v. J. Bauer, D. L. J. Clive, D. Dolphin, J. B. Paine III, F. L. Harris, M. M. King, J. Loder, S.-w. Chien Wang, R. B. Woodward, J. Arn. Chern. Soc. 105 (1983) 6429; (d) pentaphyrin: H. Rex- hausen, A. Gossauer, J. Chern. Soc. Chern. Cornrnun. 1983, 275; (e) platy- rins: E. LeGoff, R. A. Berger, 0. G. Weaver, Abstr. 10th Int. Congr. Het- erocyc/. Chern . Waterloo, Canada 1985.

24. Waluk, Jacek. "Ground-and excited-state tautomerism in porphycenes."*Accounts of chemical research* 39.12 (2006): 945-952.

25. Hollas, John Michael, Phillips D. ed. *Jet spectroscopy and molecular dynamics*. Springer, 1995.

26. Arnaut L. G., Formosinho S. J., J. Photochem. Photobiol. A: Chemistry, 1993, 75, 1.

27. Formosinho S. J., Arnaut L. G., J. Photochem. Photobiol. A: Chemistry, 1993, 75, 21.

28. Lakowicz J. R., Priciples of Fluorescence Spectroscopy. Second Edition, ed. 1999, New York: Kluwer Academic/Plenum Publisher.

29. Turro N. J., Modern Molecular Photochemistry. 1978, San Francisco, California, U.S.A.: Benjamin/Cummings Publishing Company.

30. Chattopadhyay N., J. Photochem. Photobiol. A: Chemistry, 1995, 88, 1.

31. See, for example: (a) Birks, J. B. *Photophysics of Aromatic Molecules,* John Wiley and Sons; London, 1970; (b) Birks, J. B. (Ed.) *Organic Molecular Photophysics,* Vols. 1 and 2, John Wiley and Sons; London, 1973;

32. Gilbert, A.; Baggott, J. *Essentials of Molecular Photochemistry,* CRC Press; Boca Raton, 1991.

33. Goodman M. F., Nature, 1995, 378, 237.

34. Belevich I., Verkhovsky M. I., Wikstroem M., Nature, 2006, 440, 829.

35. Faxen K., Gilderson G., Aedelroth P., Brzezinski P., Nature, 2005, 437, 286.

36. Crofts A. R., Biochim. Biophys. Acta, 2004, 1655, 77.

37. Watson J. D., Crick F. H. C., Nature (London), 1953, 171, 964.

38. Bell, Ronald Percy. "The tunnel effect in chemistry." (1980).

39. Löwdin, Per-Olov. "Proton tunneling in DNA and its biological implications."*Reviews of Modern Physics* 35.3 (1963): 724-732.

40. Wolfe, Megan, Drexel Univerisity. "Quantum Tunneling in DNA." (2013).

41. MacKenzie, Valerie Jane. "Photophysics and spectroscopy of tropolone and its van der Waals complexes." (1999).

42. C.J. Seliskar, R.E. Hoffman, J. Mol. Spectrosc. 88 1981 30.

43. E.B. Wilson, Z. Smith, Acc. Chem. Res. 20 1987. 257, and references therein.

44. (a) Y. Tomioka, M. Ito, N. Mikami, J. Phys. Chem. 87 1983. 4401. (b) P.F. Barbara, P.K. Walsh, L.E. Brus, J. Phys. Chem. 93 1989. 29.

45. J. Sepioł, Y. Stepanenko, A. Vdovin, A. Mordzinski, E. Vogel, and J. Waluk, Chem. Phys. Lett. 296, 549 (1998).

46. (a) Florio, G. M.; Sibert, E. L.; Zwier, T. S. *Faraday Discussions* **2001**, *118*, 315.
(b) Florio, G. M.; Zwier, T. S.; Myshakin, E. M.; Jordan, K. D.; Sibert, E. L. *Journal of Chemical Physics* **2003**, *118*, 1735.

47. Dennison, David M., and G. E. Uhlenbeck. "The two-minima problem and the ammonia molecule." *Physical Review* 41.3 (1932): 313.
48. Brillouin, L. (1926), C. R. Acad. Sci., 153, 24
49. Brillouin, L. (1926), J. de Physique, 7, 353.
50. Wentzel, G. (1926), Z. Phys., 38, 518.
51. Krammers, H. A. (1926), Z. Phys., 39, 828.
52. Jeffreys, H. (1923), Proc. London Math. Soc., (2), 23, 428.
53. Brickmann J. and Zimmermann, H. (1969), J. Chem. Phys., 50, 1608.
54. Brickmann J. and Zimmermann, H. (1966), Ber. Bunsenges. Phys. Chem., 70, 157.
55. RL Somorjai, DH Hornig; J. Chem. Phys., 36 (1962), 1980.
56. M.C. Flanigan and J.R. de la Vega, J. Chem. Phys. 61. (1974) 1882.
57. Busch, Jan H., and Jose R. De la Vega. "Symmetry and tunneling in proton transfer reactions. Proton exchange between methyloxonium ion and methyl alcohol, methyl alcohol and methoxide ion, hydronium ion and water, and water and hydroxyl ion." *Journal of the American Chemical Society* 99.8 (1977): 2397-2406.
58. Harmony, M. D. (1972), Chem. Soc. Reviews, 1, 211.
59. Sanchez-Garcia, D.; Sessler, J. L. *Chem. Soc. Rev.* **2008**, *37*, 215.
60. Waluk, J. In *Handbook of Porphyrin Science*; Smith, K., Kadish, K., Guilard, R., Ed.; World Scientific: Singapore, 2010; Vol. 7, p 359.
61. Braslavsky, S. E.; Muller, M.; Martire, D. O.; Porting, S.; Bertolotti, S. G.; Chakravorti, S.; KocWeier, G.; Knipp, B.; Schaffner, K. *Journal of Photochemistry and Photobiology B-Biology* **1997**, *40*, 191.
62. Stockert, J. C.; Cañete, M.; Juarranz, A.; Villanueva, A.; Horobin, R. W.; Borrell, J.; Teixidó, J.; Nonell, S. *Current Medicinal Chemistry* **2007**, *14*, 997.

63. Richert, C.; Wessels, J. M.; Müller, M.; Kisters, M.; Benninghaus, T.; Goetz, A. E. *Journal of Medicinal Chemistry* **1994**, *37*, 2797.
64. Nonell, S.; Bou, N.; Borrell, J. I.; Teixido, J.; Villanueva, A.; Juarranz, A.; Canete, M. *Tetrahedron Letters* **1995**, *36*, 3405.
65. Milanesi, C.; Biolo, R.; Jori, G.; Schaffner, K. *Lasers in Medical Science* **1991**, *6*, 437.
66. Mak, N. K.; Kok, T. W.; Wong, R. N. S.; Lam, S. W.; Lau, Y. K.; Leung, W. N.; Cheung, N. H.; Huang, D. P.; Yeung, L. L.; Chang, C. K. *Journal of Biomedical Science* **2003**, *10*, 418.
67. Baumer, D.; Maier, M.; Engl, R.; Szeimies, R. M.; Baumler, W. *Chemical Physics* **2002**, *285*, 309.
68. Waluk, J.; Müller, M.; Swiderek, P.; Köcher, M.; Vogel, E.; Hohlneicher, G.; Michl, J. *Journal of the American Chemical Society* **1991**, *113*, 5511.
69. Walewski, Ł., D. Krachtus, S. Fischer, Jeremy C. Smith, P. Bała, and B. Lesyng. "SCC-DFTB energy barriers for single and double proton transfer processes in the model molecular systems malonaldehyde and porphycene."*International journal of quantum chemistry* 106, no. 3 (2006): 636-640.
70. Walewski, L.; Waluk, J.; Lesyng, B. *Journal of Physical Chemistry A* **2010**, *114*, 2313.
71. Yoshikawa, T., Sugawara, S., Takayanagi, T., Shiga, M., & Tachikawa, M. (2010). Theoretical study on the mechanism of double proton transfer in porphycene by path-integral molecular dynamics simulations. *Chemical Physics Letters*, *496*(1), 14-19.
72. Vdovin, A.; Sepioł, J.; Urban´ska, N.; Pietraszkiewicz, M.; Mordzin´ski, A.; Waluk, J. *J. Am. Chem. Soc.* **2006**, *128*, 2577.
73. Kumagai, T., Hanke, F., Gawinkowski, S., Sharp, J., Kotsis, K., Waluk, J., ... & Grill, L. (2013). Controlling intramolecular hydrogen transfer in a porphycene molecule with single atoms or molecules located nearby. *Nature chemistry*.
74. Schlabach, M.; Wehrle, B.; Rumpel, H.; Braun, J.; Scherer, G.; Limbach, H. H. *Berichte Der Bunsen-Gesellschaft-Physical Chemistry Chemical Physics* **1992**, *96*, 821.
75. Braun, J.; Schlabach, M.; Wehrle, B.; Kocher, M.; Vogel, E.; Limbach, H. H. *Journal of the American Chemical Society* **1994**, *116*, 6593.
76. Braun, J.; Limbach, H. H.; Williams, P. G.; Morimoto, H.; Wemmer, D. E. *Journal of the American Chemical Society* **1996**, *118*, 7231.
77. Wehrle, B.; Limbach, H. H.; Kocher, M.; Ermer, O.; Vogel, E. *Angewandte Chemie-International Edition in English* **1987**, *26*, 934.
78. Langer, U.; Hoelger, C.; Wehrle, B.; Latanowicz, L.; Vogel, E.; Limbach, H. H. *Journal of Physical Organic Chemistry* **2000**, *13*, 23.
79. Pietrzak, M.; Shibl, M. F.; Bröring, M.; Kühn, O.; Limbach, H. H. *Journal of the American Chemical Society* **2007**, *129*, 296.
80. Shibl, M. F.; Pietrzak, M.; Limbach, H. H.; Kuhn, O. *Chemphyschem* **2007**, *8*, 315.

81. del Amo, J. M. L.; Langer, U.; Torres, V.; Pietrzak, M.; Buntkowsky, G.; Vieth, H. M.; Shibl, M. F.; Kuhn, O.; Broring, M.; Limbach, H. H. *Journal of Physical Chemistry A* **2009**, *113*, 2193.

82. Kozlowski, P. M.; Zgierski, M. Z.; Baker, J. *Journal of Chemical Physics* **1998**, *109*, 5905.

83. Smedarchina, Z.; Shibl, M. F.; Kuhn, O.; Fernandez-Ramos, A. *Chem. Phys. Lett.* **2007**, *436*, 314.

84. Smedarchina, Z.; Siebrand, W.; Fernandez-Ramos, A.; Meana-Paneda, R. *Zeitschrift Fur Physikalische Chemie-International Journal of Research in Physical Chemistry & Chemical Physics* **2008**, *222*, 1291.

85. Duran-Frigola, M.; Tejedor-Estrada, R.; Sanchez-Garcia, D.; Nonell, S. *Physical Chemistry Chemical Physics* **2011**, *13*, 10326.

86. Waluk, J. In *Hydrogen-Transfer Reactions*; Hynes, J. T., Klinman, J. P., Limbach, H. H., Schowen, R. L., Eds.; Wiley-VCH, Weinheim: 2007; Vol. 1, p 245.

87. Waluk, J. In *CRC Handbook of Organic Photochemistry and Photobiology*; Oelgemoeller, M., Griesbeck. A. Ghetti, F., Ed.; Taylor and Francis: 2011.

88. Gil, M.; Waluk, J. *Journal of the American Chemical Society* **2007**, *129*, 1335.

89. Piwonski, H.; Hartschuh, A.; Urbanska, N.; Pietraszkiewicz, M.; Sepiol, J.; Meixner, A. J.; Waluk, J. *Journal of Physical Chemistry C* **2009**, *113*, 11514.

90. Piwonski, H.; Sokolowski, A.; Kijak, M.; Nonell, S.; Waluk, J. *Journal of Physical Chemistry Letters* **2013**, *4*, 3967.

91. Piwoński, H.; Stupperich, C.; Hartschuh, A.; Sepioł, J.; Meixner, A.; Waluk, J. *Journal of the American Chemical Society* **2005**, *127*, 5302.

92. Gil, M.; Dobkowski, J.; Wiosna-Salyga, G.; Urbanska, N.; Fita, P.; Radzewicz, C.; Pietraszkiewicz, M.; Borowicz, P.; Marks, D.; Glasbeek, M.; Waluk, J. *Journal of the American Chemical Society* **2010**, *132*, 13472.

93. Gil, M.; Organero, J. A.; Waluk, J.; Douhal, A. *Chem. Phys. Lett.* **2006**, *422*, 142.

94. Fita, P.; Urbanska, N.; Radzewicz, C.; Waluk, J. *Zeitschrift Fur Physikalische Chemie-International Journal of Research in Physical Chemistry & Chemical Physics* **2008**, *222*, 1165.

95. Fita, P.; Urbanska, N.; Radzewicz, C.; Waluk, J. *Chemistry-a European Journal* **2009**, *15*, 4851.

96. Gawinkowski, S.; Orzanowska, G.; Izdebska, K.; Senge, M. O.; Waluk, J. *Chemistry-a European Journal* **2011**, *17*, 10039.

97. Gawinkowski, S.; Walewski, L.; Vdovin, A.; Slenczka, A.; Rols, S.; Johnson, M. R.; Lesyng, B.; Waluk, J. *Physical Chemistry Chemical Physics* **2012**, *14*, 5489.

98. Sobolewski, A. L.; Gil, M.; Dobkowski, J.; Waluk, J. *Journal of Physical Chemistry A* **2009**, *113*, 7714.

99. Kumagai, T.; Hanke, F.; Gawinkowski, S.; Sharp, J.; Kotsis, K.; Waluk, J.; Persson, M.; Grill, L. *Physical Review Letters* **2013**, *111*.

100. Mengesha, E. T.; Sepiol, J.; Borowicz, P.; Waluk, J. *Journal of Chemical Physics* **2013**, *138*.
101. Vdovin, A.; Waluk, J.; Dick, B.; Slenczka, A. *Chemphyschem* **2009**, *10*, 761.
102. Ensminger, F. A.; Plassard, J.; Zwier, T. S.; Hardinger, S. *Journal of Chemical Physics* **1995**, *102*, 5246.
103. Nash, J. J.; Zwier, T. S.; Jordan, K. D. *Journal of Chemical Physics* **1995**, *102*, 5260.
104. Levy, D. H. (1980). Laser spectroscopy of cold gas-phase molecules. *Annual Review of Physical Chemistry*, *31*(1), 197-225.
105. Amirav, Aviv, Uzi Even, and Joshua Jortner. "Analytical applications of supersonic jet spectroscopy." *Analytical Chemistry* 54.11 (1982): 1666-1673.
106. Gouterman, M. "The Porphyrins"; Dolphin, I)., Ed.; Academlc Press: New York, 1978; Vol. 111. p 1.
107. Malsch, Karsten, and Georg Hohlneicher. "The force field of porphycene: A theoretical and experimental approach." *The Journal of Physical Chemistry A*101.45 (1997): 8409-8416.
108. Stepanenko, Y., Laser spectroscopy of molecular complexes, PhD thesis, 2002, Warszawa.
109. N. Seurre, Université Paris XI, Orsay, 21 septembre 2004, "Etude par spectroscopie de double résonance IR-UV de complexes à liaisons hydrogène formés en jet supersonique : application aux intéractions énantiosélectives."
110. Sen, Ananya. *Reconnaissance chirale dans des complexes moléculaires neutres et ioniques*. Diss. Université Paris Sud-Paris XI, 2012.
111. Kang, W. K., Kim, E. J., Choi, C. J., Jung, K. W., & Jung, K. H. (1995). Time resolved molecular beam characteristic in a pulsed supersonic jet. *Bull. Korean. Chem. Soc*, *16*(3), 238-243.
112. R. J. Levis, Annual Review of Physical Chemistry **45**, 483 (1994).
113. John, F. Ready, Effects of high-power laser radiation." (1971): 115-116. New York Academic press.
114. Hicks JM, Urbach LE, Plummer EW, Dai HL. 1988. *Phys. Rev. Lett.* 61 : 2588-91.

115. Paddock CA, Eesley GL. *J. Appl. Phys.* 60: 285 90.

116. Bechtel JH. 1975. *J. Appl. Phys.* 46 (4): 1585- 93.

117. Burgress D., Stair P. C., Weitz E., (1986). J. Vac. Sci. Technol. A 4 1362-66.

118. Phillippoz J. M., Zenobi R., Zare R.N, (1989) Chem.Phys.Lett. 158:12-17.

119. Brand J.I., George S.M., 1986 Surf. Sci. 167, 341-62.

120. Eesley G.L. 1986, Phys. Rev. B 33 (4) 2144-51.

121. Elsayed-Ali H.E, Norris T.B, Pessot M.A., Mourou G.A, 1987. Phys.Rev. Lett. 58: 1212-15.

122. Schoenlein R.W., Lin W.Z., Fujimoto J.G., Eesley G.L., 1987, Phys. Rev. Lett. 58 1680-83.

123. Culter J, Li M, John LG, Hochstrasser RM, Yodh AG. 1993. Chem. Phys. Lett. 214: 431-37.

124. Hall RB, 1987. J. Phys. Chem. 91: 1007-15.

125. Van der Peyl GJQ, Isa K, Haverkamp J, Kistemaker PG. 1983. Int. J. Mass Spectrom. Ion Phys. 47: 11-14.

126. Zenobi R, Hahn JH, Zare RN, 1988. Chem. Phys. Lett. 150: 361-65.

127. Hall RB, DeSantolo AM, Bares SJ, 1985. Surf.Sci. 161: L533-L42.

128. George SM, DeSantolo AM, Hall RB, 1985. Surf. Sci. 159: L425-L32.

129. Deckert AA, George SM. 1987. Surf. Sci. 182: L215-L20.

130. Land DP, Wang DTS, Tai TL, Sherman MG, Hemminger JC, McIver RT. 1990. See ref.11 pp. 157-78

131. Redhead PA. 1962. Vacuum 12; 203-11.

132. Lucchese RR, Tully JC. 1984. J.Chem.Phys. 81 (12) : 6313-19.

133. Zhdanov VP, Zamaraev KI. 1982. Catal. Rev. Sci. Eng. 24: 373-413.

134. Zare RN, Levine RD. 1987. Chem. Phys. Lett. 136:593-99.

135. Levine RD, Bernstein RB, 1987, In Molecular Reaction Dynamics and Chemical Reactivity, pp. 314-16. New York: Oxford Univ.Press

136. Rosenzweig Z, Asscher M. 1992. J. Chem. Phys. 96 (5): 4040-43.

137. Levy D. 1981. Science 214: 263-69.

138. Schafer B, Hess P. 1984. Chem. Phys. Lett. 105: 563-66.

139. Natzel WC, Padowitz Q, Sibener SJ, 1988. J. Chem. Phys. 88: 7975-94.

140. Cousinsv LM, Lwvis RJ, Leone SR. 1989. J. Chem. Phys. 91: 5731-42

141. Noorbatcha I, Lucchese RR, Zeiri Y, 1988. Surf. Sci. 200: 113-34.

142. Noorbatcha I, Lucchese RR, Zeiri Y, 1988. J. Chem. Phys. 89: 5251-63.

143. Noorbatcha I, Lucchese RR, Zeiri Y, 1987. Phys. Rev: 36: 4978-81.

144. (a) Lahmani, F., Le Barbu-Debus, K., Seurre, N., & Zehnacker-Rentien, A. (2003). Laser spectroscopy of a chiral drug in a supersonic beam: conformation and complexation of S-(+)-< i> Naproxen</i>. *Chemical physics letters*, *375*(5), 636-644.

(b) Sen, A., Lepere, V., Barbu-Debus, L., & Zehnacker, A. (2013). How do Pseudoenantiomers Structurally Differ in the Gas Phase? An IR/UV Spectroscopy Study of Jet-Cooled Hydroquinine and Hydroquinidine.*ChemPhysChem*, *14*(15), 3559-3568.

145. Michał Kijak, Ephriem Mengesha, Anna Grabowska, Jerzy Sepioł*, Michał Gil*, 'Supersonic jet spectroscopy of 1,4-diazatriphenylene and its complexes. Structural distortion and state inversion effects.' (unpublished manuscript)

146. Frisch, M.J.T., G. W.; Schlegel, H. B.; Scuseria, G. E.; Robb, M. A.; Cheeseman, J. R.; Montgomery Jr., J. A.; Vreven, T.; Kudin, K. N.; Burant, J. C.; Millam, J. M.; Lyengar, S. S.; Tomasi, J.; Barone, V.; Mennucci, B.; Cossi, M.; Scalmani, G.; Rega, N.; Petersson, G. A.; Nakatsuji, H.; Hada, M.; Ehara, M.; Toyota, K.; Fukuda, R.; Hasegawa, J.; Ishida, M.; Nakajima, T.; Honda, Y.; Kitao, O.; Nakai, H.; Klene, M.; Li, X.; Knox, J. E.; Hratchian, H. P.; Cross, J. B.; Bakken, V.; Adamo, C.; Jaramillo, J.; Gomperts, R.; Stratmann, R. E.; Yazyev, O.; Austin, A. J.; Cammi, R.; Pomelli, C.; Ochterski, J. W.; Ayala, P. Y.; Morokuma, K.; Voth, G. A.; Salvador, P.; Dannenberg, J. J.; Zakrzewski, V. G.; Dapprich, S.; Daniels, A. D.; Strain, M. C.; Farkas, O.; Malick, D. K.; Rabuck, A. D.; Raghavachari, K.; Foresman, J. B.; Ortiz, J. V.; Cui, Q.; Baboul, A. G.; Clifford, S.; Cioslowski, J.; Stefanov, B. B.; Liu, G.; Liashenko, A.; Piskorz, P.; Komaromi, I.; Martin, R. L.; Fox, D. J.; Keith, T.; Al-Laham, M. A.; Peng, C. Y.; Nanayakkara, A.; Challacombe, M.; Gill, P. M. W.; Johnson, B.; Chen, W.; Wong, M. W.; Gonzalez, C.; Pople, J. A., Gaussian Inc, 2004. Revision C.02 ed; Wallingford CT(,).

147. S. Takada and H. Nakamura: Multidimensional tunneling in tropolone, J. Chem. Phys., Vol. 102, No. 10, 8 March 1995.

148. E. Bosch, M. Moreno, J. M. Lluch, and J. Bertra´n, J. Chem. Phys. **93**, 5685 (1990).

149. A. Auerbach and S. Kivelson, Nucl. Phys. B **257** [FS14], 799 (1985).

150. S. Takada and H. Nakamura: WKB theory of multidimensional tunneling, J. Chem. Phys. **100** (1), 1 January 1994.

151. H. Iga, T. Isozaki, T. Suzuki, and T. Ichimura, J. Phys. Chem. A **111**, 5981 (2007).

152. T. Isozaki, K. Sakeda, T. Suzuki, and T. Ichimura, J. Chem. Phys. **126**, 214304 (2007).

153. T. Isozaki, T. Suzuki, and T. Ichimura, Chem. Phys. Lett. **449**, 63 (2007).

154. G. N. Patwari and S. Wategaonkar, Proc. Indian Natn. Sci. Acad. **69A**, 61 (2003).

155. C. J. Seliskar and R. E. Hoffmann, J. Mol. Spectrosc. **88**, 30 (1981).

156. S. L. Baughcum, Z. Smith, E. B. Wilson, and R. W. Duerst, J. Am. Chem. Soc. **106**, 2260 (1984).

157. C. Duan and D. Luckhaus, Chem. Phys. Lett. **391**, 129 (2004).

158. T. N. Wassermann, D. Luckhaus, S. Coussan, and M. A. Suhm, Phys. Chem. Chem. Phys. **8**, 2344 (2006).

159. R. L. Redington and T. E. Redington, J. Mol. Spectrosc. **78**, 229 (1979).

160. R. Rossetti and L. E. Brus, J. Chem. Phys. **73**, 1546 (1980).

161. Y. Tomioka, M. Ito, and N. Mikami, J. Phys. Chem. **87**, 4401 (1983).

162. H. Sekiya, Y. Nagashima, and Y. Nishimura, Bull. Chem. Soc. Jpn. **62**, 3229 (1989).

163. R. L. Redington, J. Chem. Phys. **92**, 6447 (1990).

164. H. Sekiya, Y. Nagashima, and Y. Nishimura, J. Chem. Phys. **92**, 5761 (1990).

165. H. Sekiya, H. Hamabe, H. Ujita, N. Nakano, and Y. Nishimura, J. Chem. Phys. **103**, 3895 (1995).

166. R. K. Frost, C. Hagemeister, C. A. Arrington, T. S. Zwier, and K. D. Jordan, J. Chem. Phys. **105**, 2595 (1996).

167. T. Ikoma, K. Akiyama, S. Tero-Kubota, and Y. Ikegami, J. Chem. Phys.

168. A. E. Bracamonte and P. H. Vaccaro, J. Chem. Phys. **120**, 4638 (2004).

169. R. L. Redington and T. E. Redington, J. Chem. Phys. **122**, 124304 (2005).

170. J. C. Keske, W. Lin, W. C. Pringle, S. E. Novick, T. A. Blake, and D. F. Plusquellic, J. Chem. Phys. **124**, 074309 (2006).

171. R. L. Redington, T. E. Redington, and R. L. Sams, J. Phys. Chem. A **112**, 1480 (2008).

172. D. Murdock, L. A. Burns, and P. H. Vaccaro, Phys. Chem. Chem. Phys. **12**,

8285 (2010).

173. H. Sekiya, H. Takesue, Y. Nishimura, Z. H. Li, A. Mori, and H. Takeshita, Chem. Lett. **17**, 1601 (1988).

174. H. Sekiya, H. Takesue, Y. Nishimura, Z. H. Li, A. Mori, and H. Takeshita, J. Chem. Phys. **92**, 2790 (1990).

175. T. Tsuji, H. Sekiya, Y. Nishimura, R. Mori, A. Mori, and H. Takeshita, J. Chem. Phys. **97**, 6032 (1992).

176. H. Sekiya, H. Hamabe, T. Nakajima, A. Mori, H. Takeshita, and Y. Nishimura, Chem. Phys. Lett. **224**, 563 (1994).

177. K. Nishi, H. Sekiya, H. Kawakami, A. Mori, and Y. Nishimura, J. Chem. Phys. **109**, 1589 (1998).

178. R. Rossetti, R. C. Haddon, and L. E. Brus, J. Am. Chem. Soc. **102**, 6913 (1980).

179. R. Rossetti, R. Rayford, R. C. Haddon, and L. E. Brus, J. Am. Chem. Soc. **103**, 4303 (1981).

180. V. E. Bondybey, R. C. Haddon, and J. H. English, J. Chem. Phys. **80**, 5432 (1984).

181. H. Sekiya, N. Nakano, K. Nishi, H. Hamabe, T. Sawada, M. Tashiro, and Y. Nishimura, Chem. Lett. **24**, 893 (1995).

182. K. Nishi, H. Sekiya, H. Hamabe, Y. Nishimura, T. Mochida, and T. Sug- awara, Chem. Phys. Lett. **257**, 499 (1996).

183. K. Nishi, H. Sekiya, T. Mochida, T. Sugawara, and Y. Nishimura, J. Chem. Phys. **112**, 5002 (2000).

184. T. Matsuo, S. Baluja, Y. Koike, M. Ohama, T. Mochida, and T. Sugawara, Chem. Phys. Lett. **342**, 22 (2001).

185. G. D. Gillispie, B. M. H. Van, and M. Vangsness, J. Phys. Chem. **90**, 2596 (1986).

186. K. Okuyama, T. Hasegawa, M. Ito, and N. Mikami, J. Phys. Chem. **88**, 1711 (1984).

187. A. Gorski, S. Gawinkowski, J. Herbich, O. Krauss, B. Brutschy, R. P. Thummel, and J. Waluk, J. Phys. Chem. A **116**, 11973 (2012).

188. Nash, J. J.; Zwier, T. S.; Jordan, K. D. *Journal of Chemical Physics* **1995**, *102*, 5260.

189. Tsuji, Takeshi, et al. "Electronic spectra of jet-cooled 5-phenyltropolone. The effect of excitation of the torsional vibrational levels on proton tunneling."*Chemical physics letters* 278.1 (1997): 49-55.

190. See, for example, Y. Udagawa, M. Ito, and I. Suzuka, ***Chem. Phys.* 46,** 237 (1980).

191. Okuyama, Katsuhiko, et al. "Electronic spectra of tolan in a supersonic free jet: large-amplitude torsional motion." *The Journal of Physical Chemistry* 88.9 (1984): 1711-1716.

192. Harmony, M. D. *Chem. Phys. Lett.* **1971**, *10*, 337.

193. Ksenofontova, N. M., Gradyushko, A. T., Solov'ev, K. N., Starukhin, A. S., & Shul'Ga, A. M. (1976). Resonance raman spectra of porphin and its deuterium derivatives. *Journal of Applied Spectroscopy*, *25*(5), 1398-1404.

194. Fita, P.; Garbacz, P.; Nejbauer, M.; Radzewicz, C.; Waluk, J. *Chemistry-a European Journal* **2011**, *17*, 3672.

195. Piuzzi, F.; Dimicoli, I.; Mons, M.; Tardivel, B.; Zhao, Q. C. *Chem. Phys. Lett.* **2000**, *320*, 282.

196. Nosenko, Yevgeniy, et al. "Laser spectroscopy of porphycene derivatives: a search for proton tunneling in 2, 7, 12, 17-tetra-tert-butylporphycene."*Chemical physics letters* 399.4 (2004): 331-336.